A THERMAL MODEL FOR IGBT MODULES AND ITS IMPLEMENTATION IN A REAL TIME SIMULATOR

by

Zhaohui Luo

BS in EE, Tianjin University, 1990

MS in EE, University of Pittsburgh, 1999

Submitted to the Graduate Faculty of

School of Engineering in partial fulfillment

of the requirements for the degree of

Doctor of Philosophy

University of Pittsburgh

2002

UNIVERSITY OF PITTSBURGH

SCHOOL OF ENGINEERING

This dissertation was presented

by

Zhaohui Luo

It was defended on

October 15th, 2002

and approved by

Mahmoud El Nokali, Associate Professor, Department of Electrical Engineering

Dietrich Langer, Professor, Department of Electrical Engineering

Hong Koo Kim, Associate Professor, Department of Electrical Engineering

George Kusic, Associate Professor, Department of Electrical Engineering

Patrick Smolinski, Associate Professor, Department of Mechanical Engineering

Dissertation Director: Mahmoud El Nokali
Associate Professor, Department of Electrical Engineering

ABSTRACT

A THERMAL MODEL FOR IGBT MODULES AND ITS IMPLEMENTATION IN A REAL TIME SIMULATOR

Zhaohui Luo, PhD

University of Pittsburgh, 2002

As the power density and switching frequency increase, thermal analysis of power electronics system becomes imperative. The analysis provides valuable information on the semiconductor rating, long-term reliability and efficient heat-sink design. The aim of this thesis is to build a comprehensive thermal model for the power IGBT modules used in three-phase inverters in order to predict the dynamic junction temperature rise under real operating conditions. The thermal model is developed in two steps: first, the losses are calculated and then the junction temperature is estimated. The real-time simulation environment dictates the requirements for the models: easy implementation on the software platform SIMULINK and fast calculation time.

The power losses model, which is based on the look-up table method for calculating the conduction and switching losses, are successfully built and implemented in the real time simulation environment. The power losses equations are derived from the experimental data. Several algorithms are developed to catch every switching event and to solve the synchronization problem in a real-time system.

An equivalent RC network model is built to perform the thermal analysis. The parameters of the thermal network are extracted from the junction to case and case to ambient dynamic thermal impedance curves. Two separate approaches are followed in deriving these thermal characteristic curves. The first approach uses the experimental data available while the second approach uses the commercial software package ANSYS. The 3-D simulation results using ANSYS agree well with the experimental data and therefore can be relied upon to extract the parameters of the thermal RC network. The latter is successfully implemented using the transfer

parameters of the thermal RC network. The latter is successfully implemented using the transfer function method, and is then built in SIMULINK environment for the use in a real time simulator.

The power losses and thermal RC network models are extensively tested in a real time simulator environment. The accuracy of the models is confirmed by comparing their predictions with the experimental data.

ACKNOWLEDGEMENT

First, I would like to express my sincere gratitude to my advisor, Prof. El Nokali for his guidance and encouragement throughout this research. I learned a lot from him and enjoyed working with him.

This work would not have been possible without the contribution of Valeriu Rusu who worked with me on the real time simulator. And I benefited from Shawn West for his many constructive suggestions and from Diep Bains from Bombardier who provided the experimental data. I would also like to acknowledge the help from Hilmar Lorenz, Frank and Bruce Williams from Bombardier who helped me with the use of the real time simulator.

My sincere thanks to my friends at the university of Pittsburgh: Yong Liu and Qiang Li who provided invaluable help on using ANSYS software and to Yizhang Yang from CMU who helped me with the thermal model.

I would also want to thank Prof. Hong Koo Kim, Prof. Joel Falk and Ms. Sandy Weisberg from the Department of Electrical Engineering for their help during my Ph.D study. I would like to take the opportunity to thank Miss Wanying Kang and Mr. Mingjiao Liu for their friendship.

Finally, I want to thank my parents and my husband for their understanding, support and sacrifice during this journey in graduate school. Especial thank to my dear sweet baby Bambi for bringing me so much joy. This accomplishment is dedicated to my dear brother Feng Luo, who died in the summer of 2000 at age of 36. Finishing this tough work is my way of showing how much I love him.

This work was funded by Bombardier under the supervision of Mr. Lance. C. Schnur who manages the power control group.

TABLE OF CONTENTS

1.0 INTRODUCTION……………………………………………………………………….1
1.1 Power Electronics 1
1.2 Thermal Analysis Of IGBT Module 2
1.3 Organization.. 9
2.0 POWER LOSSES IN IGBT MODULES…………………………………………………11
2.1 Introduction.. 11
2.2 Device Description.. 12
2.2.1 Physics Of IGBT.. 12
2.2.2 Free Wheeling Diode (Fwd) 14
2.3 Power Losses Of IGBT.. 14
2.3.1 Conduction Losses.. 14
2.3.2 Switching Losses 14
2.4 Diode Recovery Energy Losses 19
2.5 IGBT & Diode In PWM Three-Phase Inverter... 21
2.6 Models For Calculating Power Losses Of IGBT Module In Three-Phase Inverter 23
2.6.1 Previous Work 23
2.6.2 Transient Energy Losses Model Of IGBT And Diode 25
2.6.3 Conduction Power Losses Of IGBT And Diode.. 28
2.7 Discussion 32
3.0 THERMAL MODEL OF IGBT MODULE……………………………………………33
3.1 Introduction.. 33
3.2 Thermal Analysis Of IGBT Module And Previous Work 33
3.3 Thermal RC Network... 35
3.4 Transient Thermal Impedance Curve (TTIC) From Junction-To-Case 37
3.5 Thermal RC Model Of IGBT Module From Junction To Case.. 41
3.6 Thermal RC Model Of IGBT Module With Heatsink 44
3.6.1 Experimental Data: Thermal Impedance From Case-To-Ambient............................ 44
3.6.2 Extension Of The Thermal RC Network 47
3.6.3 Thermal Model Of IGBT Module On Heatsink 50
3.6.4 Thermal Coupling 52
3.7 Thermal Model For The Diode 54
3.8 Summary And Discussion.. 56
4.0 MODEL IMPLEMENTATION IN REAL TIME SIMULATOR…………………………...60
4.1 Introduction.. 60
4.2 Introduction Of The Real-Time Simulator And Simulink 60
4.3 Power Losses Model Implementation In Simulink... 62
4.3.1 Sub-Function Blocks Of Calculating Energy Losses Of IGBT And Diode 63
4.3.2 Synchronization Of Switching Event In Simulink.. 63
4.3.3 Switching Power Losses And Switching Energy Losses 66

4.3.4 The Peak Value I_c Catching Algorithm 70
4.3.5 Instantaneous Vs. Average Power Losses Over A Long Time Period 70
4.4 Power Losses Model Result From Real Time Simulator 71
4.4.1 Power Losses Waveforms 71
4.4.2 Instantaneous Vs. Average Power Losses Of IGBT And Diode 71
4.5 Thermal RC Network Model Implementation In Simulink 78
4.5.1.Transfer Function For Solving The Thermal RC Circuit In Simulink 78
4.5.2 Calculating Junction And Case Temperature Of IGBT 79
4.5.3 Calculating Junction And Case Temperature Of Diode 81
4.6 Thermal RC Model Results From Real Time Simulator 86
4.6.1 Junction Temperature Of IGBT 86
4.6.2 Case Temperature Of IGBT 86
4.6.3 Junction Temperature Of Diode 86
4.6.4 Case Temperature Of Diode 86
4.7 Model Verification By Off-Line Simulation In Matlab 89
5.0 3-D THERMAL SIMULATION OF IGBT MODULE 95
5.1 Introduction 95
5.2 Governing Differential Equations Of Heat Transfer 96
5.3 Thermal Behavior Of The IGBT Module 98
5.3.1 Structure Of The IGBT Module 98
5.3.2 3-D Thermal Modeling 98
5.4 Thermal Behavior Of The IGBT Module With Heatsink In The Three-Phase Inverter ... 103
5.4.1 System Description 103
5.4.2 3-D Thermal Modeling 103
5.5 Summary 115
6.0 CONCLUSION 119
6.1 Summary 119
6.2 Suggestion For Future Work 120
APPENDIX A 123
Modeling Approach Including Temperature-Dependency Of Power Losses 123
BIBLIOGRAPHY 139

LIST OF TABLES

Table 2.1 Coefficients in Equations (2.8) for Switching Losses 29
Table 3.1 Thermal –electrical Analogous Quantities 39
Table 3.2 Exponential terms extracted from the transient thermal impedance curve.................. 45
Table 3.3 Parameters of the RC network of IGBT from junction to case. 45
Table 3.4 Parameters of the RC network of diode from junction to case.................................. 45
Table 3.5 Parameters of the RC network of IGBT from junction to ambient. 58
Table 3.6 Parameters of the RC network of diode from junction to ambient............................. 58
Table 5.1 Model physical dimensions and material properties used for simulation.................. 102
Table 5.2 Temperature dependent thermal conductivity of silicon used for simulation 102
Table 5.3 Dimensions of finned heatsink 109
Table 5.4 Thermochemical properties of air at room temperature used in the calculation 109
Table A.1 Data from Fig. A.1 124
Table A.2 Scaling–up data on Table A.1 124
Table A.3 Dividing data on Table A.2 by 2.. 124
Table A.4 Data from Fig.A.2 126
Table A.5 Scaling-down the data from Table A.4 126

LIST OF FIGURES

Figure 1.1 Qualitative representation of the switching cycle of an IGBT. 3
Figure 1.2 A power-cycle lifetime curve for IGBT module. 5
Figure 1.3 Coupling between thermal and electrical model of a power device............................. 5
Figure 2.1 Cross section of the IGBT structure. 13
Figure 2.2 I-V characteristics of IGBT. 13
Figure 2.3 IGBT and anti-parallel diode block. 15
Figure 2.4 Testing circuit for the explanation of Eon, Eoff. 15
Figure 2.5 IGBT turn-on transient. 17
Figure 2.6 IGBT turn-off transient.. 17
Figure 2.7 Diode reverse recovery voltage and current waveforms. 20
Figure 2.8 Single phase full-bridge circuit. 20
Figure 2.9 Voltage and current waveforms of the load of Fig.2.8. 22
Figure 2.10 Three-phase inverter. 22
Figure 2.11 Switching losses curve of the IGBT module. 26
Figure 2.12 Polynomial curve-fitting result for turn-off losses of IGBT: *Eoff*............................ 26
Figure 2.13 Polynomial curve-fitting result for turn-on losses of IGBT: *Eon*............................. 27
Figure 2.14 Polynomial curve-fitting result for recovery losses of diode: *Erec*........................... 27
Figure 2.15 DC characteristics of IGBT: $I_c=f(V_{CE})$. 29
Figure 2.16 Polynomial curve-fitting of DC characteristics of IGBT: $V_{CE}=f(I_c)$ at Tj=125°C. ... 30
Figure 2.17 DC characteristics of diode: $I_d=f(V_d)$. 30
Figure 2.18 Polynomial curve-fitting of DC characteristics of diode: $V_d=f(I_d)$ at Tj=125°C....... 31
Figure 2.19 Values of V_{CE} and $E_{total}=E_{on}+E_{off}$ vs load current and junction temperature [40]. ... 31
Figure 3.1 Transmission line equivalent circuit diagram.. 39
Figure 3.2 Thermal RC network based on the physical structure of power module. 40
Figure 3.3 Simple structure for illustration of Equation (3.4). 40
Figure 3.4 Linear system representing the thermal behavior of IGBT from junction to case. 42
Figure 3.5 Transient thermal impedance curve of IGBT module including the diode. 42
Figure 3.6 Geometry of the IGBT module on the heatsink in three-phase inverter. 48
Figure 3.7 Circuit used to get thermal data of the case. 48
Figure 3.8 Thermal RC network with extension to include heatsink. 51
Figure 3.9 Transient thermal impedance from case-to-ambient of IGBT. 51
Figure 3.10 RC network representing the thermal behavior of IGBT with heatsink.................... 53
Figure 3.11 The principle of superposition applied to the IGBT module..................................... 53
Figure 3.12 Transient thermal impedance from case-to ambient of IGBT unpowered. 55
Figure 3.13 RC circuit representing the thermal coupling effect of diode on the IGBT. 55
Figure 3.14 Transient thermal impedance from case-to-ambient of IGBT. 57
Figure 3.15 RC network for the thermal behavior of diode inside the module with heatsink...... 57
Figure 3.16 RC circuit representing the thermal coupling effect of IGBT on the diode. 59

Figure 3.17 Transient thermal impedance from case-to ambient of diode unpowered. 59
Figure 4.1 Generic hardware-in-the-loop setup. 61
Figure 4.2 The synchronization between the gate-firing signal and the subblock....................... 64
Figure 4.3 Simulink model of implementation of Equation (2.8).. 65
Figure 4.4 Simulink model of calculating conduction losses of IGBT and diode. 65
Figure 4.5 The synchronization between the firing signal and the trigger signal. 67
Figure 4.6 Simulink model of generating trigger signal for E_{on} and E_{off}. 68
Figure 4.7 Two forms of energy losses of 1 Joules. 69
Figure 4.8 Demonstration of the lag between the I_c(peak) and the trigger signal for E_{off}. 69
Figure 4.9 Simulink model of implementation of catching I_c peak algoritm. 72
Figure 4.10 The delay between I_c (peak) and trigger signal for E_{on}. 73
Figure 4.11 Simulink model of averaging function for power losses. 73
Figure 4.12 Waveforms of Turn-on energy losses of IGBT E_{on}. 74
Figure 4.13 Waveforms of Turn-on energy losses of IGBT E_{off}. 74
Figure 4.14 Waveforms of switching and conduction energy losses of IGBT. 75
Figure 4.15 Waveforms of switching and conduction energy losses of diode. 75
Figure 4.16 Instantaneous power losses waveform of IGBT for a 200 seconds run 76
Figure 4.17 Average power losses waveform of IGBT for a 200 seconds run 76
Figure 4.18 Instantaneous power losses waveform of diode for a 200 seconds run..................... 77
Figure 4.19 Average power losses waveform of diode for a 200 seconds run 77
Figure 4.20 Transfer function approaches of calculating each term in Equ. (3.21) for IGBT. 80
Figure 4.21 Simulink model of calculating the junction temperature of IGBT. 82
Figure 4.22 Simulink model of calculating the case temperature of IGBT. 82
Figure 4.23 Transfer function approaches of calculating each term in Equ. (3.21) for diode. 83
Figure 4.24 Simulink model of calculating the junction temperature of diode. 85
Figure 4.25 Simulink model of calculating the case temperature of diode. 85
Figure 4.26 Junction temperature above the ambient profile of IGBT for a 200-second run....... 87
Figure 4.27 Case temperature above the ambient profile of IGBT for a 200-second run. 87
Figure 4.28 Junction temperature above the ambient profile of diode for a 200-second run 88
Figure 4.29 Case temperature above the ambient profile of diode for a 200-second run. 88
Figure 4.30 Model testing process. 91
Figure 4.31 Demonstration of power losses and the junction temperature relation 91
Figure 4.32 Power losses profile of IGBT and diode during train's service period. 92
Figure 4.33 Power losses profile of IGBT and diode in the off-line simulation. 93
Figure 4.34 Off-line simulation model block in Simulink. 93
Figure 4.35 Off-line simulation results: temperature profile of IGBT. 94
Figure 4.36 Off-line simulation results: temperature profile of diode. 94
Figure 5.1 Schematics of the IGBT module. 99
Figure 5.2 Mesh structure for half of the IGBT module. 99
Figure 5.3 Temperature distribution of the module after power applied on IGBT chips. 101
Figure 5.4 Transient thermal impedance from junction to case of IGBT chips. 101
Figure 5.5 Temperature distribution of the module after power applied on diode chips............ 104
Figure 5.6 Transient thermal impedance from junction to case of diode chips. 104
Figure 5.7 Schematic of the whole system. 105
Figure 5.8 Simplified structure of the system. 105
Figure 5.9 Schematics of the heatsink and the serrated fins. 107

Figure 5.10 Mesh structure of the system. 112
Figure 5.11 Temperature distribution of the system after power applied on IGBT chips. 112
Figure 5.12 Transient thermal impedance from junction to ambient of IGBT chips. 113
Figure 5.13 Transient thermal impedance from case to ambient of IGBT chips. 113
Figure 5.14 Thermal coupling effect of IGBT chips on the diode chips. 114
Figure 5.15 Transient thermal impedance representing the thermal coupling effect of IGBT... 114
Figure 5.16 Temperature distribution of the system after power applied on diode chips. 116
Figure 5.17 Transient thermal impedance from junction to ambient of diode chips. 116
Figure 5.18 Transient thermal impedance from case to ambient of diode chips. 117
Figure 5.19 Thermal coupling effect of diode chips on the IGBT chips. 117
Figure 5.20 Transient thermal impedance representing the thermal coupling effect of diode ... 118
Figure 5.21 Transient thermal impedance Z_{ja} of IGBT at different power levels. 118
Figure 6. 1 Relation between different approaches of thermal modeling of IGBT module. 121
Figure A.1 Typical switching losses vs. junction temperature 123
Figure A.2 Typical output characteristics 126
Figure A.3 Simulation models built in Simulink : with and without temperature dependency 127
Figure A.4 Input Ic waveform. X-time(second); Y-current(A) 128
Figure A.5 Power losses waveform. X-time(second); Y-power losses(Watts) 129
Figure A.6 Junction temperature waveform. X-time(second); Y-temperature(°C) 129
Figure A.7 Junction temperature Tj simulation results by two model when ambient =0°C 131
Figure A.8 Junction temperature Tj simulation results by two model when ambient =25°C 132
Figure A.9 Junction temperature Tj simulation results by two model when ambient =40°C 133
Figure A.10 Averaged power losses waveform. X-time(second); Y-power losses(Watts) 135
Figure A.11 Pulses vs. step as input function 137

1.0 INTRODUCTION

1.1 Power Electronics

Power electronics is the technology of converting electric power from one form to another using electronic power devices. It has undergone intensive developments in recent years with the advances and innovations in power semiconductor devices, power conversion techniques, microprocessors, DSP, application specific ICs, personal computers, CAD tools, control and estimation techniques [1].

The key element in a power conversion system is the power semiconductor device that operates as power switch. By some estimates, more than 60% of all the power utilized in U.S.A flows through at least one power device and more often through multiple devices [2]. The improvement in power semiconductor devices is the driving force behind the improved performance, efficiency, size and weight of power conversion systems.

The requirement for ideal power semiconductor device is the ability to control the power flow to the load with zero power dissipation. In the conducting mode, the device should have infinite current conduction capacity, while in the blocking mode, it should have infinite blocking voltage capacity. Furthermore the switching speed between the different modes should be very fast.

Commercially available since 1988, the Insulated Gate Bipolar Transistors (IGBT's) are widely used in today's power conversion systems for high switching frequency and medium power ranges. The IGBTs combine the advantage of the high current density in bipolar operation with the advantage of the fast switching and low drive power of MOS gated devices. Other advantages include low steady-state losses, very low switching losses, high short-circuit capability and easy to make parallel connection.

Today, there are 600 V, 1200V, 1700V, 2500V and 3300V IGBT with current up to 2400A on the market. And samples of 4500 V IGBTs have been tested in laboratories. Recently Eupec introduced 6500V IGBTs for current of 200A, 400A and 600 A. Samples of 6500V IGBT

modules are available [3]. The state of the art IGBT technology makes IGBT superior to GTO (gate turn-off) even at higher switching powers after having already replaced power BJTs. IGBTs operating at 150 kHz in the hard-switching mode and 300 kHz in the soft-switching mode are available [4].

1.2 Thermal Analysis Of IGBT Module

For an ideal switch, the power consumption is zero. For a real switch, however there will be static (conduction) and dynamic (switching) losses which are shown in Fig. 1.1 over one switching cycle.

When turn-on or turn-off the switch, the transient process takes time (several microseconds for IGBT) and the device consumes power while both the voltage and current are non-zero. When the switch is conducting, because there is voltage falling on the switch (several volts for IGBT), the conduction also has power dissipation.

Power losses inside an IGBT module can restrict its use and therefore it becomes an important issue that cannot be ignored in the design stage. The power losses work as a heat source inside the semiconductor device and this heat will elevate the junction temperature and change the temperature profile inside the device. This is called self-heating effect and is more severe when the device is compactly packaged.

From physics, we know that the parameters of a semiconductor are temperature-dependent. Specifically, for power semiconductor devices, with its high ambient temperature application environment and high power rating, the temperature dependence is even more critical. Generally, the power devices' properties and performance in circuits will degrade with increased temperatures. This can be attributed to the reduction of the carrier mobility with increased temperature according to the following relation [5]:

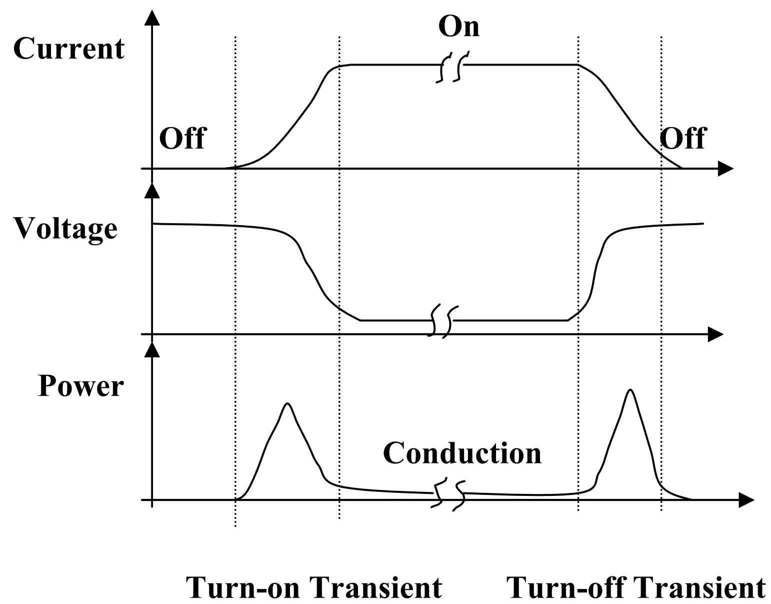

Figure 1.1 Qualitative representation of the switching cycle of an IGBT.
(a) Current waveform, (b) Voltage waveform, (c) Instantaneous power losses waveform.

$$\mu_T(T) = \mu_{300}\left(\frac{T}{300}\right)^{-2.3}$$

(1.1)

where μ_T is the electron (or hole) mobility at temperature T and μ_{300} is the mobility at 300 K. The degradation has significant effects on the voltage rating, conduction losses and switching losses [6].

In order to avoid destruction and permanent damage of the device, the junction temperature T_j must be kept under a safe operating value T_{jmax} that is normally specified by the manufacturer. For a silicon device, the temperature rating is usually 150 °C and can be as high as 600 °C for silicon carbide which has higher temperature capacity [6]. Keeping the junction temperature in the safe operating range is not enough for the devices long-term reliability. Due to loading in the circuit, power losses vary and the temperatures of the power devices fluctuate while operating. This fluctuation causes mechanical stress due to the different thermal expansion coefficients of the layers inside a device. The stress affects the solder and wire bond connections. Mechanical failure is expected when a device experiences a certain number of thermal cycles. So it is not the absolute temperature value T_j but also the temperature cycling value ΔT_j matters.

Fig. 1.2 [7] shows the power cycle lifetime curve as a function of the change in junction temperature during the power cycling of an IGBT module. From the graph we conclude that in order to increase the long-term reliability of the power module, the change in the junction temperature during operation should be as small as possible. For example, the IGBT module is used in traction applications such as locomotive, elevator and subway which generally require a service lifetime of about 30 years and then demand IGBT modules of a long term reliability to withstand as much as 10^6 to10^7 power cycles [8].

In order to guarantee a safe operating condition for a system, a designer may be conservative by allowing wider margins than normally required: such as attaching a larger heatsink than necessary, or reduce the current through the IGBT, or reduce the switching frequency. All these choices reduce the performance of the system while increasing its price. A

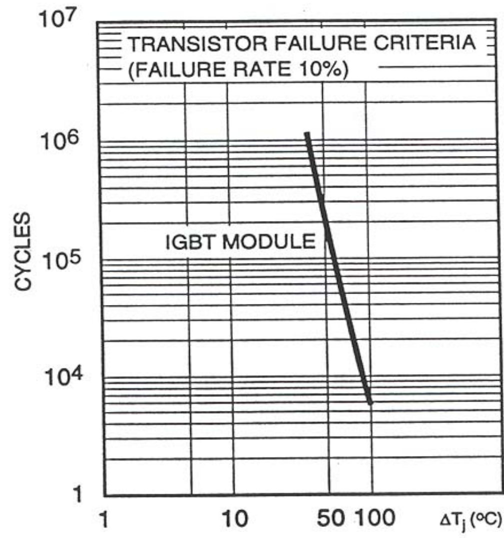

Figure 1.2 A power-cycle lifetime curve for IGBT module.

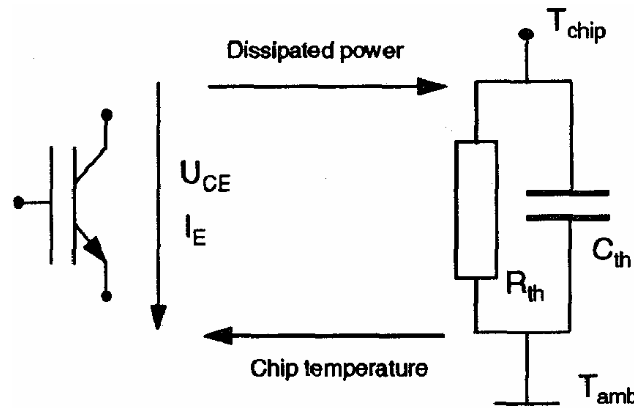

Figure 1.3 Coupling between thermal and electrical model of a power device.

better design is offered if one can accurately predict the temperature gradient within the device under existing operating conditions.

Thermal analysis is therefore a fundamental issue in the design of power conversion systems. It provides us with information that can be used for the analysis of the device long-term reliability, maximum ratings characterization, package design optimization, correct choice of heatsink [9].

Besides the need to keep the device junction temperature below a safe operating value, an circuit designer need to know the junction temperature to calculate the operating current and voltage in a circuit that uses the device.

So through self-heating effect, there is a connection between the electrical and thermal performances of the semiconductor device as shown in Fig. 1.3 [10]. The voltage across the device U_{CE} and the current through the device I_E will determine the power dissipated. This in turn will generate heat and thus changes the junction temperature of the device. This new junction temperature will affect the parameters U_{CE} and I_E for they are temperature-dependent.

An electro-thermal analysis, which accounts for the coupling, will provide more realistic and accurate information for a device in operation. For some applications, only an electro-thermal model can give reasonable results. An example is the case for predicting the output characteristics of a semiconductor device under short-circuit condition [11].

Estimating of the junction temperature of an operating power switching device is not an easy task. On the semiconductor device level, an electrical engineer views the junction as the active region of the device, and it is more easier for him to calculate the electric field, current density in this region than to determine its temperature. A mechanical engineer regards the active region as a rather small region (around micrometer) build from silicon with high temperature gradients. The coupling between the electronics and thermal parameters makes this microscopic picture more complex. On the package and system level, the IGBT is not only made of various layers of material but also several IGBT chips are paralleled inside a module in order to provide

high current. Outside the module, various cooling methods are used, and these factors complicate the thermal analysis of the system.

For thermal analysis, there is no “best” or “exclusive” model or method to use. However given the different application requirements and objectives of the model, application-specific thermal analysis models are used to simplify the problem.

It usually takes the following steps to perform the thermal analysis of a power semiconductor device. The power losses in the device are first calculated. This calculation requires the availability of the current and voltage waveforms in the device that can be obtained through measurement, simulation, or analytical solution. The non-invasive measurement for high current and high voltage in an IGBT module is not an easy task when the environment is full of EMI, especially that the measurement need to be fast enough to catch the fast transient process. An alternative choice is to derive analytical expressions for the power losses under simplified operating condition e.g. sinusoidal output and inductive load [12]. If these conditions are far from the ones encountered in real operation, the accuracy of the power losses calculation will be affected. This method is also invalid in some cases. For example, in three-phase inverter circuits, space vector pulse width modulation technique (SVPWM) is used and the waveforms of the current and voltage vary cyclically with time and change with the mode of operation [13]. This renders the analytical calculation for power losses extremely difficult. A second choice consists of using circuit simulation tools to get power losses profile. The advantage of simulation lies in the fact that one can estimate the losses under various operating conditions. In this choice, decisions need to be made on the model needed to describe the static and dynamic behavior of the IGBT module and what simulator to use and how to implement the model within the simulator. IGBTs model can be classified into two categories: physics based and behavioral models also known as compact models. The models in the first category are based on the analytical solution derived from the physics of the device and have high accuracy. Hefner’s IGBT model implemented in commercially available simulator SABER [14] is the most comprehensive one and involves tens of parameters that need to be extracted for each device. The parameter extraction process is very time consuming and test systems need to be devised [15]. The simulation of a power circuit gives the details of the transient analysis and power

losses are directly obtained from the product of the current and voltage waveforms of an IGBT. The simulation time need to be long enough to catch the cycle of the power circuit (usually around several milliseconds) while the time step need to be small enough to catch the transient detail (the transient process happens within several microseconds). So the computation time of the power losses profile is prohibitively long. In order to avoid extracting too-many parameters in the physics model and to accelerate the simulation speed, behavioral or empirical models are developed for specific devices. The detailed physical mechanism of the device is not considered. Curve-fitting and interpolation methods are used to extract the model parameters from the measured data provided by the manufacturer [16].

After calculating the power losses of a semiconductor device, a model is built to describe its thermal behavior. The thermal model of the semiconductor device should be added with the package and the cooling system in order to simulate the entire system performance. Generally, there are four kinds of thermal analysis models: thermal numerical, analytical, thermal RC network and electro-thermal models.

The thermal numerical model is often done on package level or system level. The analysis is focused on the detail structure of the power module, overall air flow and temperature field of the application system. Now the IGBT module technology is based on multichip silicon die mounted in a complex structure of several materials that are connected by bonding techniques. Free wheeling diodes are integrated inside the module. In order to simulate the thermal behavior of the complex hybrid structure, numerical methods such as finite element method (FEM) [11], finite difference method (FDM) [17] or computational fluid dynamic (CFD) [18] are used. 3-D software packages based on these methods are available and are widely used [19] [20]. The 3-D analysis will provide the following information on the module: the temperature distribution inside the module, the hot spot location, and the temperature rise in devices. The information will benefit the following aspects of thermal design: the optimization of the internal geometry of the module to avoid localized heating, minimization of the rises in the device temperature. For the power module user, the analysis will provide information on the efficiency of the heatsink design. And from the step response of the thermal system, the thermal resistance from junction to ambient Z_{ja} can be calculated.

Before the use of numerical software, analytical methods were used for the important for the thermal analysis. In order to obtain closed-form solution for the heat diffusion equation, the structure of the device, boundary and initial conditions are simplified. The analytical solution is usually mathematically complex. With the power device's structure becomes more complicated and the advantage of the numerical software of thermal analysis, this method is much less popular now.

Building equivalent electrical circuit is another alternative to carry thermal analysis [21]. The model can be implemented in existing circuit simulators and provide a simple way for the simulation of thermal and electrical models simultaneously. The thermal RC network's parameters can be derived from FDM, FEM simulations (step response) [22] [23] or transient temperature measurement data [24].

Some models have the ability to simulate the thermal and electrical models simultaneously [25]. The temperature of the device is not a constant during simulation. The electro-thermal model is built in three steps: first the electronics model of the device is developed, followed by the thermal model, and finally the coupling between the two models is provided. The coupling can be implemented by setting the temperature in the electrical models as the state variable instead of being a global parameter. The device's temperature is determined by iteration at each simulation step. Self-heating effect is taken into account through temperature-dependent parameters that modified by the device's dynamic temperature.

1.3 Organization

This Ph.D. dissertation deals with the thermal analysis of power IGBT modules that are used in three-phase inverters. The objective is to develop a thermal model that can be implemented in a real time simulator. The experimental data available are used to extract the thermal model parameters. In addition, 3-D Finite Element Method thermal simulations are performed on the module to provide an alternative avenue for the extraction of the thermal model

parameters. Both the on-line and off-line simulation results of the device temperature are presented.

Chapter 2 describes the physics of IGBTs and free wheeling diode and examines the origin of the power losses in these devices when used in three-phase inverters. Assuming that these losses are function of current, voltage and temperature, and based on the experimental data from the manufacturer, the formulas to calculate the conduction and switching losses are derived. The effect of excluding the temperature as a variable in the model is analyzed.

The general concepts of thermal analysis that are familiar to electrical engineers are introduced in Chapter 3. The thermal RC model is then described. The process of extracting the parameters of the thermal model from the dynamic thermal impedance data is outlined. Finally, the limitation of the RC thermal model is discussed.

Chapter 4 describes the implementation of the power losses and thermal RC models in the real time simulator. First the real time simulator and software platform Simulink are introduced. Based on the models developed in Chapters 2 and 3, function blocks in Simulink are described in detail. Special function blocks to handle the synchronization in the real time simulator are derived. The results of the model implemented in the real time simulator are given and discussed. An off-line simulation block is built in Simulink, and the simulation results are compared with the experimental data.

In Chapter 5, the 3-D FEM software ANSYS is used to predict the model thermal behavior of the IGBT modules in three-phase inverters. From the step response of the system in the 3-D model, the dynamic thermal impedance curves are derived. This approach provides an alternative avenue for extracting the parameters of the thermal RC models outlined in Chapter 3.

In Chapter 6, the conclusions of the thesis are presented and future work is suggested. An interesting topic for future work would be the electro-thermal simulation of the IGBT module.

2.0 POWER LOSSES IN IGBT MODULES

2.1 Introduction

The first step in performing the thermal analysis in an IGBT module is to calculate the power losses in the module. The losses will also provide information to the system engineer to optimize the pulse pattern generation [26] and to design the gate-drive circuit topology [27] of a power conversion system.

There are two kinds of losses in power devices: conduction losses (static losses) and switching losses (transient losses). Increasing the switching frequency will increase switching losses so that it becomes the dominant factor in the total power losses. In order to understand the origin of these losses, the physics of IGBTs and free wheeling diodes and their operation as switching elements in inverters are reviewed.

The current and voltage transient waveforms are not always available to us which is a prerequisite for computing the power losses. Simulation and analytical solution becomes therefore important.

In this chapter, we review various approaches used in the literature to calculate the power losses of IGBT in operation. We also show that these approaches cannot be used in real time simulator. The ideal approach is to develop empirical equation to calculate the power losses. Based upon the assumption that the power losses of IGBT and diode in the turn-on and turn-off transient depend on the DC link voltage and current through the IGBT and diode, an analytical expression for the power losses is extracted from the experimental data provided by the manufacturer.

2.2 Device Description

2.2.1 Physics Of IGBT

The cross-section of the IGBT is illustrated in Fig. 2.1 [28]. We can see that the IGBT is a four-layer power semiconductor device having a MOS gate.

When a negative voltage is applied to the collector with respect to the emitter, there will be no current flow through the device for the lower junction (J_1) is reverse biased. This provides the reverse blocking capacity of the IGBT.

When the gate is attached to the emitter (V_{GE}= 0 volt), and a positive voltage is applied to the collector with respect to the emitter (the same voltage as gate), the upper junction (J_2) is reverse biased and the device operates in the forward blocking mode.

If a positive voltage higher than the threshold voltage is now applied between the gate and the emitter ($V_{GE} > V_{th}$), the surface of the P base region is inverted and an N channel will appear. The electrons will then flow from the N+ emitter to the N drift region forming the base current for the vertical P-N-P transistor of the IGBT. An increase in the positive voltage between the collector and emitter leads to an increase in the injected holes concentration until it exceeds the background doping level of the N drift region. In this region of operation, the device behaves like a P-I-N device and this explains the IGBT's ability to handle high current densities. If we further increase the voltage between the collector and the emitter, the N-channel will get pinched-off. The base current for the P-N-P transistor will be limited and so will the hole current through the path. The collector to emitter current reaches the saturation point and the IGBT operates in the active region. The output characteristics of the IGBT are similar to that of the MOS and the output current is controlled by the gate voltage V_{GE}. The I-V characteristics of IGBT are shown in Fig. 2.2.

From the above, one concludes that IGBT integrates the physics of MOS and bipolar junction transistors. The P-I-N behavior of the BJT part provides high forward conduction density, and the MOS gate structure determines the low drive power and fully gate-controlled output characteristics.

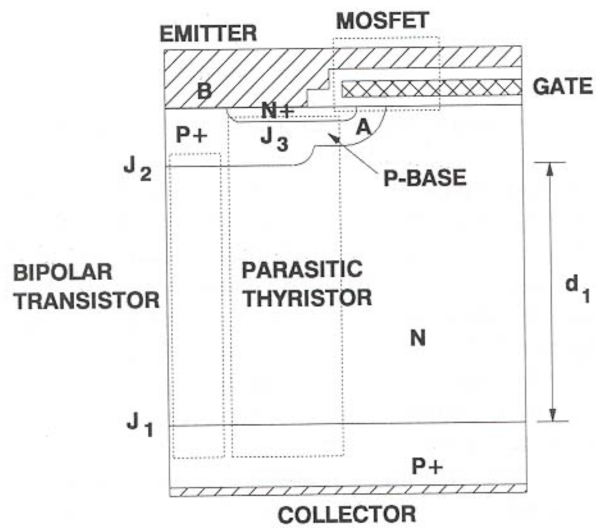

Figure 2.1 Cross section of the IGBT structure.

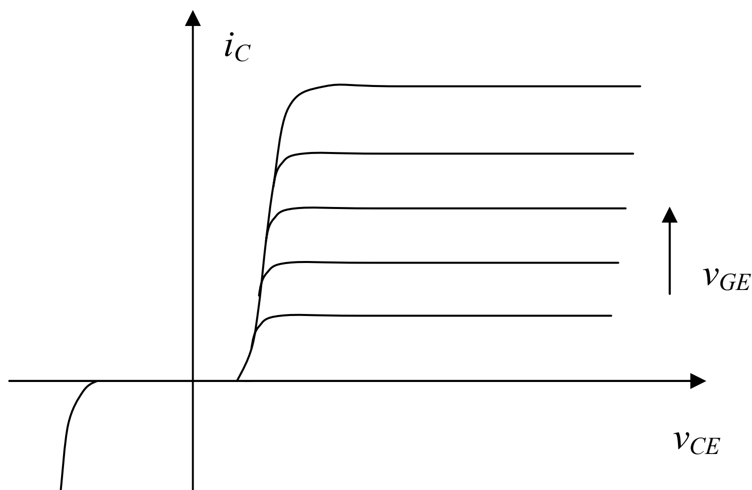

Figure 2.2 I-V characteristics of IGBT.

2.2.2 Free Wheeling Diode (Fwd)

In a three-phase inverter circuit, each IGBT is connected in parallel with a diode as shown in Fig.2.3 in order to handle the regenerative or inductive current of a motor. The principle of operation of power diode is not different from that of the common diode. It has two regions of operation: reverse blocking region and forward conduction region. This diode is also called free wheeling diode (FWD). The diode and the IGBT form a switching "block" which has bi-directional switching ability. The reverse recovery process of diode will produce undesired stress on the IGBT during operation. So the reverse recovery losses of the diode are related to the switching losses of the IGBT. The diode being co-packaged with the IGBT inside the module, one cannot conduct the thermal analysis of IGBT module without taking account of the FWD.

2.3 Power Losses Of IGBT

2.3.1 Conduction Losses

The IGBT is not an ideal switch. Therefore there will be a voltage drop, v_{CE}, across the device while it conducts current, i_C. The voltage drop has these parts: the voltage drop across junction J_1, the voltage drop across the epitaxial region N. The analytical equations that calculate these voltage drops along with the current through the device while conducting can be found in [28].

The conduction losses is the product of the instantaneous current $i_{CE}(t)$ and the corresponding voltage $v_{CE}(t)$.

$$P_{conduction}(t) = i_{CE}(t) \times v_{CE}(t) \tag{2.1}$$

2.3.2 Switching Losses

Switching losses occur in the IGBT when it is turned on and off due to the finite time taken by the charges to respond to applied voltages. The conduction in the MOSFET part of the IGBT depends on the charges on the gate and under the channel. The conduction in the BJT part

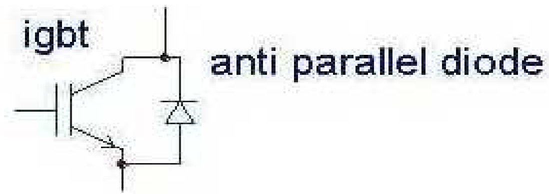

Figure 2.3 IGBT and anti-parallel diode block.

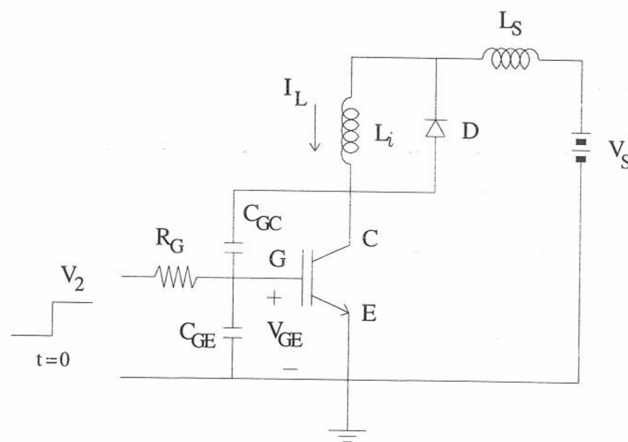

Figure 2.4 Testing circuit for the explanation of Eon, Eoff.

is influenced by the stored minority charge in the vicinity of the PN junction. In power conversion systems, the IGBT is usually connected to inductors or capacitors that will store or release energy in the transient process. All these storing and losing charge and energy process takes time and consumes power [29].

The circuit in Fig. 2.4 [30] is used to examine the switching transient exhibited by an IGBT. The input characteristics of IGBT are the same as of MOSFET, and hence the capacitance C_{GC} (between gate and collector) and C_{GE} (between gate and emitter) are taken into consideration when transient analysis is conducted. An inductive load L_i is connected in parallel with a free wheeling diode D. The stray circuit inductance is denoted by L_S and the supply voltage is V_S.

Let's assume initially that the IGBT is in its OFF state. The load current I_L is therefore circuiting through the diode turning it ON. The supply voltage V_S is supported by the IGBT and appears across its collector (C) and emitter (E) terminals.

Suppose that at time t =0, a step voltage is applied at the gate terminal. This voltage will not turn ON the IGBT immediately i.e. the collector current will not flow instantaneously. Rather v_{GE} will increase exponentially with a time constant equal to $R_G(C_{GC}+C_{GE})$. Once v_{GE} reaches the threshold voltage V_T of the IGBT, the collector current starts to flow. The time taken for v_{GE} to reach the threshold voltage V_T represents the turn-on delay period t_1 as shown in Fig. 2.5. Beyond t_1, V_{GE} will continue to increase past V_T leading to an increase in the IGBT collector current. However, the diode is still forward biased albeit with less current flowing in it ($I_d=I_L-I_C$). Hence, the IGBT must still support the entire supply voltage. This time period will end when the collector current reaches the value of the load current I_L i.e., when all the circulating current is transferred to the IGBT. Beyond this point in time, the diode enters its recovery mode allowing the collector voltage to fall from V_S to the steady state on-sate voltage drop V_f. From the turn-on waveforms as shown in Fig.2.5, it can be concluded that power dissipation occurs during the

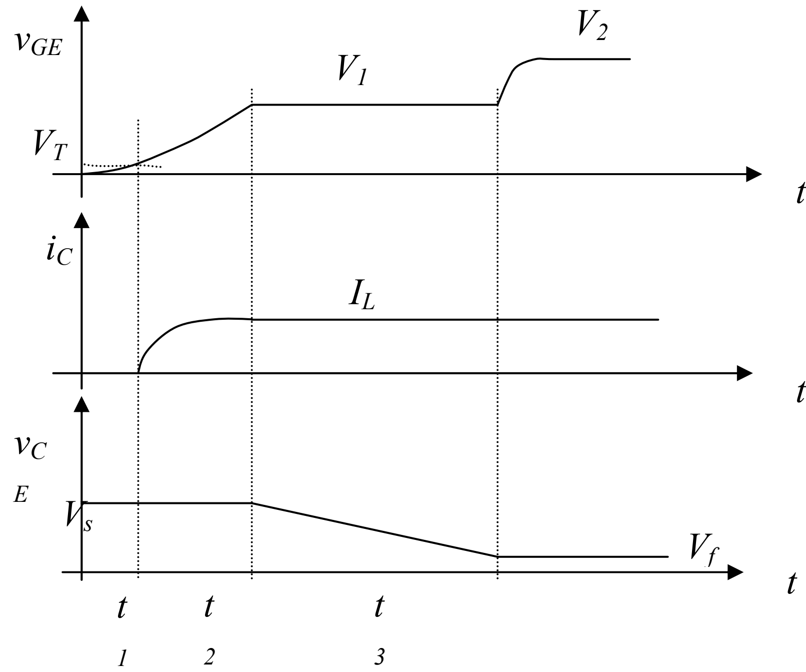

Figure 2.5 IGBT turn-on transient.

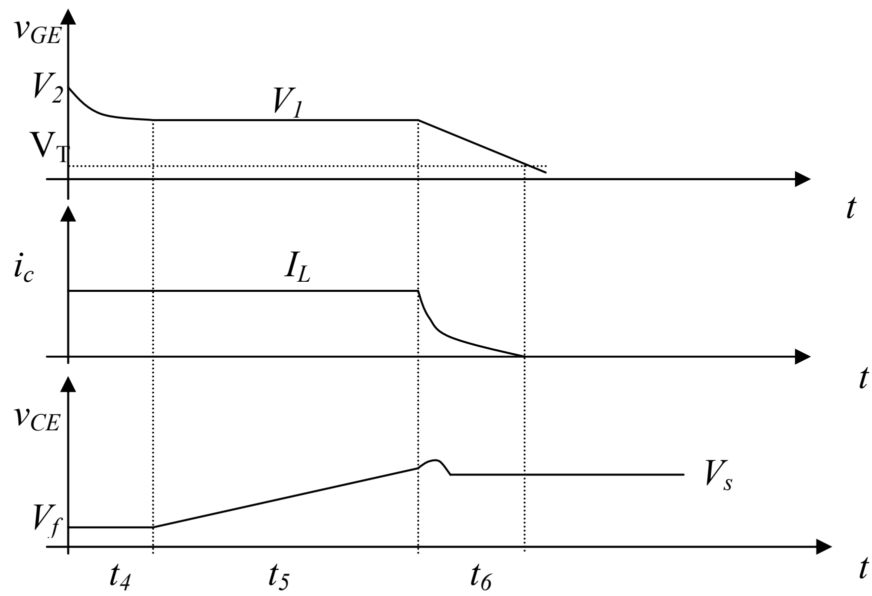

Figure 2.6 IGBT turn-off transient.

interval t_2 and t_3 where high current and voltage are sustained by the device simultaneously. The instantaneous power $p(t)$ dissipated by the IGBT is equal to $i_C(t)v_{CE}(t)$. The energy losses during the IGBT turn-on transient is denoted by E_{on} and integral of $p(t)$ over the switching transition period (t_2+t_3).

$$E_{on} = \int_{t2}^{t3} i_c(t) \times v_{CE}(t) \cdot dt \qquad (2.2)$$

To explain the origin of the turn OFF losses, assume that the IGBT is in its ON-state with $v_{GE} = V_2$ and $v_{CE} = V_f$. All the load current I_L is flowing through the IGBT with no current flows through the diode which is now in its reverse blocking state. Suppose that at t =0, the applied gate voltage is abruptly reduced to zero. Once again the IGBT will not turn OFF instantaneously i.e., the collector current will not reduce to zero momentarily. Rather, v_{GE} decreases exponentially with time due to the discharging of the gate capacitance via the gate series resistance R_G. There will be no change in either v_{CE} or i_C until v_{GE} reaches V_1 which is the magnitude required to saturate the collector current at a value equal to the load current I_L. The period t_4 at which this occurs corresponds to the turn off delay. Beyond t_4, the collector current remains at I_L and v_{CE} rises towards V_S. This is because the load current cannot be diverted from the IGBT into the diode until the diode voltage exceeds V_S. As long as the collector current is constant, V_{GE} will also remain constant. The collector-emitter voltage rises linearly from the on-state voltage drop V_f to V_S during period t_5. At the end of t_5, the free wheeling diode D turns ON. Both v_{GS} and i_C decrease since a transfer of current occurs from the IGBT to the diode. This period will extend until v_{GS} reaches the threshold voltage V_T and the drain current is reduced to zero. From the turn-off waveforms as shown in Fig. 2.6, it can be concluded that high power dissipation occurs during interval t_5 and t_6 where high current and voltage are sustained by the device simultaneously. Switching turn off energy E_{off} is defined as:

$$E_{off} = \int_{t5}^{t6} i_c(t) \times v_{CE}(t) \cdot dt \qquad (2.3)$$

2.4 Diode Recovery Energy Losses

The free wheeling diode also exhibits conduction losses and switching losses during its operation.

When the diode is conducting a current i_d, there is a forward voltage drop v_d across the diode that leads to a conduction loss which is equal to $i_d \times v_d$.

$$p_{conduction}(t) = i_d(t) \times v_d(t) \tag{2.4}$$

When the diode is turned on, the switching time is usually short and the switching losses can be ignored.

Reverse recovery occurs when a forward conducting diode is turned off abruptly. The build-in charges accumulated in the drift region when the diode was forward biased need time to be removed through recombination, diffusion or be swept out by the high electric field. The resulting transient reverse current flows through the circuit at high reverse voltage and this will generate switching losses. The recovery phenomenon of diode will limit the switching speed, the current and voltage rate of the IGBT.

The waveform when the diode turns off with an inductive load is shown in Fig. 2.7. Stage 0 ends at the moment when the diode is turned OFF. In stage 1 the excess charge is removed from the P region of the P-N junction. At the beginning of Stage 2 the total excess carrier concentration in the junction is reduced to zero and during this stage, the voltage across the diode increases, and the depletion region gets wider until it reaches its maximum.

From the turn-off waveforms of diode it can be concluded that power dissipation occurs during stage 1 and stage 2 where current and voltage are sustained by the diode simultaneously. The diode recovery energy *Erec* is defined:

$$E_{rec} = \int_{(stage1, stage2)} i_d(t) \times v_d(t) \cdot dt \tag{2.5}$$

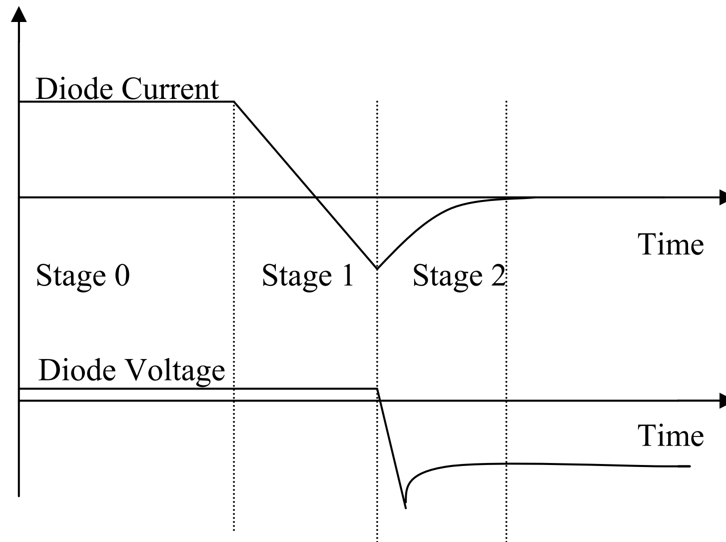

Figure 2.7 Diode reverse recovery voltage and current waveforms.

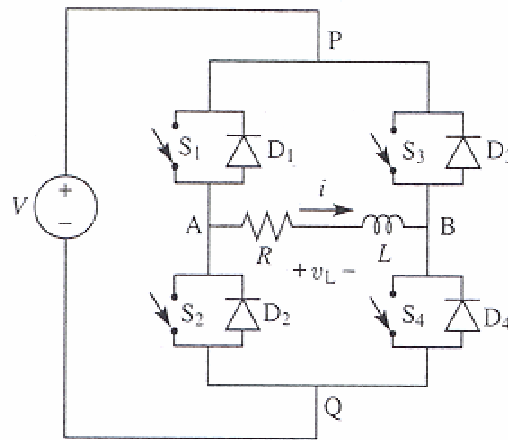

Figure 2.8 Single phase full-bridge circuit.

2.5 IGBT & Diode In PWM Three-Phase Inverter

The total energy losses (conduction and switching) of IGBT and diode in a three-phase inverter are function of the internal physics of the device, external load condition (capacitance and inductance load) and the circuit topology (modulation method, gate driving circuit). It is therefore instructive to understand the operation of three-phase inverter, so we can decide when and what losses occur during operation.

An inverter converts a DC supply voltage to an AC output delivered to a load. Fig.2.8 [31] shows a simple implementation of an inverter: a single-phase, full-bridge configuration that consists of four blocks. A block consists of an IGBT (S) in parallel with a diode (D). We turn ON blocks 1 and 4 for half the period of the desired AC output to obtain the positive voltage +V, then blocks 2 and 4 are turned ON for the other half period to get the negative voltage. The output voltage and the current in the load are shown in Fig.2.9. It is instructive to note that a block is turned ON either by turning ON its IGBT or its diode. For example in the period $t_1<t<t_2$, D_1 and D_4 are ON, while $t_2<t<t_3$, S_1 and S_4 are ON.

Fig.2.10 shows the configuration of three-phase inverter.

For many inverters applications, one needs to adjust the frequency and amplitude of the output AC signal. Pulse width modulation (PWM) is the technique being used. By controlling the switching pattern (the combination of the on-off) of the various switching elements, the amplitude of the output voltage and the frequency of its fundamental are adjusted. They are two types of PWM techniques being used: sinusoidal pulse width modulation (SPWM) or space vector pulse width modulation (SVPWM). The former generates the gate control signal by comparing a reference sine wave with a carrier triangular wave. The latter sequences the switches to certain states (described by space vector) according to the position of the reference vector in a coordinate plane. The switching pattern in this case is controlled through software in SVPWM.

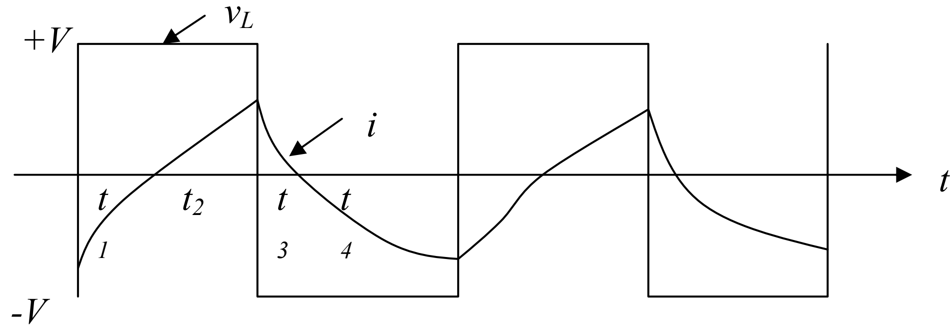

Figure 2.9 Voltage and current waveforms of the load of Fig.2.8.

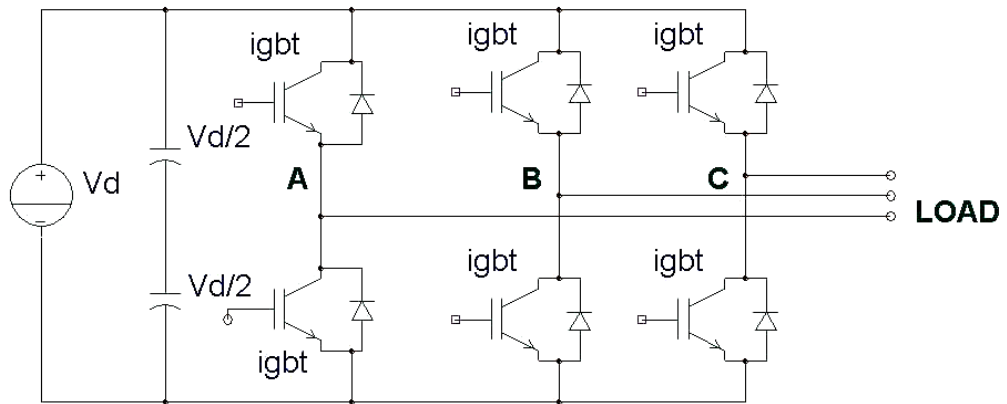

Figure 2.10 Three-phase inverter.

2.6 Models For Calculating Power Losses Of IGBT Module In Three-Phase Inverter

2.6.1 Previous Work

One approach is to find the analytical equations [32] [33] that calculate the conduction and switching losses of power device in a given application. The equations use the phase angle between the phase voltage and current of the fundamental as a variable and require that we express the modulation method mathematically. Since we do not know the phase angle in advance in a real time system, this method is therefore not suitable for us.

Other models concentrate on the switching behavior of the IGBT. In reference [34], the turn-off process is studied under different switching operation modes such as hard-switching, emission-open operation mode etc., and analytical equations are derived to calculate the turn-off losses of IGBT under different modes. In reference [35], power losses of IGBT are divided into parts that include as losses due to diode recovery, losses resulting from the current tail, losses during turn-on process with the rise of collector current, and losses due to the output capacitance. Equations to calculate the power losses due to each mechanics are derived. In reference [36], a loss summation method is used in which the curves of voltage and current during switching transient are divided into segments, then calculate the power losses in each segment and add them up. For example for the IGBT turn-off process, two segments are identified: one in which the collector voltage rises linearly and the other is characterized by a decrease in the collector current. The parameters needed in the calculation such as the reverse charge during the diode recovery, the current slope *di/dt* during the IGBT turn-on process can be extracted from the experimental or simulation data of the transient curve of the device. The parameters necessary to calculate the power losses are too many and some are not available to us. So this is still not our choice to implement our model in the real time simulator.

The above methods are examples of physics-based approaches. Behavior models can be also used to calculate losses. Reference [16] presents a behavior model to estimate the power dissipation in an IGBT. In the model the IGBTs and diodes are treated as ideal switches and some user-defined turn-on and turn-off functions are extracted from the measured transient waveforms. The on-state characteristics are also defined by the measured saturation voltage of

the IGBT and the forward voltage of the diode. The direct output of the model is the transient waveforms of IGBT and diode in the application. The switching transient lasts about several microseconds. This prohibits the use of this method in the real time simulator because the step size in the simulator is around 50 microseconds and it cannot describe a process that lasts a shorter time than the step size.

From equations (2.1) and (2.4), we know that the conduction losses depends on three parameters: the current through the device I_C (I_d for the diode), the voltage across it V_{CE} (V_d for the diode) and the junction temperature T_j. Using the DC characteristics extracted from experiment or simulation, the on-stage voltage V_{CE} (V_d for the diode) can be expressed as a function of the current through the device I_C (I_d for the diode). So the conduction losses can generally be expressed as:

$$P_{conduction} = f(I, T_j) \tag{2.6}$$

where $I = I_c$ for the IGBT and $I = I_d$ for a diode.

For the switching energy losses, an assumption is made and verified by experiment: the switching energy losses have an almost linear dependency on the switched current [7]. The dependency of the switching losses on the DC link voltage V_{DC} and junction temperature T_j, for a specific device, can be extracted from experimental data or simulation results. In general, the empirical relation between the switching losses and the three parameters can be found by curve fitting methods [37] [38] [39]:

$$E_{switching} = f(I, V_{DC}, T_j) \tag{2.7}$$

In the real time simulator, the instantaneous current of the IGBT and diode are available to us. We need to find the empirical equations to calculate the IGBT switching and conduction losses as well as the diode switching and conduction losses by using the instantaneous current as input. Our model will take care of the power losses dependency on the DC link voltage V_{DC} through scaling. In all this process, the junction temperature is assumed as constant at 125°C and the effect of this will be mentioned in the discussion. The process is described below.

2.6.2 Transient Energy Losses Model Of IGBT And Diode

The manufacturer's data sheet reports the measured turn-on and turn-off energy dissipation per switching pulse as function of the collector current *Ic* for the IGBT. It also reports the recovery energy losses per pulse as function of the diode current I_d. These energy losses are measured at certain DC-link voltage, applied gate-voltage, gate-resistor and device junction temperature.

Fig.2.11 [12] shows a typical switching losses of the IGBT module at junction temperature T_j equals to 125°C.

Using data from Fig.2.11, and applying to it curve-fitting method by Kaleidagraph™, yield the results of switching losses E_{off}, E_{on} and E_{rec} shown in Fig. 2.12, Fig. 2.13, and Fig. 2.14 respectively. Here a third order or fourth order polynomial is used, and the curve fitting has almost no error on the given data point which is indicated by the correlation coefficient R >0.999. It is instructive to note that each curve should pass through the point of origin (0,0), which is reasonable since zero energy loss is expected when the current through the device is zero. To achieve this, data point (0,0) is included in curve fitting besides the experimental data from Fig. 2.11.

The function that describes the relation between the switching losses and the current can be expressed as:

$$E_{switching} = f(I) = c_0 + c_1 \cdot I^1 + c_2 \cdot I^2 + c_3 \cdot I^3 + c_4 \cdot I^4 \tag{2.8}$$

The units of *I* is Kilo*Ampere*.

The polynomial coefficients for the switching energy losses are listed in Table 2.1.

The lack of experiment data that relate switching losses to the DC voltage forced us to use a scaling factor to get the energy losses at different V_{DC} values. For example, if the energy model is build using curve-fitting result at V_{DC}=900 *Volts*, energy losses at different voltages can be calculated by the following equation:

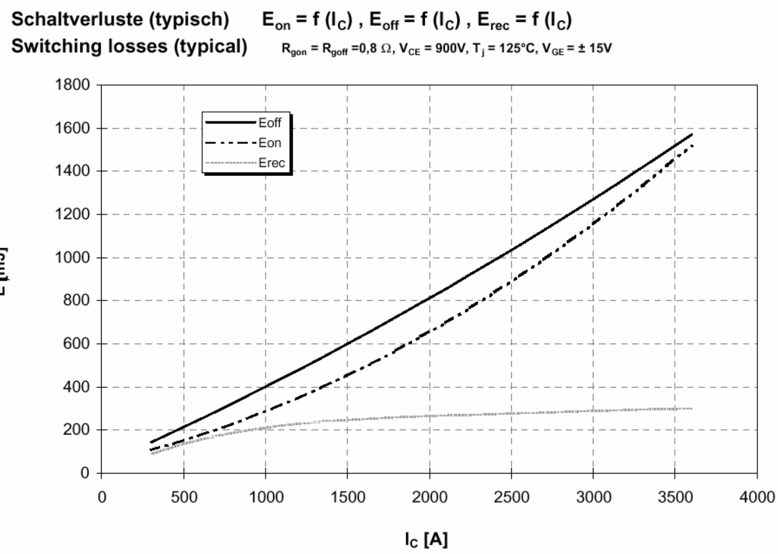

Figure 2.11 Switching losses curve of the IGBT module.

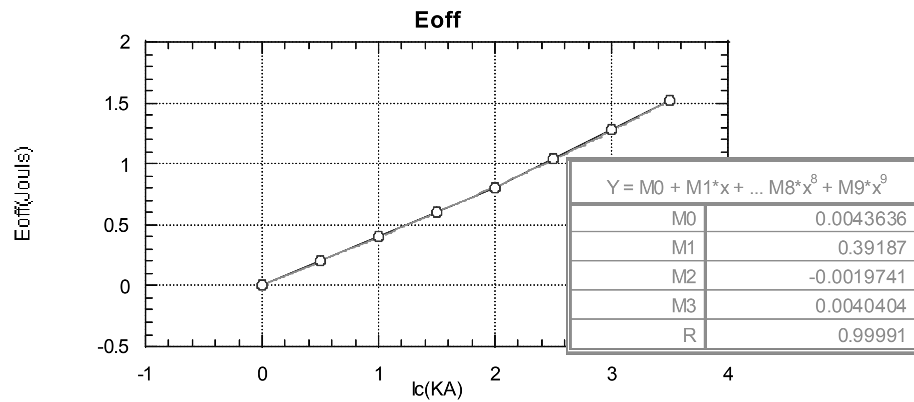

Figure 2.12 Polynomial curve-fitting result for turn-off losses of IGBT: *Eoff*.

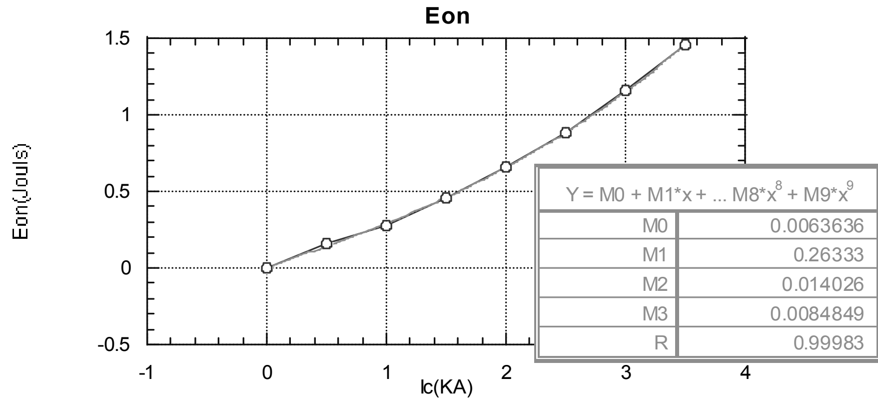

Figure 2.13 Polynomial curve-fitting result for turn-on losses of IGBT: *Eon*.

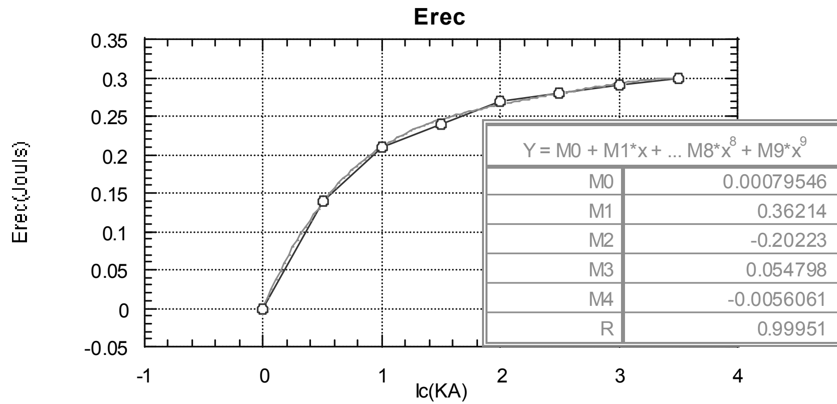

Figure 2.14 Polynomial curve-fitting result for recovery losses of diode: *Erec*.

$$Energyloss\,es_{V_{DC}} = Energyloss\,es_{V_{DC}=900Volts} \times \frac{V_{DC}}{900} \times \alpha \tag{2.9}$$

Here α is an adjusting factor which can be calculated by simulation switching losses at different DC link voltages or from the data sheet of the manufacturer.

2.6.3 Conduction Power Losses Of IGBT And Diode

First, we want to express the conduction losses as a function of I_c or I_d and get rid of the dependence on voltage V_{CE} and V_d. From the DC characteristic of the IGBT module shown in Fig.2.15 [12], we used curve-fitting method as shown in Fig.2.16 to find the relation of *Vce* and *Ic* to be:

At junction temperature T_j=125°C with gate voltage V_{GE}=15 Volts:

$$V_{CE}(I_c) = -0.079117 \cdot I_c^{\;4} + 0.64764 \cdot I_c^{\;3} - 1.8444 \cdot I_c^{\;2} + 3.012 \cdot I_c + 0.67889 \tag{2.10}$$

when $V_{CE} > 0.6$ volts.
The unit of V_{CE} is *Volt*, while the unit of I_c is Kilo*Ampere*.

From the DC characteristic of the diode for the IGBT module shown in Fig.2.17 [12], we used curve-fitting method as shown in Fig.2.18 to find the relation of V_d and I_d to be:

At junction temperature T_j=125°C with gate voltage *Vge*=15 Volts:

$$V_d(I_d) = -0.05714 \cdot I_d^{\;4} + 0.48705 \cdot I_d^{\;3} - 1.4569 \cdot I_d^{\;2} + 2.213 \cdot I_d + 0.41936 \tag{2.11}$$

when $V_d > 0.5$ *volts*.
The unit of V_d is *Volt*, while the unit of I_d is Kilo*Ampere*.

Table 2.1 Coefficients in Equations (2.8) for Switching Losses

$E_{switching(Joules)}$	c_0	c_1	c_2	c_3	c_4
E_{on}	0.0063636	0.26333	0.014026	0.0084849	0
E_{off}	0.0043636	0.39187	-0.0019741	0.0040404	0
E_{rec}	0.00079546	0.36214	-0.20223	0.054798	-0.0056061

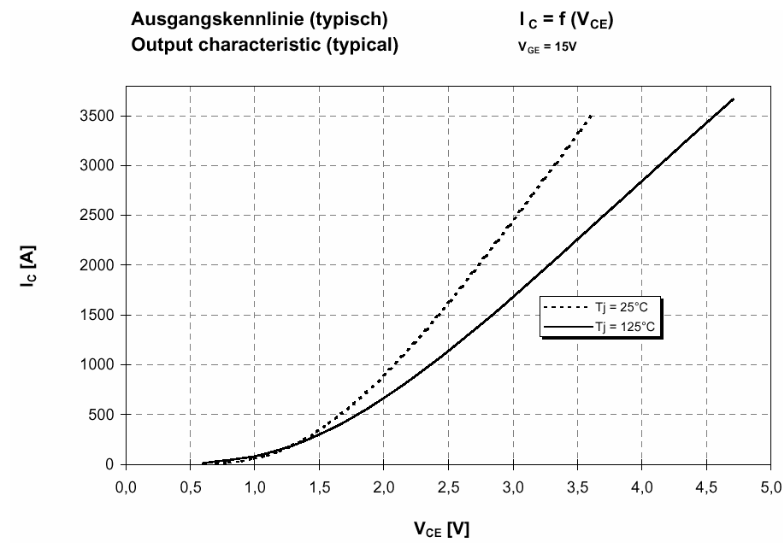

Figure 2.15 DC characteristics of IGBT: I_c=$f(V_{CE})$.

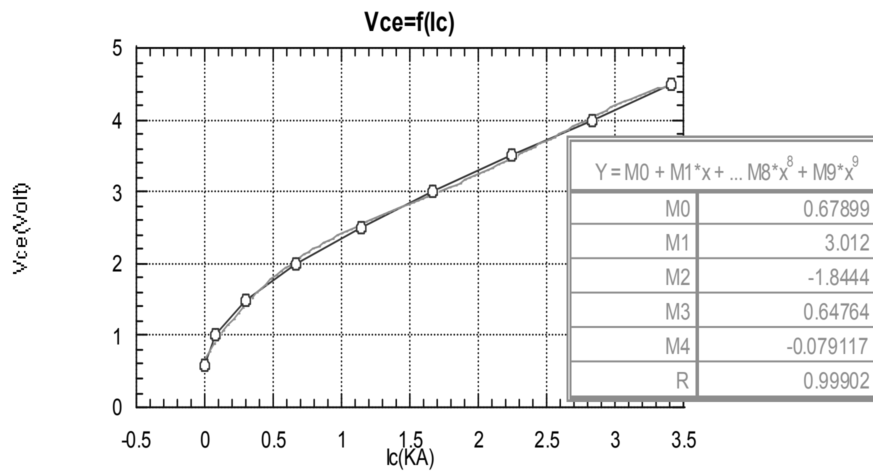

Figure 2.16 Polynomial curve-fitting of DC characteristics of IGBT: $V_{CE}=f(I_c)$ at Tj=125°C.

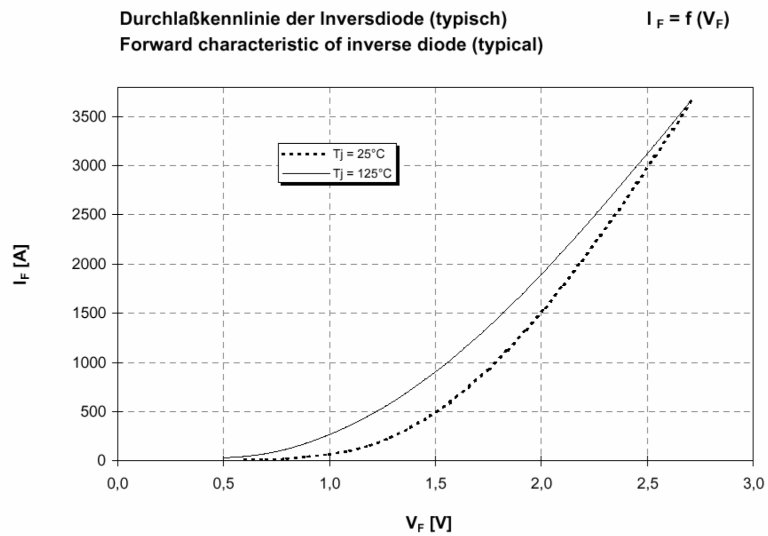

Figure 2.17 DC characteristics of diode: $I_d=f(V_d)$.

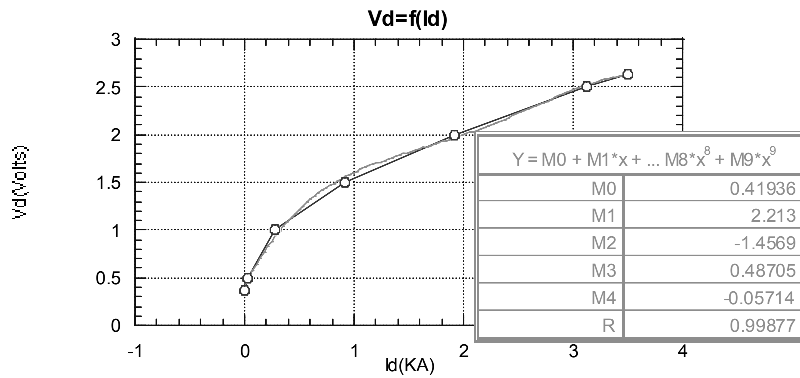

Figure 2.18 Polynomial curve-fitting of DC characteristics of diode: $V_d=f(I_d)$ at Tj=125°C.

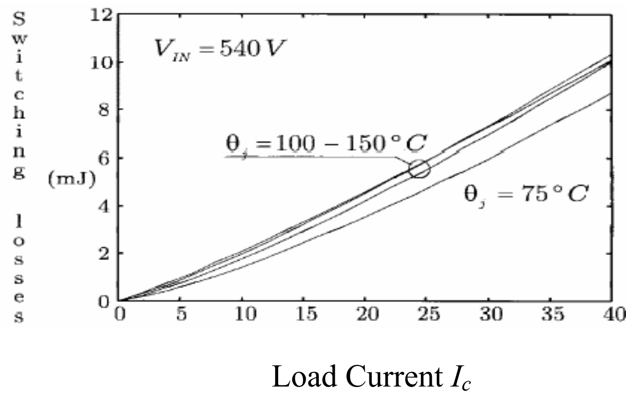

Load Current I_c

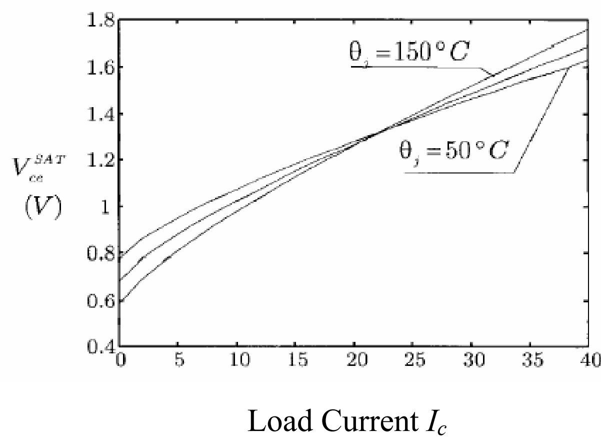

Load Current I_c

Figure 2.19 Values of V_{CE} and $E_{total}=E_{on}+E_{off}$ vs load current and junction temperature [40].

2.7 Discussion

As mentioned in Chapter 1, there is thermal coupling between the electronics and thermal behavior. The dynamic junction temperature is determined by iteration. But our analytical solution of the power losses neglects the temperature dependence and all the equations is built under condition of T_j=125°C, and we'll use the calculated power losses at this temperature in the thermal model to calculate the junction temperature. So there is no iteration involved.

The direct reason that not including the temperature dependency of the power losses on the temperature is that the performance of the IGBT module at temperature other than 125°C such as room temperature is not available from the manufacturer. Because the IGBT module most of the time works at temperature much higher than the room temperature, such as 80°C to 90°C, so this approximation is not bad. For example, for the IGBT module manufactured by ABB, at a certain DC link voltage and current, the average difference between the switching losses at 125°C and room temperature is less than 10 %. So we can expect much less than 10% error for our approximation. This approximation can also be supported by the observation in reference [40] that the switching energy losses have mildly temperature dependency as shown in Fig. [2.19] (a). Moreover, for V_{CE} shows a mild dependency on temperature too as shown in Fig. [2.19] (b), so the conduction losses dependency on the temperature is also mild.

Because the switching losses increases with the temperature, so the power losses we calculated based on 125°C performance is an overestimation, and so does the temperature from the thermal analysis which use the power losses value as input.

3.0 THERMAL MODEL OF IGBT MODULE

3.1 Introduction

Beside measurement, the junction temperatures of IGBT and free wheeling diode in power conversion systems can be estimated numerically by building thermal analysis models of the system.

In Chapter 2, the power dissipated in IGBT modules used in three-phase inverters was analyzed. This power is used in this chapter as the stimulus current source in a thermal model built to calculate the junction temperature of operational IGBTs and free wheeling diode. The thermal model will be incorporated in an on-line or real time simulator. Hence the model should be simple to implement and fast to execute in the software platform. In addition, the parameters of the thermal model should be extracted from the available experimental data. For these reasons, we choose the thermal RC network model to describe the thermal behavior of IGBT modules.

A review of different approaches used in the literature to perform thermal analysis is given. These include analytical, numerical and behavioral models. The thermal RC network approach is then selected for special investigation. The actual thermal RC networks for the IGBT and diode from the experimental transient thermal impedance curves available are then derived.

3.2 Thermal Analysis Of IGBT Module And Previous Work

Heat can transfer from one material to another through one of the three mechanisms: conduction, convection or radiation [41]. Conduction occurs when two materials physically touch each other, convection happens when the material is surrounded by gas or fluid, and radiation implies that heat is lost from surface by radiating infrared light. In practical applications, the IGBT modules are cooled by mounting them on a heatsink and natural air-cooling or forced air-cooling method is used. There is conduction between different layers of

materials, the heat generated inside the IGBT module can also get into the air by convection (airing cooling) or radiate into the air directly.

Analytical methods have long been used in thermal analysis to predict the operating temperatures of semiconductor devices. The methods provide us with better physical insight through the use of meaningful parameters. Various assumptions for the boundary and initial conditions are made in order to solve the heat conduction equation. By assuming that the semiconductor chip is a semi-infinite solid with uniform initial temperature and that the flux of heat at the top surface is a prescribed function of time, the surface temperature is solved [42]. A correction to the solution is derived [43] by removing the previous assumptions when the thickness of the silicon is assumed infinite and the heat source is considered an infinite thin layer at the surface. Using the equation derived for pulse widths shorter than the thermal transit time (in the order of 300 μs), the peak temperature can be more accurately calculated. An analytical 3-D transient temperature solution of a two-layer semi-finite plane structure with embedded heat source is derived [44]. In the model, the first layer which represents the semiconductor chip has finite thickness while the second layer which accounts for the package has infinite thickness. For a practical device which has a finite thickness package, the method of images is utilized to approximate the temperature calculation. The method can be extended to solve the 3-D temperature distribution for structures consisting of more than two layers. The superposition principle is applied to obtain the thermal response if a structure has multiple heat sources. A 3-D thermal model based on the two-port network theory for hybrid or monolithic integrated power circuit is presented by Dorkel et al [45]. The power dissipation is assumed flat (infinite small of the thickness of heat source) and can take any shape (multiple heat sources can therefore be modeled). The power module is treated as a multilayered rectangular parallel structure. The lateral bounding planes are adiabatic. Fast Fourier transform algorithms are used to calculate the temperature distribution in an IGBT module with FWD in transient and steady states and the results are confirmed by experiment. The analytical solution is usually mathematically complex and not suitable to implement in the real time simulator.

Numerical methods are another choice for thermal analysis. Finite element method (FEM), or finite difference method (FDM) are used to discretize the differential equation for heat

conduction. Computational fluid dynamic (CFD) is used to solve the equations governing the conservation of mass, momentum and energy. Finite element method (FEM) is used by Shammas et al [46] to model the thermal fatigue effects in the IGBT module. The output of numerical the model can be thermal resistance, heat flux distribution (information on the heat path inside the device) through different layers and the maximum die temperature. Temperature excursion can be estimated from dynamic analysis. FDM is used by Hefner [25] to discretize the thermal conduction equation and a dynamic electro-thermal model of IGBT is derived. Lee [18] analyzes the fluid and heat transfer inside an IGBT module with integrated liquid-cooling method by using CFD technique.

RC ladder networks are more popular to use for thermal analysis. They are easy to integrate into existing circuit simulator making the latter capable of it simulating both electrical and thermal characteristics of circuits. The RC thermal model is flexible and can be used to describe 1-D [25], 2-D [11], or 3-D [47] problems. It can be build through the discretization of the thermal conduction equation by either using finite difference or finite element method. The accuracy of the two approaches is analyzed and compared in reference [21]. Hefner [25] uses the finite difference method to build the thermal RC network for the IGBT module by including thermal nonlinearity. Tzer et al [48] follow a parallel approach while using finite element method. The same method is used by Ammous et al [11] to build a thermal model for analyzing IGBT module under short circuit condition. RC networks are also used to analyze multichip power package such as a power Hbridge module [49]. The RC thermal model can be also build by behavioral approach. In such case, the elements of the network are extracted from the thermal dynamic curve [24]. Building equivalent thermal RC model is our choice in real time simulator for its easy implementation and short calculation time.

3.3 Thermal RC Network

For electronic components, usually the heat conduction dominates the heat transfer process, and convection and radiation are assumed negligible [21]. In a homogeneous isotropic material, the conduction is described as:

$$\nabla \cdot \left(\kappa\left(\nabla T\right)\right) = \rho c \frac{\partial T}{\partial t} \tag{3.1}$$

where κ is the thermal conductivity, ρ is the mass density, c is the specific heat. T is the temperature.

IGBT as a vertical power device, the thickness L is smaller than other dimensions. A one-dimensional conduction process is therefore assumed [8]. The thermal characteristics of silicon chip (such as the conductivity) is also assumed independent of temperature. The above two assumptions simplify Equation (3.1) into:

$$\kappa \frac{\partial^2 T}{\partial x^2} = \rho c \frac{\partial T}{\partial t} \tag{3.2}$$

where x denotes the coordinate in the direction of heat propagation.

The RC network description of thermal property of a device is based on the similarity between Equation (3.2) and the differential equation of a transmission line namely [50]:

$$\frac{\partial^2 V}{\partial x^2} = C' R' \frac{\partial V}{\partial t} \tag{3.3}$$

where C' is the capacitance per unit length, R' is the resistance per unit length of the line.

Since a transmission line can be described by a RC ladder network, it follows that the thermal properties of a device can also be described by a ladder network. Based on Equation (3.2) and Equation (3.3), the analogy between the thermal and electrical variables is listed in Table 3.1[51].

For a power transistor such as an IGBT, we can use a transmission line equivalent circuit as shown in Fig.3.1 to describe the heat conduction path from the silicon chip to the heatsink. The power dissipated by an IGBT (or a diode) acts as a stimulus current source in the thermal circuit.

The “R” s and “C”s in the circuit shown in Fig.3.1 are the thermal resistors and thermal capacitors per unit length. Fig.3.1 is a distributed RC model while the number of the RC ladders can be infinite. Practically, a finite number will suffice to model the module, we can therefore combine the single elementary volume element and get the equivalent lumped elements with finite number RC ladders.

The parameters value of the lumped thermal RC network are found by segment of the device into substructures as shown in Fig.3.2. Each substructure will correspond to a different layer of material in the IGBT module. The following equations are then used to estimate the thermal resistors and capacitors’ of each layer (substructure):

$$R_{th} = \frac{d}{A \cdot \kappa} \qquad C_{th} = c \cdot \rho \cdot d \cdot A \tag{3.4}$$

where d is the length along the heat conduction direction, A is the area perpendicular to the heat conduction direction as shown in Fig. 3.3.

An alternative approach to determine the values of the various “R”s and “C”s would be to extract their values from the dynamic thermal impedance curve available from experiment [24] or from simulation by FEM [52].

3.4 Transient Thermal Impedance Curve (TTIC) From Junction-To-Case

Usually the manufacturer of power semiconductor devices will provide the user with the transient thermal impedance curve. In order to understand the definition, derivation, assumption and application of the curve, the measurement process is introduced.

By using environment thermal control system [53], set the temperature of the power module’s case, T_c, to a fixed value (such as the ambient temperature). Apply a single square power pulse with amplitude P to the module until the junction temperature reaches its steady

state at time t_{ss}. Measure the module junction temperature variation with time $T_j(t)$ by way of thermal imaging or using temperature-sensitive electrical parameter as thermometer.

The transient thermal impedance is defined at time t as:

$$Z_{jc} = \frac{T_j(t) - T_c(t)}{P} = \frac{\Delta T_{jc}}{P} \tag{3.5}$$

From a circuit point of view, the transient thermal impedance curve is a step response curve with zero-initial conditions. It is well known that the step response of a linear system contains the full description of the system. This process is described in Fig. 3.4 in which the fixed case temperature is represented by a constant voltage source.

Before extracting of the thermal RC network's parameters, the curve-fitting method is applied to the experimental transient thermal impedance data which resulting in a finite series of exponential terms that are provided by the manufacturer:

$$Z_{jc}(t) = \sum_{i=1}^{n} \gamma_i \cdot \left(1 - \exp\left(-\, {t}/{\tau_i}\right)\right) \tag{3.6}$$

The transfer function (input impedance) of the thermal RC network is found by applying Laplace Transform to equation (3.6):

$$Z_{jc}(s) = \sum_{i=1}^{n} \frac{{\gamma_i}/{\tau_i}}{s + {1}/{\tau_i}} \tag{3.7}$$

In order to derive the thermal RC network parameters' value, we need to transfer Equation (3.7) in the following form:

Table 3.1 Thermal –electrical Analogous Quantities

	Thermal	Electrical
Through Variable	Heat transfer rate, q, watts	Current, i, amps
Across Variable	Temperature, T, K or C, degC/watt	Volatge, v, volts
Dissipation Element	Thermal resistance, $R_{th,}$ degC/watt	Elect. Resistance, R, ohms
Storage Element	Thermal capacitance, $C_{th,}$ joules/degC	Elect. Capacitance, C, farads

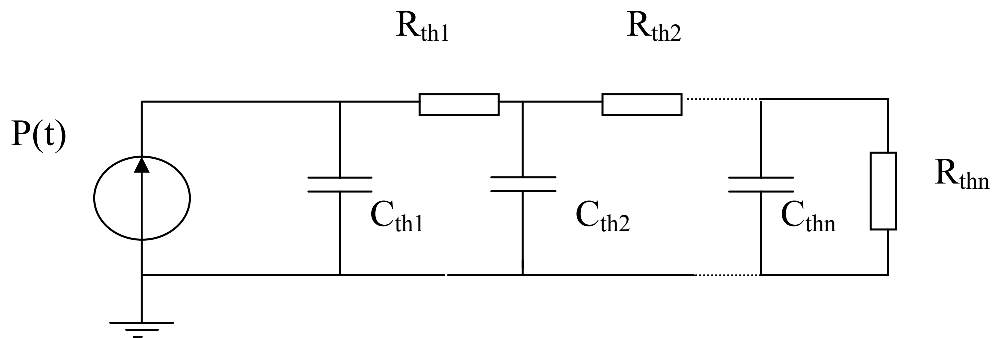

Figure 3.1 Transmission line equivalent circuit diagram.

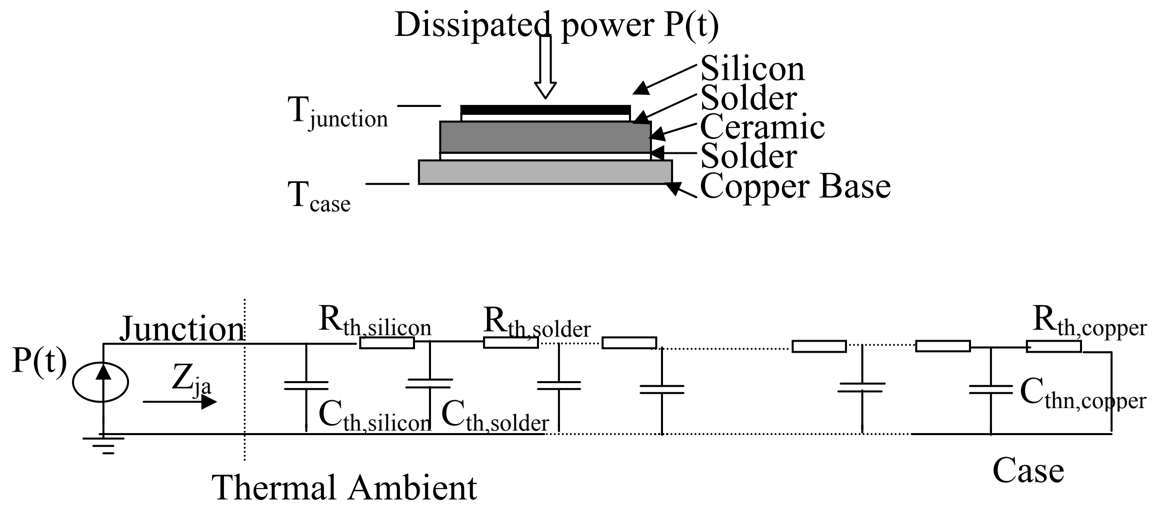

Figure 3.2 Thermal RC network based on the physical structure of power module.

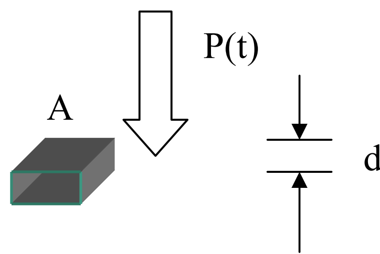

Figure 3.3 Simple structure for illustration of Equation (3.4).

$$Z_{jc}(s) = \cfrac{1}{sC_{th1} + \cfrac{1}{R_{th2} + \cfrac{1}{sC_{th2} + \ldots + \cfrac{1}{R_{thn}}}}}$$

(3.8)

This can be achieved by using a continuous-fraction expansion (denominator divided by numerator continuously) as carried out in a program written in **Matlab**.

Usually four or five exponential terms are enough to curve-fit $Z_{thjc}(t)$ with desired accuracy for the intended applications. The number of exponential terms will determine the number of RC rings in the thermal RC network.

3.5 Thermal RC Model Of IGBT Module From Junction To Case

Usually the IGBT module' manufacturer will provide the transient thermal impedance curve of junction to case to the users. By using the method outlined above, the RC model describing the thermal behavior of a power module mounted on an ideal heatsink is derived. It is instructive to mention that only ideal or nearly ideal heatsink can keep the case temperature constant while applying power through the module.

Fig.3.5 [12] shows the transient thermal impedance curve from junction to case for the IGBT module. The solid line is the transient thermal impedance curve of the IGBT while the dotted line is of the free wheeling diode inside one IGBT power module. The exponential terms from the curve-fitting of the transient impedance curve is listed in Table 3.2 [12]. So for the IGBT, the thermal impedance curve is expressed as:

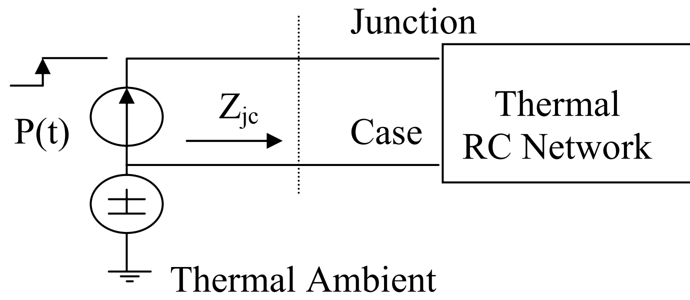

Figure 3.4 Linear system representing the thermal behavior of IGBT from junction to case.

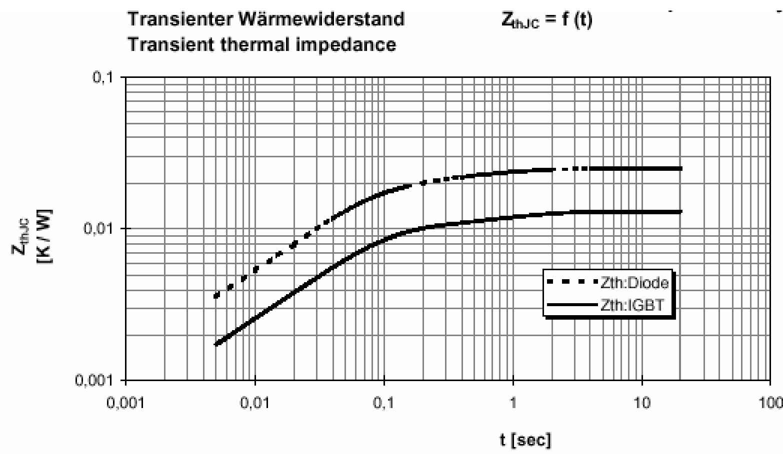

Figure 3.5 Transient thermal impedance curve of IGBT module including the diode.

$$Z_{jc}(t)=\sum_{i=1}^{4}\gamma_i\left(1-\exp\left(-{t}/{\tau_i}\right)\right)=0.001\cdot\left\{\begin{array}{l}1.25\cdot\left[1-\exp\left(-\frac{t}{0.003}\right)\right]\\+6.15\cdot\left[1-\exp\left(-\frac{t}{0.05}\right)\right]\\+2.6\cdot\left[1-\exp\left(-\frac{t}{0.1}\right)\right]\\+3\cdot\left[1-\exp\left(-\frac{t}{0.95}\right)\right]\end{array}\right\} \tag{3.9}$$

According to Equation (3.7), the input impedance of the thermal RC network representing the thermal behavior of IGBT can be written as:

$$Z_{jc}(s)=\sum_{i=1}^{4}\frac{\gamma_i/\tau_i}{s+1/\tau_i}=0.001\cdot\left(\frac{1.25/0.003}{s+1/0.003}+\frac{6.15/0.05}{s+1/0.05}+\frac{2.6/0.1}{s+1/0.1}+\frac{3/0.95}{s+1/0.95}\right) \tag{3.10}$$

Using the "**simplify**" function in **Mathcad**, equation (3.10) reduces to:

$$Z_{jc}(s)=\frac{0.56882\cdot s^3+65.659\cdot s^2+766.16\cdot s+912.28}{s^4+364.39\cdot s^3+10582\cdot s^2+77404\cdot s+70175} \tag{3.11}$$

Expressing Equation (3.11) in the form shown in Equation (3.8) results in:

$$Z_{jc}(s)=\cfrac{1}{s\cdot 1.758+\cfrac{1}{0.0023+\cfrac{1}{s\cdot 5.5872+\cfrac{1}{0.0075+\cfrac{1}{s\cdot 109.1768+\cfrac{1}{0.0012+\cfrac{1}{s\cdot 329.2682+\cfrac{1}{0.002}}}}}}}} \tag{3.12}$$

From Equation (3.12), the RC parameters of the linear RC ladder network which represent the thermal model of IGBT mounted on ideal heatsink is listed in Table 3.3.

The same analysis process is applied to the diode inside the IGBT module to yield the RC parameters' values for the diode as listed in Table 3.4.

3.6 Thermal RC Model Of IGBT Module With Heatsink

The IGBT module is usually mounted on a heatsink in order to keep the device temperature in the safe operation area. User-specific methods of cooling such as natural air, forced air or water cooling are typically used. The thermal behavior of a system is determined by the thermal impedance of the IGBT and diode from junction to case (the data is given by the IGBT module's manufacturer), the thermal impedance of the interface (thermal grease, etc.) between the IGBT and the heatsink in addition to the heatsink thermal behavior (besides conduction, convection and radiation play a more important role than within the IGBT module). Since the heatsink is usually shared by several modules, the geometrical distribution of the modules on the heatsink will influence the thermal behavior of each module. This sounds like a prohibitive complex process to model. If we still assume the system is linear and that one-dimension problem is involved here, we can extend the thermal RC network from junction-to-case to junction-to-ambient. This can be done using the thermal measurement data for the case which is accessible and easy to obtain. From this data together with the thermal impedance data provided by the IGBT module's manufacturer, the RC network parameters can be extracted. With this thermal RC network, we can predict the junction temperature of the IGBT and diode in the three-phase inverter in the real time simulator.

3.6.1 Experimental Data: Thermal Impedance From Case-To-Ambient

When an IGBT module is mounted on an ideal heatsink, the thermal RC network's parameters can be extracted from the transient thermal impedance from junction to case as outlined in Section **3.5**. When the IGBT module is mounted on a non-ideal heatsink which is more realistic to expect, then knowing the transient thermal impedance from junction to ambient can lead to the derivation of the network's parameters that describe the thermal behavior of the module.

Table 3.2 Exponential terms extracted from the transient thermal impedance curve for IGBT and diode.

i	1	2	3	4
r_i [K/kW] : IGBT	1,25	6,15	2,6	3
τ_i [sec] : IGBT	0,003	0,05	0,1	0,95
r_i [K/kW] : Diode	2,46	13,4	4,57	4,57
τ_i [sec] : Diode	0,003	0,045	0,45	0,75

Table 3.3 Parameters of the RC network of IGBT from junction to case.

i	**1**	**2**	**3**	**4**
Thermal R_{thi}(K/Watt)	0.0023	0.0075	0.0012	0.002
Thermal C_{thi}(Watt·Sec/K)	1.758	5.5872	109.1768	329.2682

Table 3.4 Parameters of the RC network of diode from junction to case.

i	**1**	**2**	**3**	**4**
Thermal R_{thi}(K/Watt)	0.0046	0.0128	0.0072	0.005
Thermal C_{thi}(Watt·Sec/K)	0.9	2.8	70.7	1372.8

The IGBT module manufacturers provide only the junction to case thermal impedance of the IGBT and the diode inside a module. For users, the junction temperature is not easy to get. The user cannot therefore get the thermal impedance curve from junction to ambient directly from experiment.

Instead, for the case temperature is easy to measure for the IGBT module user, the experiment similar to the transient thermal impedance measurement of junction to case is carried out for the IGBT module in the three-phase inverter system. In order to understand the meaning of the data, the measurement process is described here.

In a three-phase inverter used to drive motors, six IGBT modules are needed for acceleration and others are used for putting the brake on the motor. These eight modules are mounted on the same heatsink and the forced air cooling method is used. This is shown in Fig. 3.6.

The thermal data collected relate to the last module in the way of the airflow. This module is the hottest of the eight and therefore presents the worst case scenario. If the junction temperature of this module is kept under safe limit, all other modules are safe too.
Four sets of experimental data are collected for the designated last module. The four sets are as follows:

(1) Measuring the case temperature under the IGBT when it is turned ON while the diode is turned OFF. The data is called “IGBT powered”.

(2) Measuring the case temperature under the IGBT when it is turned OFF while the diode is turned ON. The data is called “IGBT unpowered”.

(3) Measuring the case temperature under the diode when it is turned ON while the IGBT is turned OFF. The data is called “Diode powered”.

(4) Measuring the case temperature under the diode when it is turned OFF while the IGBT is turned ON. The data is called “Diode unpowered”.

The circuit used collect the measurements is shown in Fig. 3.7. The 6 modules of the three-phase inverter are connected in series, and the DC current is provided by a current source. A gate control signal greater than the threshold voltage will turn-on the IGBT while its absence will turn-off the modules.

The thermal impedance data is calculated by turning on the six IGBTs. Given that the current through the circuit is I, and assuming that the voltage drop across each module is V, then the power losses of the one module is given by:

$$P = I \cdot V \tag{3.13}$$

After being subjected to this constant power losses P for a time duration t, the case temperature increase above the ambient temperature is measured as T_{ca}. The thermal impedance Z_{ca} at time t is then equal to:

$$Z_{ca}(t) = \frac{T_{ca}(t)}{P} \tag{3.14}$$

The case temperature is measured every 1 second until it reaches its steady state. Similar ways are used to get data for sets (2), (3) and (4).

3.6.2 Extension Of The Thermal RC Network

Based on the four sets of experimental data collected, we can extent the thermal RC network that appears in Section **3.5** to include the heatsink, the interface between the device and the heatsink, and the cooling effect in a real system. The thermal coupling between the IGBT and diode will be modeled using the superposition principle. This resulting model will be able to predict the junction temperature of IGBT and diode inside the module, and the case temperature of the package in a three-phase inverter application.

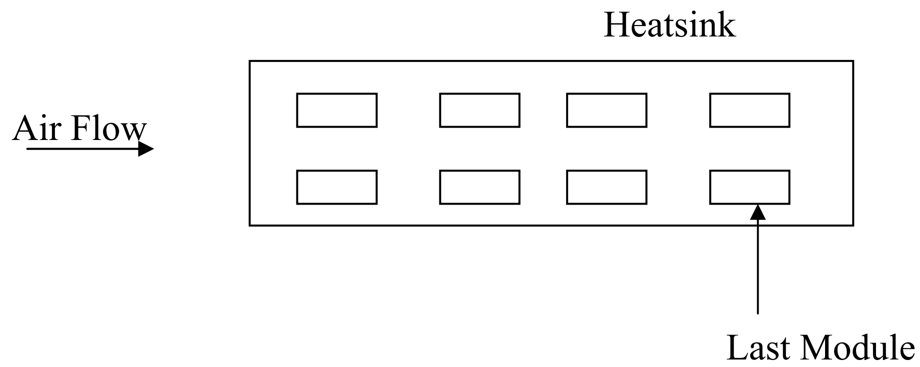

Figure 3.6 Geometry of the IGBT module on the heatsink in three-phase inverter.

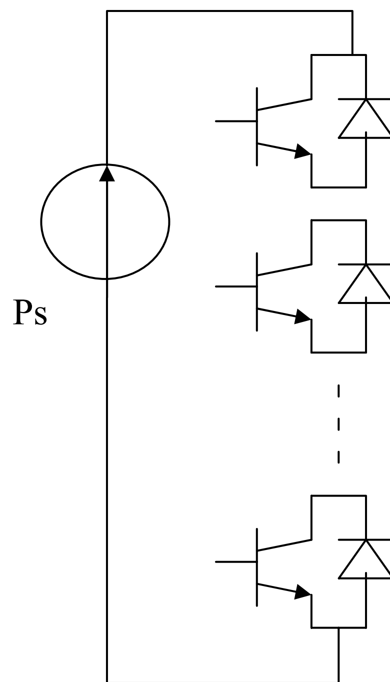

Figure 3.7 Circuit used to get thermal data of the case.

Before extending the RC network, we need to understand the meaning of the experiment data from a circuit point of view. The equivalent transmission line circuit shown in Fig. 3.1 can be correlated to the real IGBT (diode) structure with each node assigned to a structure element (different layers of material). The IGBT (or the diode) from its junction to the case can be represented by a 4-ring RC network. The heatsink connected to the IGBT module can be simulated by a second RC network. The two networks are connected at the node called "case" as shown in Fig.3.8. Strictly speaking, the experimental data obtained from Equation (3.14) is not the impedance of the RC network from case to ambient, since the current source P representing the power losses is applied to the junction and not to the case. The real thermal impedance from case to ambient should be calculated by using P_1 which unfortunately we do not know. We need to find a way to solve this dilemma.

Assume that we apply the current source P to the junction, the junction temperature above the ambient is T_{ja} and is given by:

$$T_{ja}(t) = T_{jc}(t) + T_{ca}(t) \tag{3.15}$$

The transient thermal impedance from junction to ambient is defined as:

$$Z_{ja}(t) = \frac{T_{ja}(t)}{P} \tag{3.16}$$

Combing Equation (3.15) and (3.16)

$$Z_{ja}(t) = \frac{T_{jc}(t)}{P} + \frac{T_{ca}(t)}{P} = Z_{jc}(t) + Z_{ca}(t) \tag{3.17}$$

The first term $Z_{jc}(t)$ in the right-hand-side of Equation (3.17) is the thermal impedance from junction to case which we get from the manufacturer, and the second term $Z_{ca}(t)$ can be calculated through Equation (3.14) using the data collected from the experimental data.

From Equation (3.9), we know that $Z_{jc}(t)$ can be expressed as the sum of four exponential terms. Similarly we can curve-fit the experimental data $Z_{ca}(t)$ as the sum of exponential terms . The resulting $Z_{ja}(t)$ will therefore be expressed in a series containing exponential terms. From the methods introduced before, we can derive the thermal RC network which describes the thermal behavior from junction to ambient of IGBT and diode.

3.6.3 Thermal Model Of IGBT Module On Heatsink

The first set of data referred as " **IGBT powered**" is shown in Fig. 3.9. The dots refer to the experimental data, and the solid line is the curve-fitting that resulting from **Matlab**.

The transient thermal impedance from case-to-ambient for the IGBT can be expressed as the sum of two exponential terms:

$$Z_{ca}(t) = \sum \gamma_i \left(1 - \exp\left(-\frac{t}{\tau_i}\right)\right) = 0.001 \cdot \begin{Bmatrix} 12.3 \cdot [1 - \exp(-t/5.4782)] \\ +27 \cdot [1 - \exp(-t/80.4812)] \end{Bmatrix} \tag{3.18}$$

Combing Equation (3.9), (3.16) and Equation (3.18) yields:

$$Z_{ja}(t) = \sum \gamma_i \left(1 - \exp\left(-\frac{t}{\tau_i}\right)\right) = 0.001 \cdot \begin{Bmatrix} 1.25 \cdot \left[1 - \exp\left(-\frac{t}{0.03}\right)\right] \\ +6.15 \cdot \left[1 - \exp\left(-\frac{t}{0.05}\right)\right] \\ +2.6 \cdot \left[1 - \exp\left(-\frac{t}{0.1}\right)\right] \\ +3 \cdot \left[1 - \exp\left(-\frac{t}{0.95}\right)\right] \\ +12.3 \cdot \left[1 - \exp\left(-\frac{t}{5.4782}\right)\right] \\ +27 \cdot \left[1 - \exp\left(-\frac{t}{80.4812}\right)\right] \end{Bmatrix} \tag{3.19}$$

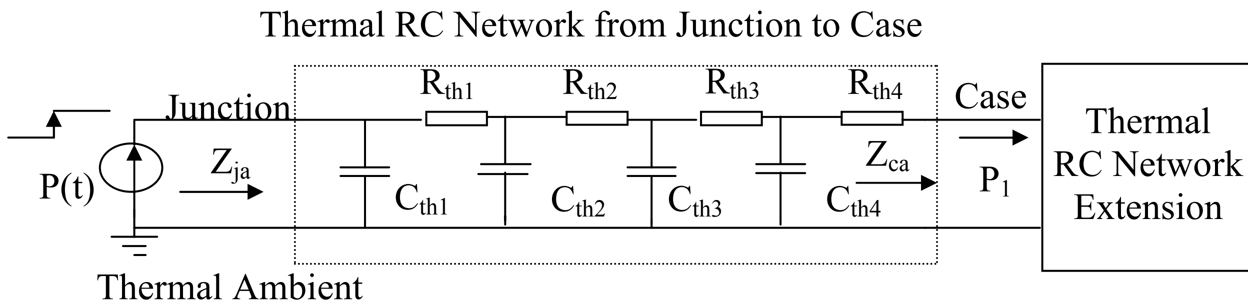

Figure 3.8 Thermal RC network with extension to include heatsink.

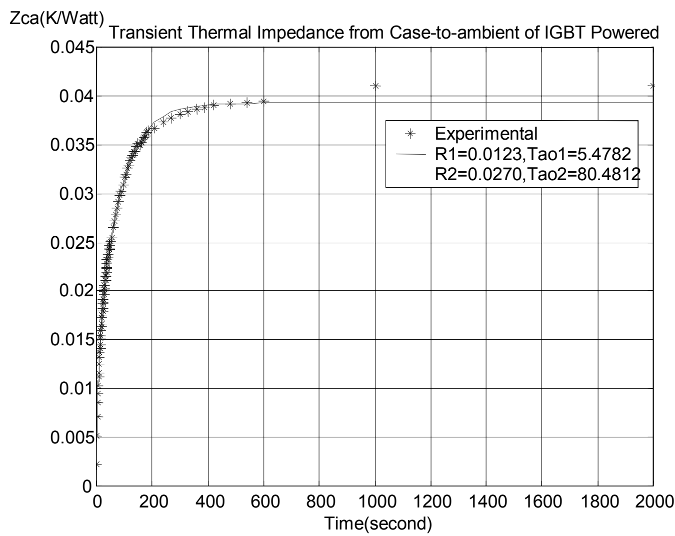

Figure 3.9 Transient thermal impedance from case-to-ambient of IGBT.

Using Laplace transform to Equation (3.19), one obtains:

$$Z_{ja}(s) = \sum_{i=1}^{6} \frac{\gamma_i / \tau_i}{s + 1/\tau_i}$$

$$= 0.001 \cdot \left(\frac{1.25/0.003}{s + 1/0.003} + \frac{6.15/0.05}{s + 1/0.05} + \frac{2.6/0.1}{s + 1/0.1} + \frac{3/0.95}{s + 1/0.95} + \frac{12.3/5.4782}{s + 1/5.4782} \frac{27/80.4812}{s + 1/80.4812} \right)$$

$$= \frac{0.57141 \cdot s^5 + 66.712 \cdot s^4 + 806.3 \cdot s^3 + 1262.5 \cdot s^2 + 367.62 \cdot s + 8.3245}{s^6 + 364.58 \cdot s^5 + 10653 \cdot s^4 + 79467 \cdot s^3 + 85287 \cdot s^2 + 13857 \cdot s + 159.16}$$

(3.20)

Equation (3.20) is used to derive a 6-ladder RC network which represents the thermal model of IGBT on the heatsink as shown in Fig. 3.10. The RC parameters of the circuits are listed in Table 3.5.

We need to locate the node that represents the case in the RC network in order to find the case temperature. The simplest way is to make the static value of the thermal resistance from junction-to-case found from Fig.3.4 equal to the sum of r_i in Table 3.2. For R_{th1}+ R_{th2} +R_{th3}=0.012°C/Watts is almost equal to Z_{jc}=0.013°C/Watts, so we can locate the case position after R_{th3} as shown in Fig. 3.10.

3.6.4 Thermal Coupling

Since the IGBT and diode inside each module share the same case, they will be coupled thermally. This means that when the IGBT is powered, the case temperature will rise, and it will affect the junction temperature of the diode and vice-versa. The model for predicting the junction temperature of the IGBT and diode will not be accurate if this coupling effect is ignored.

If the heat transfer process is dominated by conduction, then the linear superposition rules apply: namely when the system has multiple independent heat sources operating simultaneously, the temperature fields and heat fluxes will be the linear add-up of the solution of each heat source when it operates alone [54]. This is shown in Fig. 3.11.

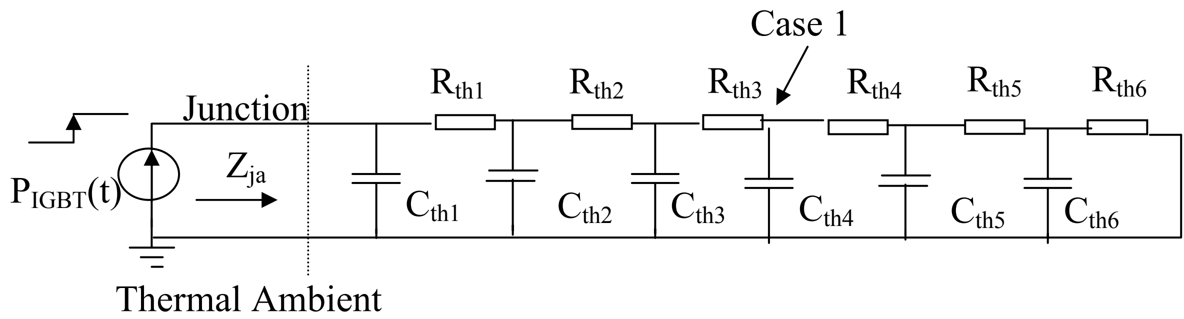

Figure 3.10 RC network representing the thermal behavior of IGBT with heatsink.

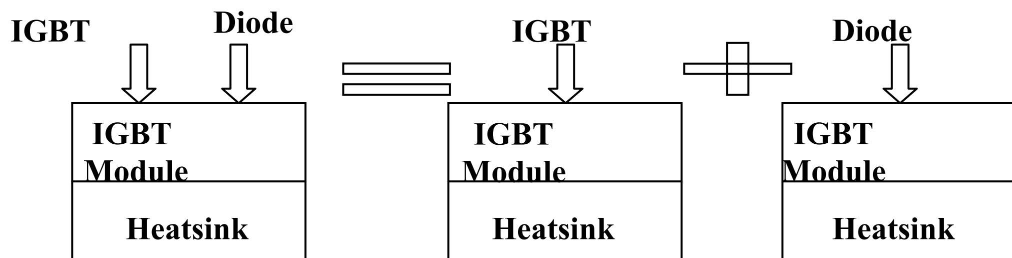

Figure 3.11 The principle of superposition applied to the IGBT module.

When the IGBT considered as heat source one is powered, the junction and case temperatures of the IGBT are calculated using Fig. 3.10, in which the current source value represents the power losses in the IGBT.

We still need to calculate the junction and case temperatures of the IGBT and the diode considered as heat source two is powered. From the second set of experimental data known as "IGBT unpowered", and using curve-fitting technique as shown in Fig. 3.12, we can extract the RC circuit of Fig.3.13. This circuit estimates the case temperature T_{case2} which has to be added to the results obtained from Fig.3.10 to account for thermal coupling. This is shown in Equation (3.21). The reason that adding T_{case2} to both junction and case temperature is: from the circuit point of view, when the current source which represents heat source power losses one as shown in Fig.3.10 is zero, the rise in junction temperature is the same as the rise in case temperature due to thermal coupling which is T_{case2}.

$$\begin{aligned} T_j &= T_{junction} + T_{case2} \\ T_c &= T_{case1} + T_{case2} \end{aligned} \qquad (3.21)$$

3.7 Thermal Model For The Diode

Based on the transient thermal impedance data from junction to case for diode as shown in Table 3.2, and the experimental data from case to ambient known as "Diode Powered" as shown in Fig. 3.14, follow the same process as shown above for IGBT, the RC thermal network which represents the thermal behavior of diode inside the module with heatsink is shown in Fig.3.15.

The parameters of the circuit are listed in Table 3.6.

In order to locate the node which represents the case, we need to divide R_{th3} into two resistors: $R_{th3}=R_{th31}+R_{th32}$ while $R_{th1}+R_{th2}+R_{th31}=0.025$ °C/Watts as shown in Fig. 3.15. Here $R_{th31}=0.0066$°C/Watts, $R_{th32}=10.2$ °C/Watts.

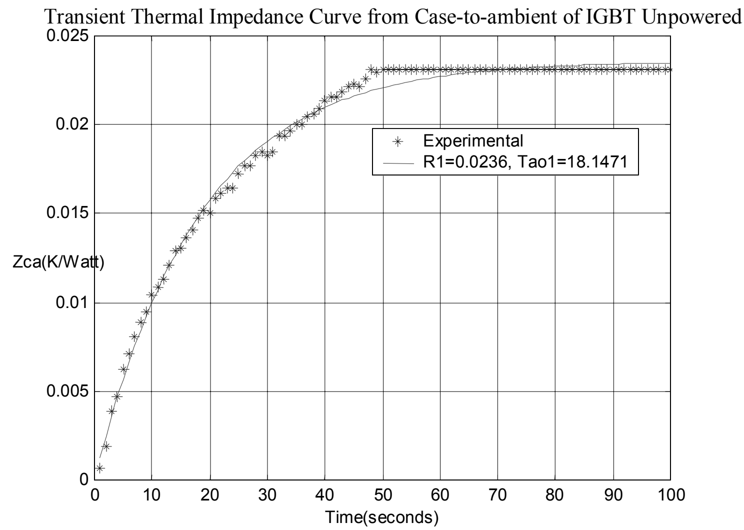

Figure 3.12 Transient thermal impedance from case-to ambient of IGBT unpowered.

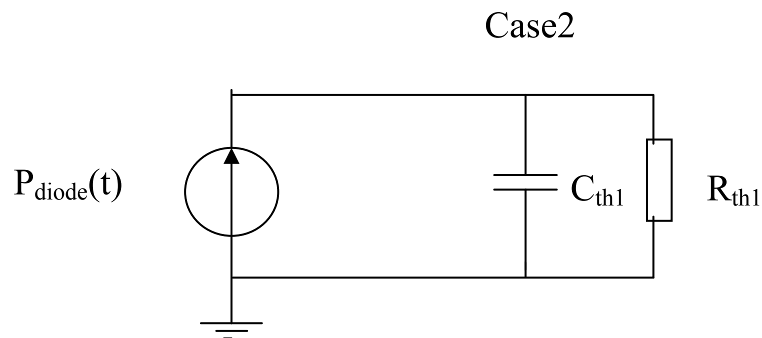

Figure 3.13 RC circuit representing the thermal coupling effect of diode on the IGBT.

With C_{th1}=Tao1/R1=18.1471/0.0236=768.948 Watt·sec/K.

The circuit describes the thermal coupling effect of IGBT on the diode is shown in Fig. 3.16. The parameters are extracted from experimental data of set (4) known as “Diode unpowered” as shown in Fig. 3.17. Equation (3.21) can still be used for the calculation of junction and case temperature of diode includes thermal coupling effect.

3.8 Summary And Discussion

Until now, we found the thermal RC network to describe the thermal behavior of the IGBT module with heatsink in real application.

RC thermal model is easy to implement and takes short execution time in the real time simulator which makes it our chioce. But there is limitation of the RC thermal model. The system is assumped linear while actually when the module is mounted on the heatsink, convection and radiation plays important roles and this makes the system not linear any more. This introduces error.

For the transient thermal impedance curve data started at 1 milliseconds as shown in Fig.3.4, therefore the thermal RC model extracted from this data is more valuable to predict the junction temperature in a long thermal run than in a transient.

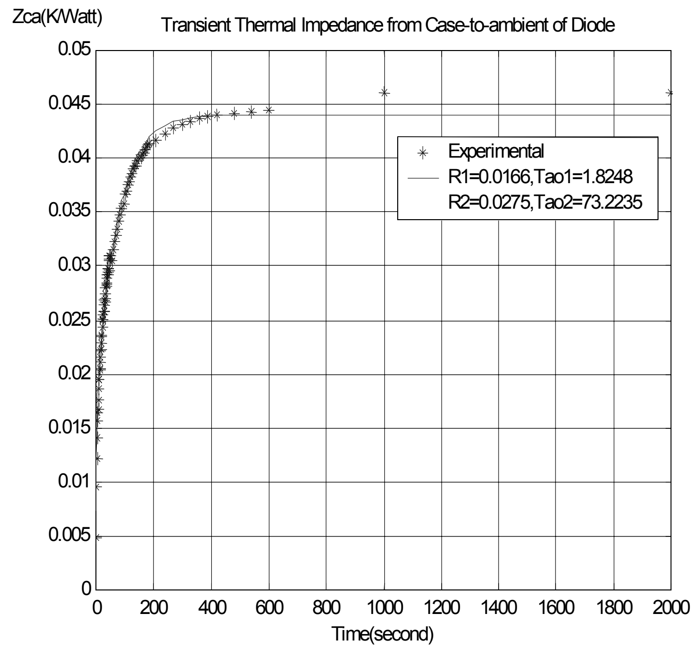

Figure 3.14 Transient thermal impedance from case-to-ambient of IGBT.

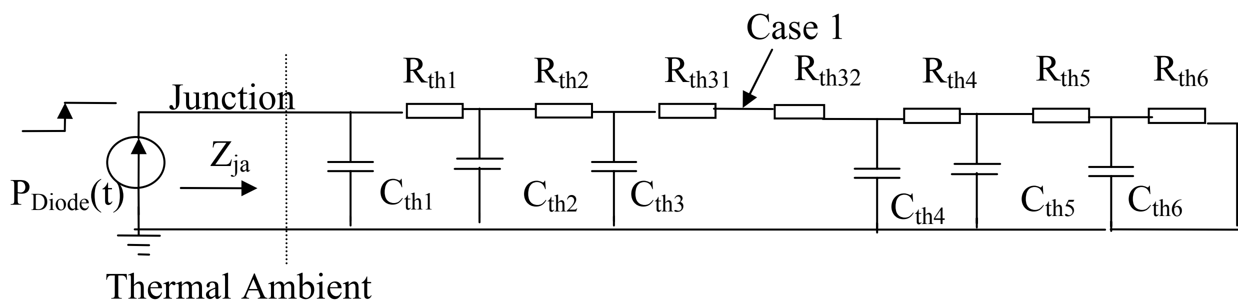

Figure 3.15 RC network for the thermal behavior of diode inside the module with heatsink.

Table 3.5 Parameters of the RC network of IGBT from junction to ambient.

i	1	2	3	4	5	6
Thermal R_{thi}(K/Watt)	0.0023	0.0078	0.0019	0.0076	0.0102	0.0225
Thermal C_{thi}(Watt·Sec/K)	1.8	5.5	82.7	123	363.2	2955.5

Table 3.6 Parameters of the RC network of diode from junction to ambient.

i	1	2	3	4	5	6
Thermal R_{thi}(K/Watt)	0.0047	0.0137	0.0168	0.0071	0.0018	0.0251
Thermal C_{thi}(Watt·Sec/K)	0.9	2.6	41	142.9	645.4	2066.1

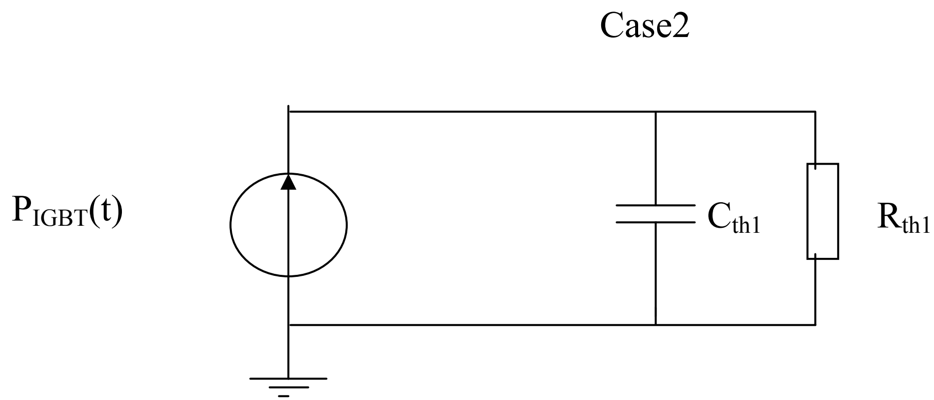

Figure 3.16 RC circuit representing the thermal coupling effect of IGBT on the diode.

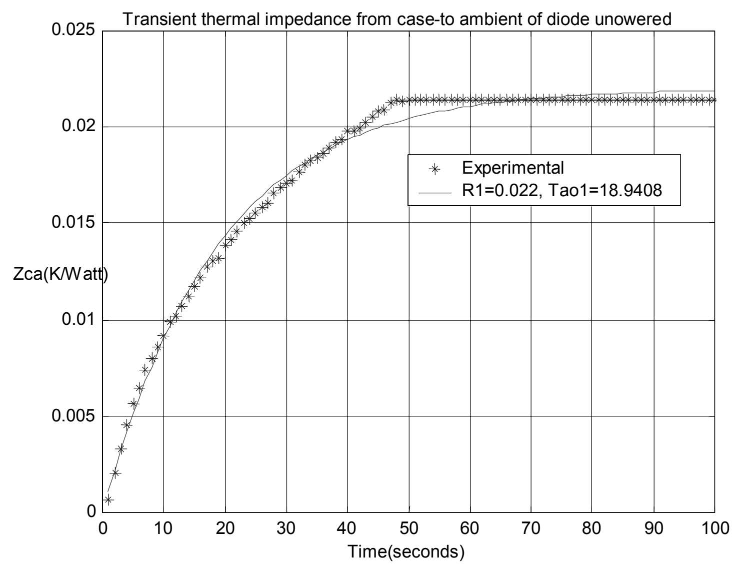

Figure 3.17 Transient thermal impedance from case-to ambient of diode unpowered.

4.0 MODEL IMPLEMENTATION IN REAL TIME SIMULATOR

4.1 Introduction

The electro/thermal model developed in Chapter 2 and 3 is implemented in a real time simulator of a rail vehicle control system. The three-phase inverter is used to provide driving force for the AC motor of the vehicle. The aim is to simulate the power losses profiles in the IGBTs and diodes and to determine in real time the junction temperature variation when the motor accelerates, in steady state and when it decelerates. This information will give a clear picture of the electrical and mechanical stresses suffered by the IGBT module and will help the designer to choose the right rating for the IGBT modules and heatsink of the three-phase inverter system.

The real time simulator requires the model to be built by **Simulink.** Hence the need to find the appropriate implementation of the power losses and thermal RC model developed in Chapters 2 and 3 in this platform. The models will be integrated into the real time simulator, and the simulation result of power losses and junction temperature profile will be compared with the profile from the power lab.

4.2 Introduction Of The Real-Time Simulator And Simulink

The IGBT modules are used in a three-phase inverter that provides variable amplitude and frequency three-phase AC signals for the induction motor drives.

In order to ensure proper operation of the rail vehicle on the track, an integration test of the vehicle control system is done before the initial roll-out. To get maximum test depth and to minimize the risk and cost, the test is implemented by connecting the original vehicle control system to the real-time dynamic vehicle simulator in closed-loop operation. Since all the control loops are closed via the simulator, it’s called hardware-in-the-loop simulation [55]. This is shown in Fig.4.1 [55].

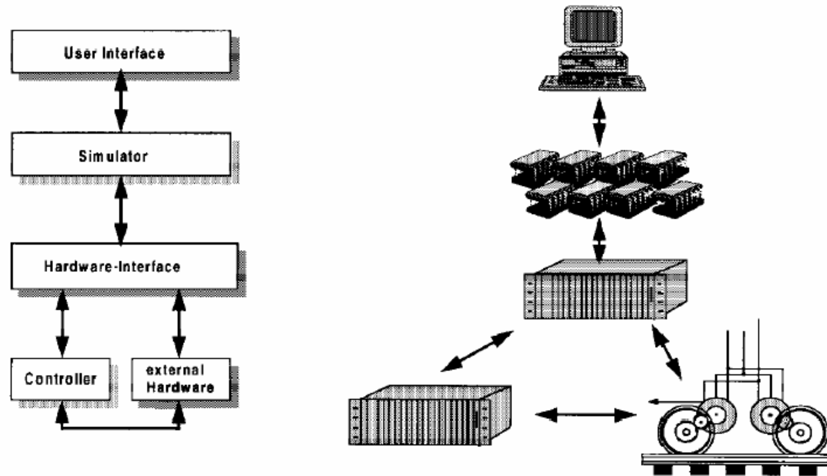

Figure 4.1 Generic hardware-in-the-loop setup.

The most important input to the simulator from the control system under test is the discrete firing signal which will control whether the IGBT modules in the three-phase inverter are conducting or not. For example, if the space vector pulse width modulation method [56] is used for the inverter, the firing signal will reflect the pattern determined by the pulse width modulation method. The output from the simulated vehicle to the control system includes the measured collector currents, voltages of the motor, etc.

Within the real time simulator, mathematical models of the mechnical and electrical systems are built in order to represent the electro-mechanical behavior of the vehicle. In this Chapter we aim to implement the thermal model of IGBT module which was developed in Chapter 3 in the real time simulator.

Simulink, an extension to **Matlab**, is a graphic block-oriented program for simulating dynamic systems [57]. It is widely used for the simulation of control systems. We will build our power losses and thermal RC network model using the block function within Simulink.

4.3 Power Losses Model Implementation In Simulink

In Chapter 2, the power losses (conduction and switching losses) of IGBT and diode in the three-phase inverter is expressed as a function of current through the device as shown in Equation (2.8). Another parameter DC link voltage will determine the scalar factor in Equation (2.9).

In the real time simulator, the current through each IGBT and the diode in each of the three phases of an inverter are available to us. The block "Fcn" in Simulink is used to implement the mathematical expression in Equation (2.8). The logic functions in Simulink are used to synchronize the power losses calculation with the switching event in the real time system.

The total power losses consist of three parts: turn-on, turn-off and conduction losses. Each sub-power losses calculation is implemented in a sub function block. The three sub

function blocks of IGBT power losses calculation are: turn-on power losses E_{on}, turn-off losses E_{off}, and conduction losses E_{con}. The sub function blocks of diode power losses calculation are: recovery losses of diode E_{rec}, conduction losses of diode E_{cond}. The total power losses is the sum of the result of each block. This is explained in Fig. 4.2.

4.3.1 Sub-Function Blocks Of Calculating Energy Losses Of IGBT And Diode

The block diagram shown in Fig.4.3 is the implementation of Equation (2.8) for calculating the switching energy losses E_{on} , E_{off} of IGBT and E_{rec} for diode. The coefficients in Equation (2.8) are implemented in the general expression "f(u)" block. The "Gain" function takes into account that the unit of I_c in Equation (2.8) is Kiloampere while the measured currents are in Amps. The "Switch" function sets the switching losses to zero when the current is zero. The block diagram shown in Fig.4.4 is used to calculate both the conduction power losses $P_{conduction}$ and the conduction energy losses $E_{conduction}$ for IGBT and diode. First using the function "f(u)", V_{CE} (or V_d) at a certain I_c (or I_d) is calculated using equation (2.10) and (2.11). The two quantities (V_{CE}, I_c) or (V_d, I_d) are then multiplied to calculate the conduction power. The frame time dt_asm is the system variable which defines the step time of the discrete system and which is used here to transform the power losses to energy losses value within each time frame.

4.3.2 Synchronization Of Switching Event In Simulink

The above models determined the power losses of IGBT and diode in the three-phase inverter. We still need to decide "when" to calculate the power losses. The power losses model in the real time simulator should have the ability to decide what kind of power losses is happening according to the firing signal. We should have trigger signal synchronized with the firing signal to turn on each power losses calculation block at the appropriate moment. And only when the trigger signal is high, the calculation result of the corresponding sub system is permitted to contribute to the total power losses waveform. The synchronization relation between the firing signal and the expected trigger signal for each function block described above is shown in Fig. 4.5.

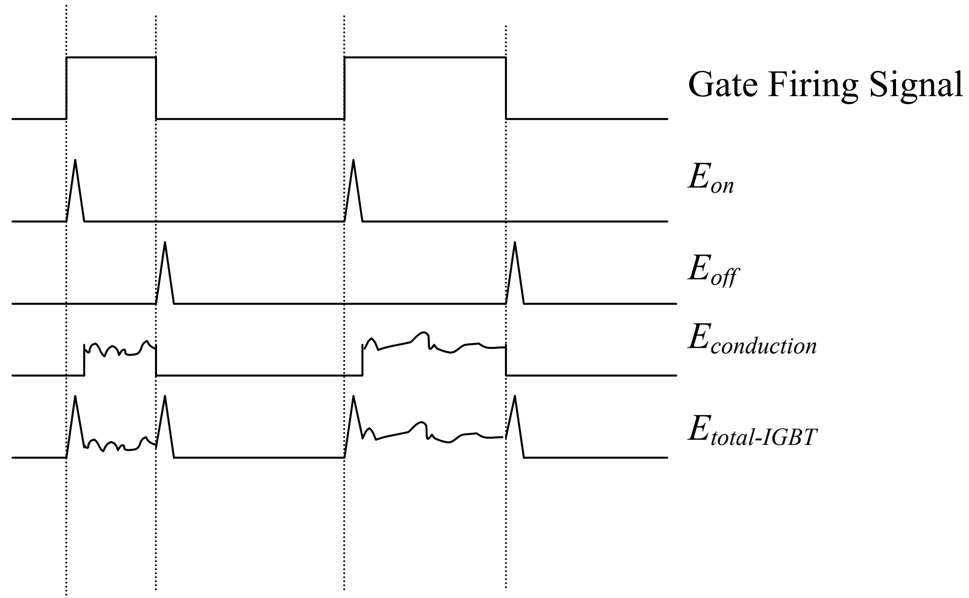

Figure 4.2 The synchronization between the gate-firing signal and the subblock.

(a) Of IGBT.

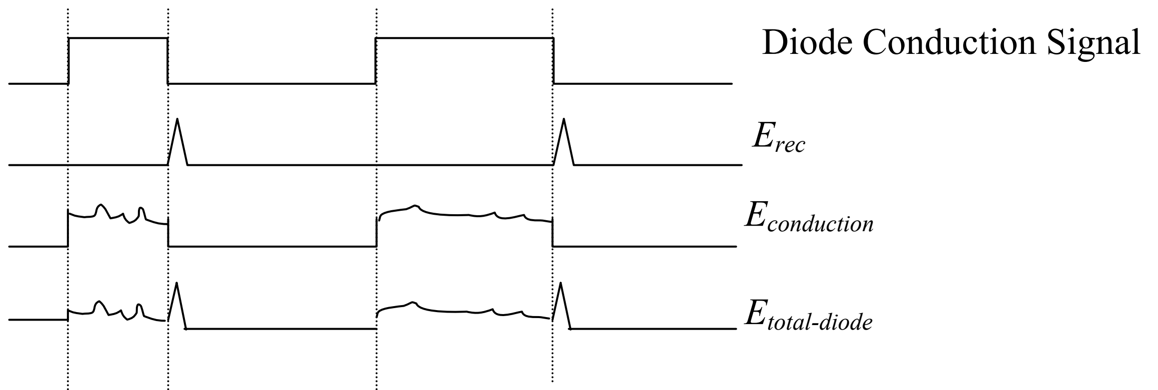

(b)of diode.

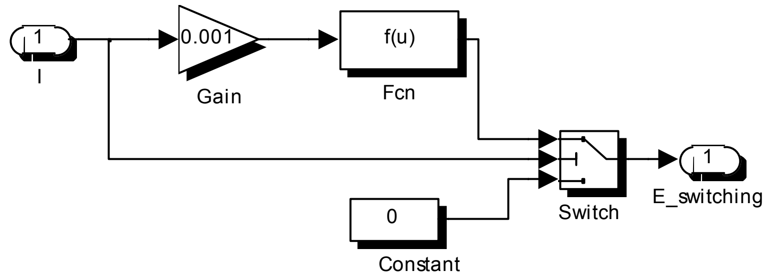

Figure 4.3 Simulink model of implementation of Equation (2.8).

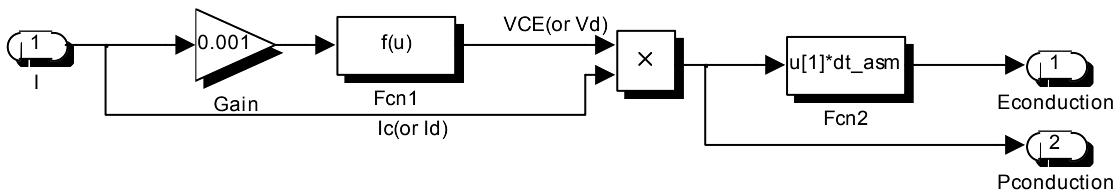

Figure 4.4 Simulink model of calculating conduction losses of IGBT and diode.

By using the logic block in Simulink, the trigger signals for sub-system E_{off}, E_{on} are generated from the models as shown in Fig.4.6 in Simulink. The trigger signals for $E_{conduction_IGBT}$ and $E_{conduction_diode}$ can be directly obtained from the gate firing signal and the diode conduction signal, respectively. For the upper free wheeling diode recovery occurs simultaneously with the turn-on energy E_{on} of the lower IGBT, so the trigger signal for calculating E_{rec} of upper diode should be the same as the trigger signal of E_{on} of the lower IGBT.

4.3.3 Switching Power Losses And Switching Energy Losses

The shortest processing time in the real time simulator is defined by the frame time. We will make the pulse width of the trigger signals for the E_{on} E_{off} and E_{rec} sub-system equal to this time in the real time simulator. This means that no matter how fast the switching transient for IGBTs and diodes are (usually around several μs), in the real time simulator, we always assume that the switching transient process takes as long as the frame time (40-60 μs [55]).

In our switching losses calculation model, every switching event will result in a rectangular pulse whose height corresponds to the appropriate energy losses and its width is equal to the frame time as shown in Fig.4.5.

The power losses is then calculated by dividing the switching energy losses by the frame time of the real time simulator.

$$P_{switching} = \frac{E_{switching}}{frametime} \tag{4.1}$$

In real case, the switching transient of IGBT and diode occurs over a much shorter period, usually around several μs and instead of a constant, it is a variable. So the power losses calculated here are smaller than the real value and it is an approximation.

This result does not adversely affect the thermal analysis result which need the power losses value as inputs. The reason is that the RC network representing the thermal model acts as

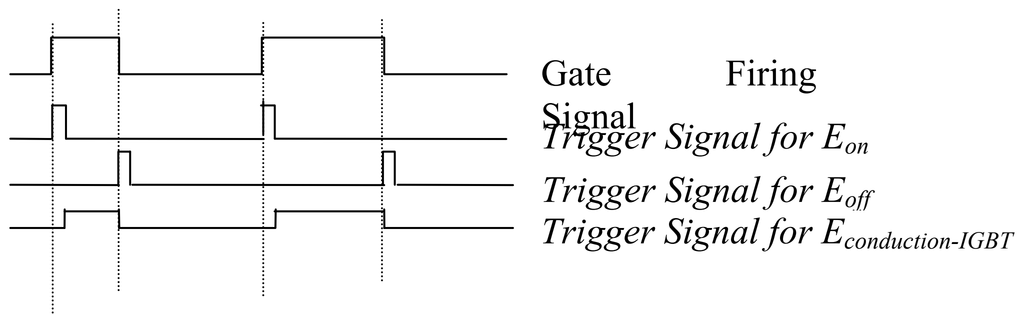

Figure 4.5 The synchronization between the firing signal and the trigger signal.

(a) For IGBT

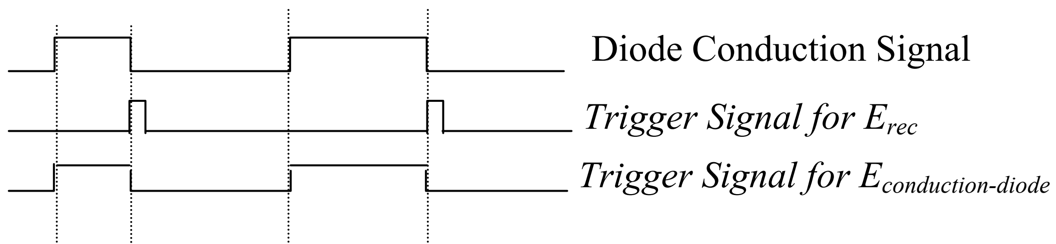

(b)For diode.

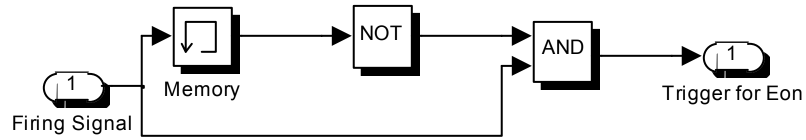

Figure 4.6 Simulink model of generating trigger signal for E_{on} and E_{off}.

(a) E_{on}

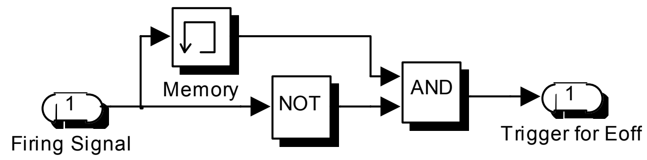

(b)E_{off}.

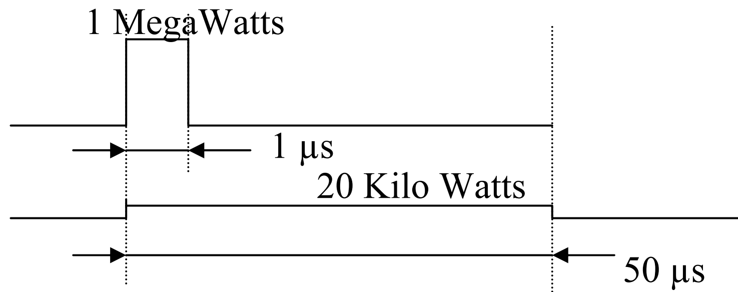

Figure 4.7 Two forms of energy losses of 1 Joules.

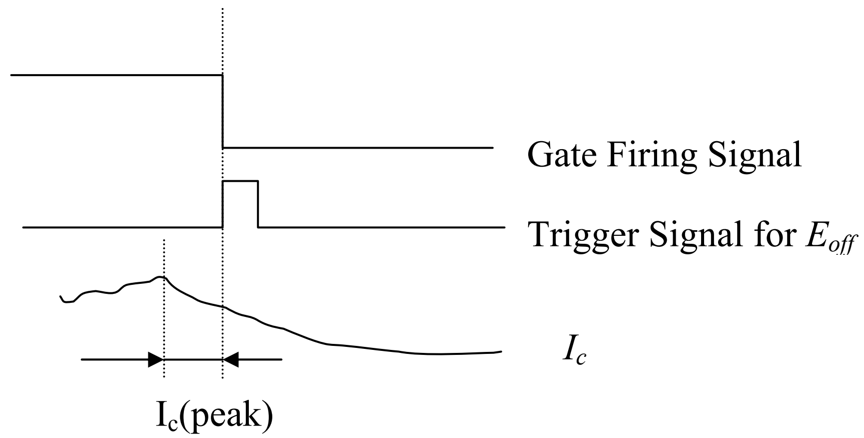

Figure 4.8 Demonstration of the lag between the I_c(peak) and the trigger signal for E_{off}.

a low-pass filter which integrates the power (current) in the time domain. So the energy and not the power value will determine the temperature. As shown in Fig.4.7, For example, if the energy losses are 1 Joules and it happens within time period as small as 1μs, then the peak power is 1 million Watts. Input this power pulses with width 1μs and peak value 1 million Watts to the thermal RC network, and the result will be the same as if time period is 50μs, the peak power=20K Watts. In both cases, the energy is the same.

4.3.4 The Peak Value I_c Catching Algorithm

Equation (2.8) that calculates E_{off} is a function of the collector current I_c before the IGBT is turned off. However in the real time simulator, the trigger signal for E_{off} lags behind the "peaking" moment of I_c by several frame times. This is shown in Fig.4.8. An algorithm is used to catch the peak collector current I_c and keep it in the memory unit until the trigger signal for calculating E_{off} arrives. Fig. 4.9 shows an implementation of this algorithm in **Simulink**.

Similarly Equation (2.8) that calculates E_{on} as a function of the peak Value of I_c after the IGBT is turned on. In the real time simulator, the trigger signal for the E_{on} occurs several time steps before the current through the IGBT reaches its peak value. This is shown in Fig. 4.10. We therefore need to delay the trigger signal to get the peak value after the IGBT is turned on. By trial and error, we found that choosing the delay time to be equal to twice frame time is appropriate. The delay function is implemented by inserting two "Memory" blocks to the block shown in Fig. 4.6(a).

4.3.5 Instantaneous Vs. Average Power Losses Over A Long Time Period

One of the advantages of the real time simulator is that we can simulate the power losses model of IGBT module under actual application condition of the three-phase inverter. For a three-phase inverter used as traction driver, the operational duty for the train is several seconds or hours. So we need to observe the power losses over a rather long time period. Instead of worrying about the instantaneous power losses at every time frame, an averaging algorithm is

used to obtain an average power losses over the observation period. The averaged power loss profile is more useful in the motor drive application.

The averaging function is implemented in **Simulink** as shown in Fig.4.11. The averaging window size can be tuned from 1 frame time to several seconds.

4.4 Power Losses Model Result From Real Time Simulator

The power losses calculation models are installed into the real time simulator. Testing of the model includes checking the signal waveform under different three-phase inverter modes, zooming in the waveform to make certain no-missing event happens and right value of energy losses are calculated. The value of power losses from the model is compared to the hand-calculation based on the waveform of current I_c (for IGBT), I_d (for diode) and the firing signal.

4.4.1 Power Losses Waveforms

Fig. 4.12, 4.13 show at a certain firing signal pattern corresponding to a particular SVPWM mode, together with the collector current and the energy losses of E_{on} and E_{off} that result from the use of from the new model. Fig.4.14 shows the waveform of energy losses of IGBT including E_{on}, E_{off} and conduction losses E_{con} from our model. Fig. 4.15 is the counterpart of 4.14 for diode.

4.4.2 Instantaneous Vs. Average Power Losses Of IGBT And Diode

4.4.2.1 Instantaneous Vs. Average Power Losses Of IGBT. Fig. 4.16 shows the instantaneous power losses waveform of IGBT for a 200 seconds run while the train accelerates and Fig.4.17 depicts the average power losses of the above signal.

4.4.2.2 Instantaneous Vs. Average Power Losses Of Diode. Fig.4.18 shows the instantaneous power losses waveform of diode for a 200 seconds run while the train accelerates and Fig.4.19 depicts the average power losses of the above signal.

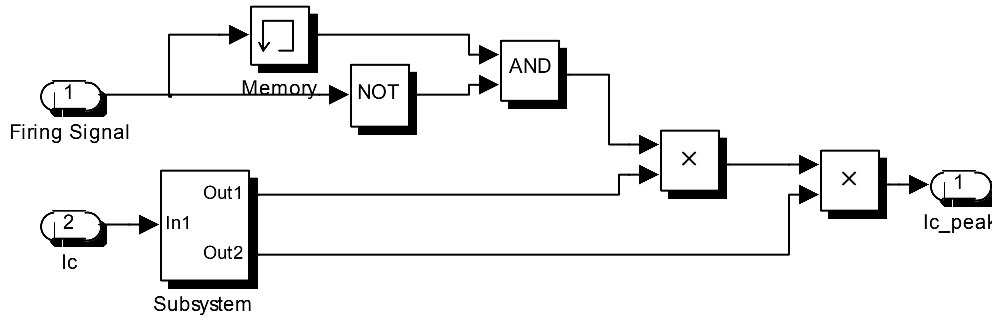

Figure 4.9 Simulink model of implementation of catching I_c peak algoritm.

(a)

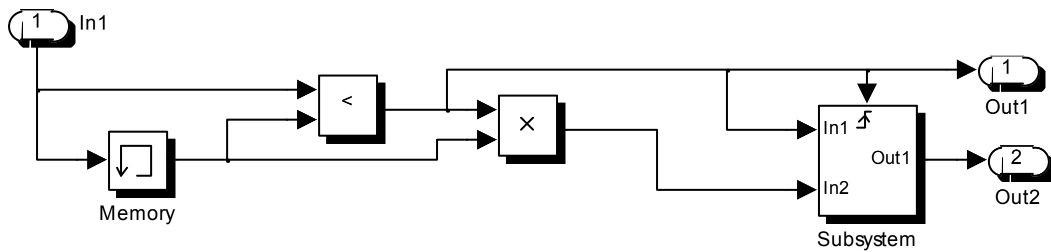

(b) Inside of the subsystem of (a).

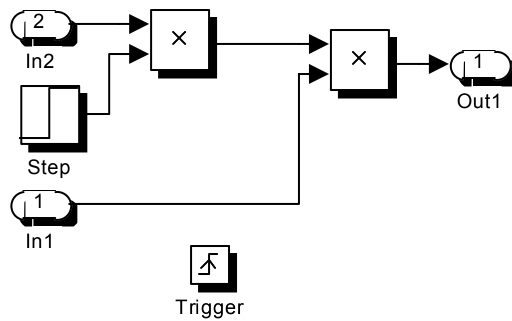

(c) Inside of the subsystem of (b).

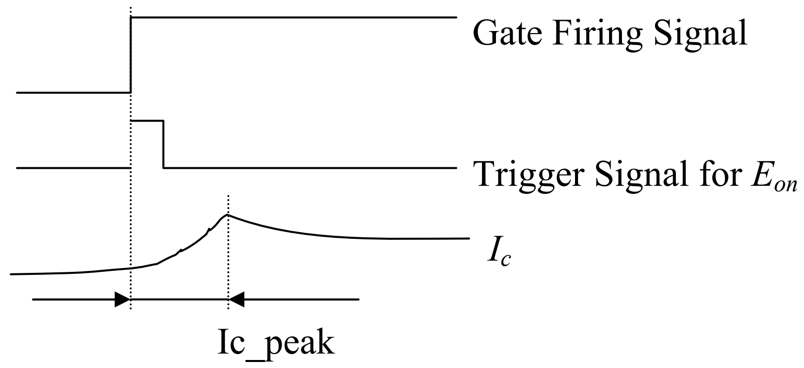

Figure 4.10 The delay between I_c (peak) and trigger signal for E_{on}.

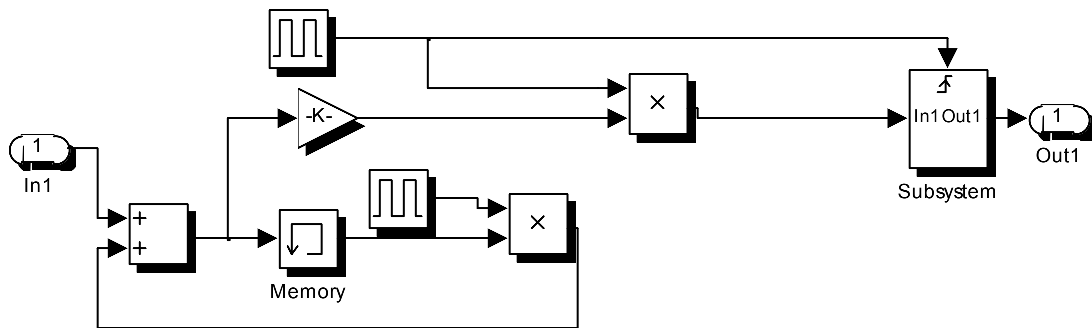

Figure 4.11 Simulink model of averaging function for power losses.

(a)

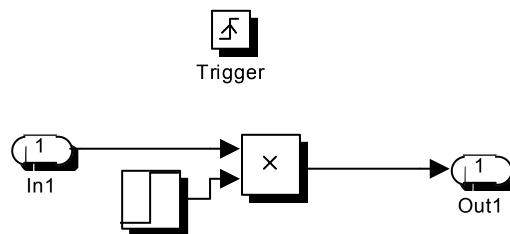

(b) Inside of subsystem of (a).

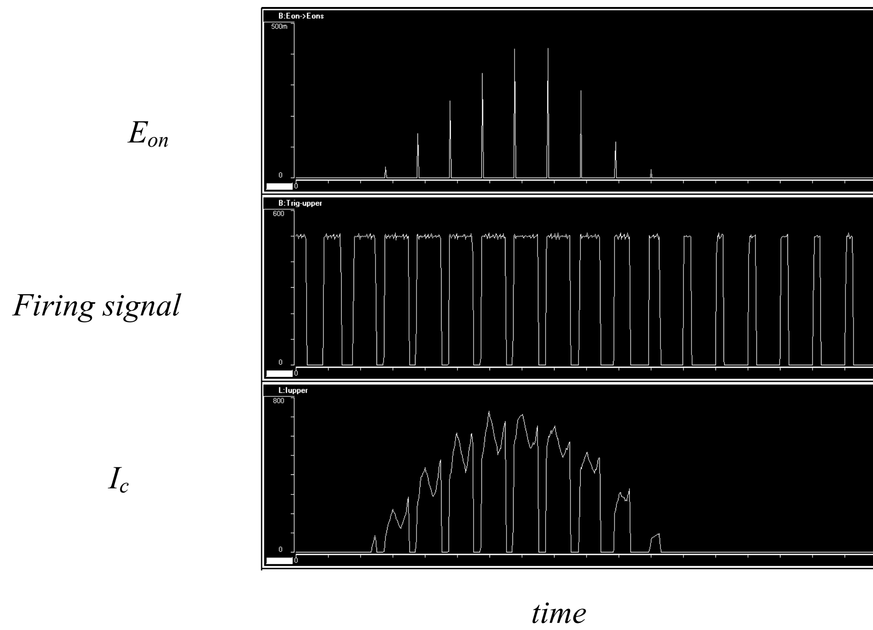

Figure 4.12 Waveforms of Turn-on energy losses of IGBT E_{on}.

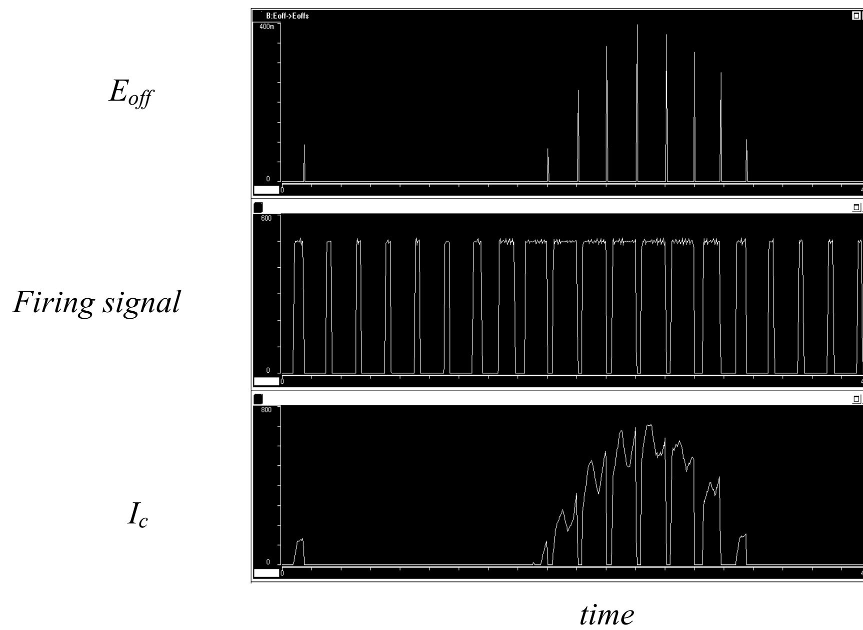

Figure 4.13 Waveforms of Turn-on energy losses of IGBT E_{off}.

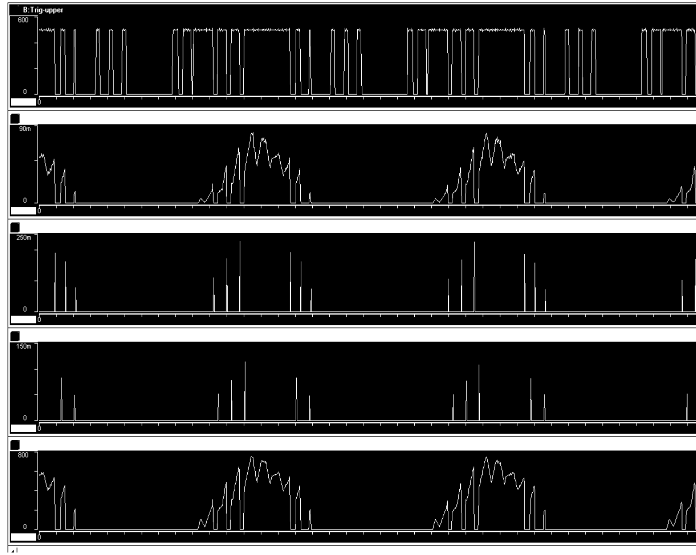

Figure 4.14 Waveforms of switching and conduction energy losses of IGBT.

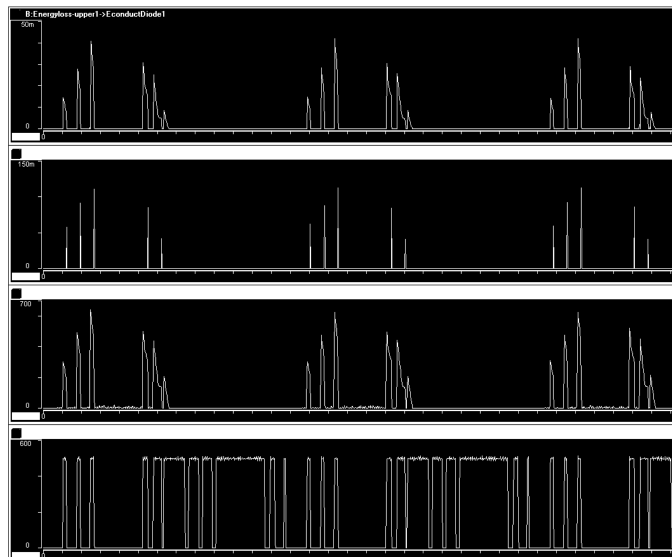

Figure 4.15 Waveforms of switching and conduction energy losses of diode.

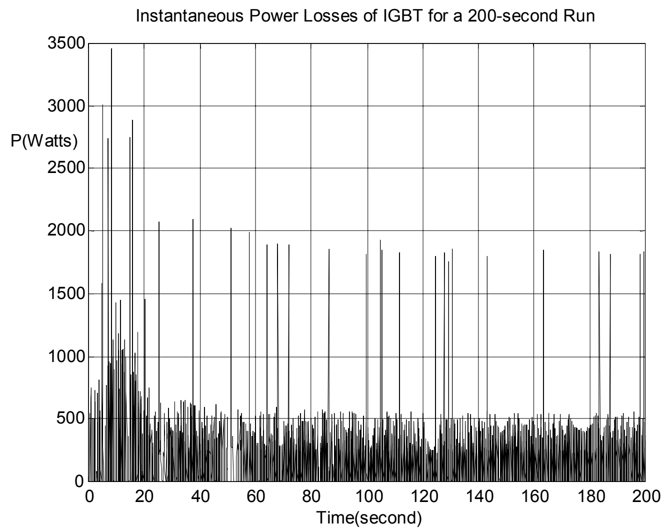

Figure 4.16 Instantaneous power losses waveform of IGBT for a 200 seconds run while the train accelerates.

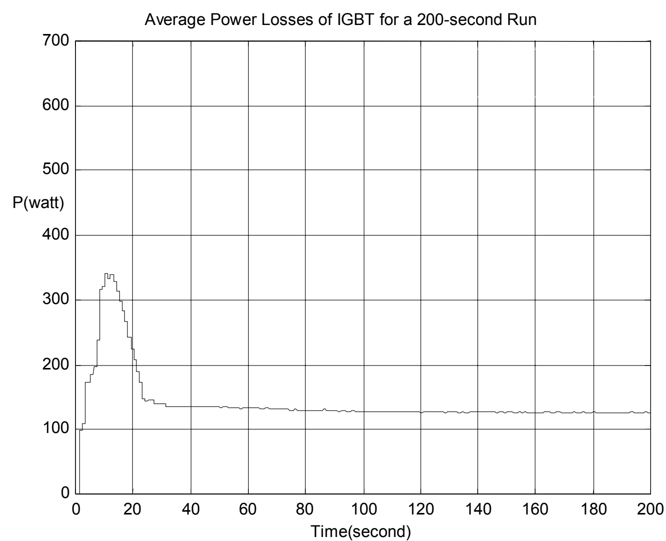

Figure 4.17 Average power losses waveform of IGBT for a 200 seconds run while the train accelerates.

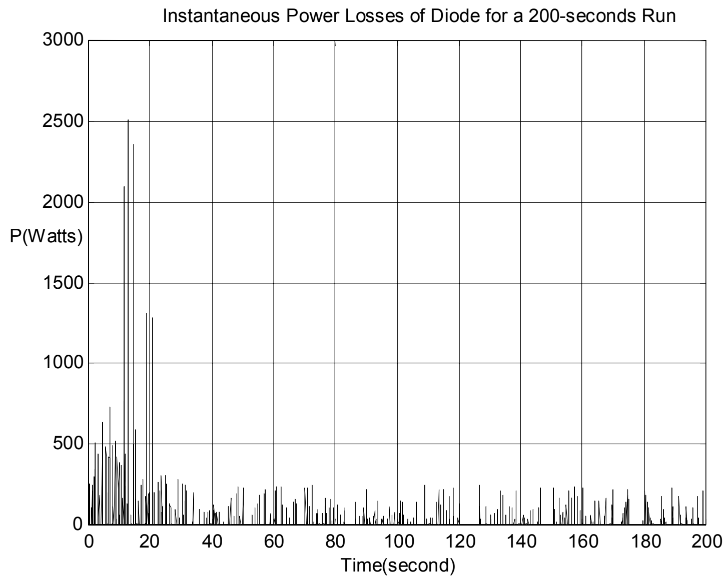

Figure 4.18 Instantaneous power losses waveform of diode for a 200 seconds run while the train accelerates.

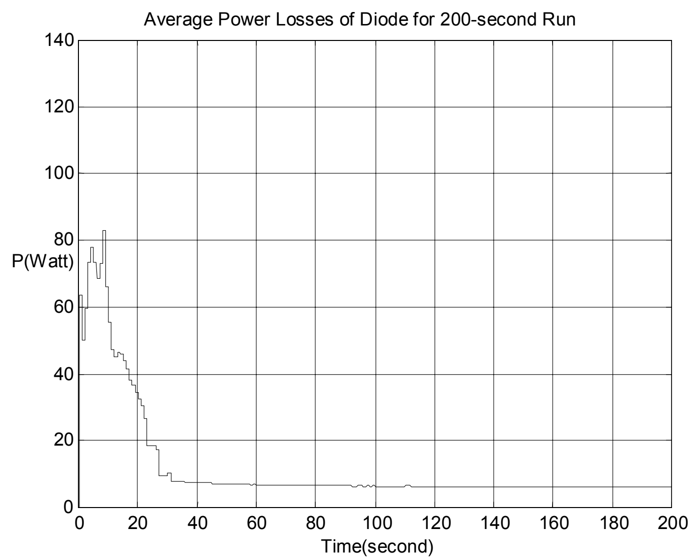

Figure 4.19 Average power losses waveform of diode for a 200 seconds run while the train accelerates.

4.5 Thermal RC Network Model Implementation In Simulink

Since 1998 the Power System Blockset has been available in **Simulink** [58] and has the electrical component blocks that can be used to build the thermal RC network. The simulation involving these discrete elements is rather long thus violating one of the requirements in the real time simulator namely speed of execution time. The “transfer” function block in Simulink is an appealing alternative. It is based on the “S” function for the RC network to calculate the junction, case temperature of IGBT and diode of the power module. The “transfer function” is easy to implement in **Simulink** and has short calculation time.

4.5.1.Transfer Function For Solving The Thermal RC Circuit In Simulink

In Chapter 3, the thermal RC circuits for IGBT and diode are built. Using the power losses as current source value in the circuit, the junction and case temperatures can be determined from the corresponding node voltages.

In the frequency domain, the power losses and the temperatures are related by the thermal impedance expressed as transfer function as shown in Equation (4.2):

$$Z_{thermal} = \frac{P(s)}{T(s)} \tag{4.2}$$

where P is the power losses and T is the temperature.

In the Simulink, if the input signal and output signal can be expressed as transfer function as the forms shown in Equation (4.3), the output can be obtained by connecting input signal to the transfer function block “transfer Fcn”.

$$H(s) = \frac{y(s)}{u(s)} = \frac{num(s)}{den(s)} = \frac{num(1)s^{nn-1} + num(2)s^{nn-2} + ... + num(nn)}{den(1)s^{nd-1} + den(2)s^{nd-2} + ... + den(nd)} \tag{4.3}$$

where *nn* and *nd* are the number of numerator and denominator coefficients, respectively. And *num* and *den* contain the coefficients of the numerator and denominator in descending powers of *s* [57].

Our aim is finding the coefficients in Equation (4.3) based on the RC thermal circuits for IGBT and diode.

4.5.2 Calculating Junction And Case Temperature Of IGBT

From the analysis in Chapter 3, we have the Equation (3.21) to calculate the junction temperature and case temperature of IGBT including the thermal coupling effect between the IGBT and diode:

$$\begin{aligned} T_j &= T_{junction} + T_{case2} \\ T_c &= T_{case1} + T_{case2} \end{aligned} \tag{3.21}$$

The method of calculating each term in Equation (3.21) for IGBT is shown in Fig.4.20.

$Z_{ja\text{-}IGBT}$ can be obtained from Equation (3.20), it is repeated here for convenience:

$$Z_{ja}(s) = \frac{0.57141 \cdot s^5 + 66.712 \cdot s^4 + 806.3 \cdot s^3 + 1262.5 \cdot s^2 + 367.62 \cdot s + 8.3245}{s^6 + 364.58 \cdot s^5 + 10653 \cdot s^4 + 79467 \cdot s^3 + 85287 \cdot s^2 + 13857 \cdot s + 159.16} \tag{4.4}$$

We can find $Z_{ca\text{-}IGBT}$ from Equation (3.18):

$$Z_{ca}(t) = 0.001 \cdot \begin{Bmatrix} 12.3 \cdot [1 - \exp(-t/5.4782)] \\ +27 \cdot [1 - \exp(-t/80.4812)] \end{Bmatrix} \tag{3.18}$$

Applying Laplace Transform to it:

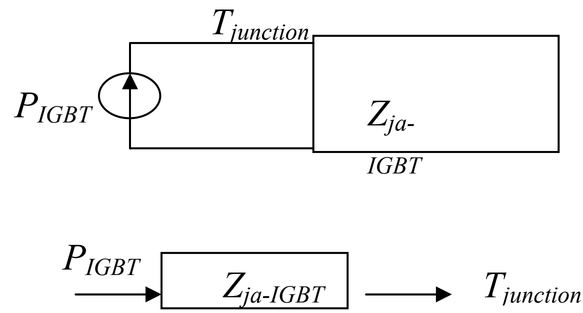

Figure 4.20 Transfer function approaches of calculating each term in Equ. (3.21) for IGBT.

(a) $T_{junction}$ for IGBT

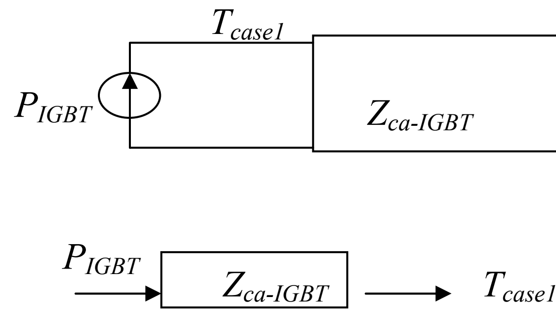

(b) T_{case1} for IGBT

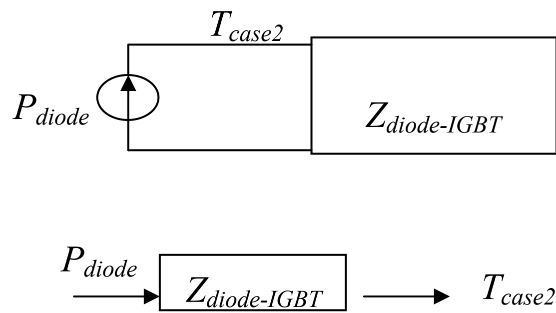

(c) T_{case2} for IGBT

$$Z_{ca}(s) = 0.001 \cdot \left(\frac{12.3/5.4782}{s + 1/5.4782} + \frac{27/80.4812}{s + 1/80.4812} \right)$$
$$= \frac{s + 0.03454}{387.49 \cdot s^2 + 75.547 \cdot s + 0.87886}$$

(4.5)

$Z_{diode\text{-}IGBT}$ which represents the thermal coupling effect of diode on the IGBT can be obtained form the circuit as shown in Fig.3.13:

$$Z_{diode-IGBT}(s) = 0.001 \cdot \left(\frac{23.6/18.1471}{s + 1/18.1471} \right)$$
$$= \frac{1}{768.95 \cdot s + 42.373}$$

(4.6)

The sub-system of calculating the junction and case temperature of IGBT in Simulink is shown in Fig.4.21, 4.22, respectively.

4.5.3 Calculating Junction And Case Temperature Of Diode

The same Equation of (3.21) can be used for the diode temperature calculation. Each terms can be calculated by the method shows in Fig.4.23.

$Z_{ja\text{-}diode}$ can be obtained from the exponential terms from Table 3.2 and Fig. 3.14:

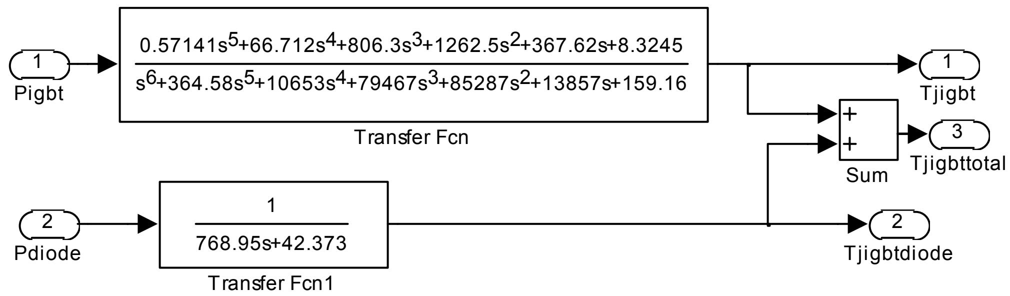

Figure 4.21 Simulink model of calculating the junction temperature of IGBT.

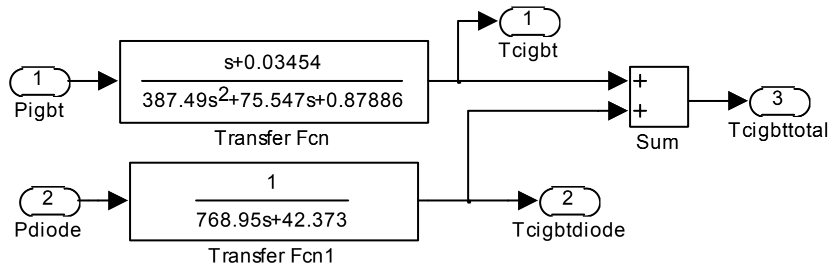

Figure 4.22 Simulink model of calculating the case temperature of IGBT.

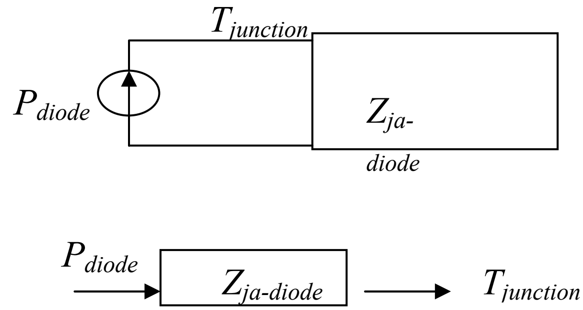

Figure 4.23 Transfer function approaches of calculating each term in Equ. (3.21) for diode.

(a) $T_{junction}$ for diode

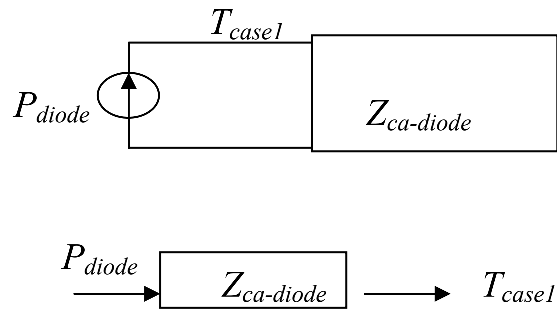

(b) T_{case1} for diode.

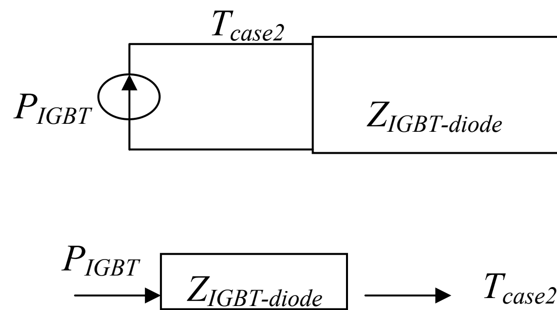

(c) T_{case2} for diode.

$$Z_{ja}(s) = \sum_{i=1}^{6} \frac{\gamma_i / \tau_i}{s + 1/\tau_i}$$

$$= 0.001 \cdot \left(\frac{2.46/0.003}{s + 1/0.003} + \frac{13.4/0.045}{s + 1/0.045} + \frac{4.57/0.45}{s + 1/0.45} + \frac{4.57/0.75}{s + 1/0.75} + \frac{16.6/1.8248}{s + 1/1.8248} \frac{27.5/73.2235}{s + 1/73.2235} \right)$$

$$= \frac{1.1435 \cdot s^5 + 131.3 \cdot s^4 + 704.77 \cdot s^3 + 1121.5 \cdot s^2 + 529.25 \cdot s + 11.35}{s^6 + 359.66 \cdot s^5 + 8876 \cdot s^4 + 32266 \cdot s^3 + 37395 \cdot s^2 + 12531 \cdot s + 164.26}$$

(4.7)

$Z_{ca\text{-}diode}$ can be obtained from the exponential terms from Fig. 3.14:

$$Z_{ja}(s) = 0.001 \cdot \left(\frac{16.6/1.8248}{s + 1/1.8248} + \frac{27.5/73.2235}{s + 1/73.2235} \right)$$

$$= \frac{s + 0.034842}{105.57 \cdot s^2 + 59.293 \cdot s + 0.79006}$$

(4.8)

$Z_{IGBT\text{-}diode}$ which represents the thermal coupling effect of IGBT on the diode can be obtained form the circuit as shown in Fig.3.16:

$$Z_{IGBT-diode}(s) = 0.001 \cdot \left(\frac{22/18.9408}{s + 1/18.9408} \right)$$

$$= \frac{1}{860.96 \cdot s + 45.454}$$

(4.9)

The sub-system of calculating the junction and case temperature of diode is shown in Fig.4.24. 4.25, respectively.

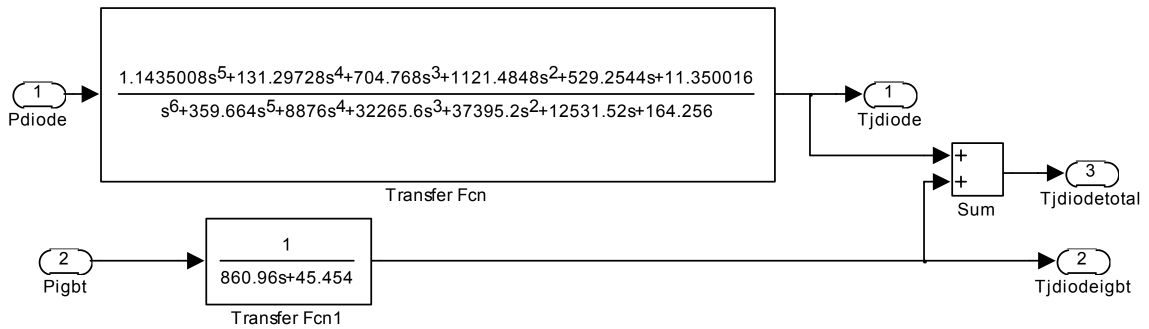

Figure 4.24 Simulink model of calculating the junction temperature of diode.

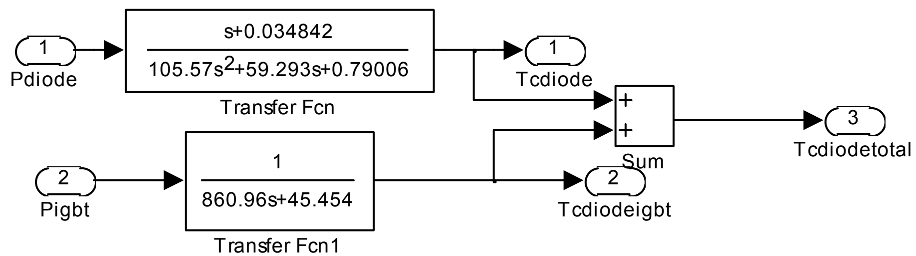

Figure 4.25 Simulink model of calculating the case temperature of diode.

4.6 Thermal RC Model Results From Real Time Simulator

4.6.1 Junction Temperature Of IGBT

Using the power losses profile as Fig.4.16 and Fig.4.18 for the IGBT and diode, the junction temperature of IGBT is shown in Fig. 4.26. The junction temperature of IGBT found was 12 °C above ambient maximum and 7 °C in steady state. Usually we assume 40°C as the ambient in the 3-phase inverter application environment, so in the acceleration process, the peak junction temperature of IGBT will be 52°C and in steady state, it will be 47°C.

4.6.2 Case Temperature Of IGBT

The case temperature profile of the case temperature of IGBT is shown in Fig. 4.27. The case temperature of IGBT found was 7 °C above ambient maximum and 5 °C in steady state. Using 40°C as the ambient temperature, this means 47°C maximum and 45°C in steady state.

4.6.3 Junction Temperature Of Diode

The junction temperature of diode found was 6 °C above ambient maximum and 3 °C in steady state. Using 40°C as the ambient temperature, this means 46°C maximum and 43°C in steady state. This is shown in Fig. 4.28.

4.6.4 Case Temperature Of Diode

The case temperature of diode is 5 °C above ambient maximum and 3 °C in steady state. Using 40°C as the ambient temperature, this means 45°C maximum and 43°C in steady state. For the case of IGBT and diode is at different position of the module package, so there is a difference between the two temperatures. This is shown in Fig. 4.29.

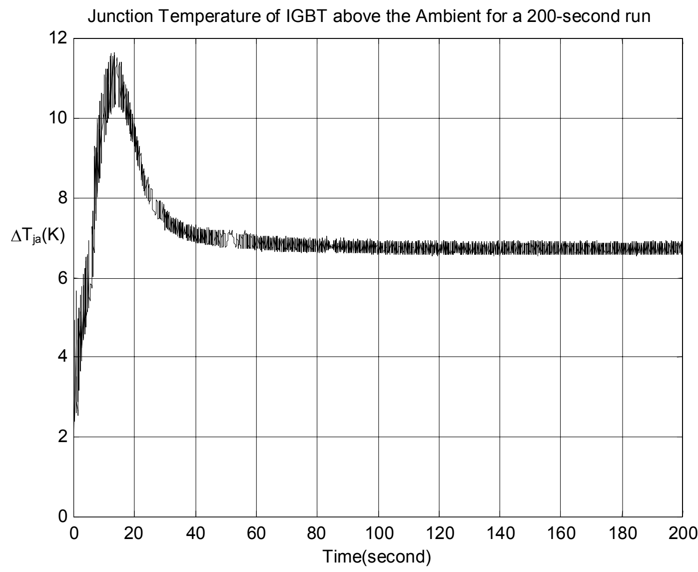

Figure 4.26 Junction temperature above the ambient profile of IGBT for a 200-second run.

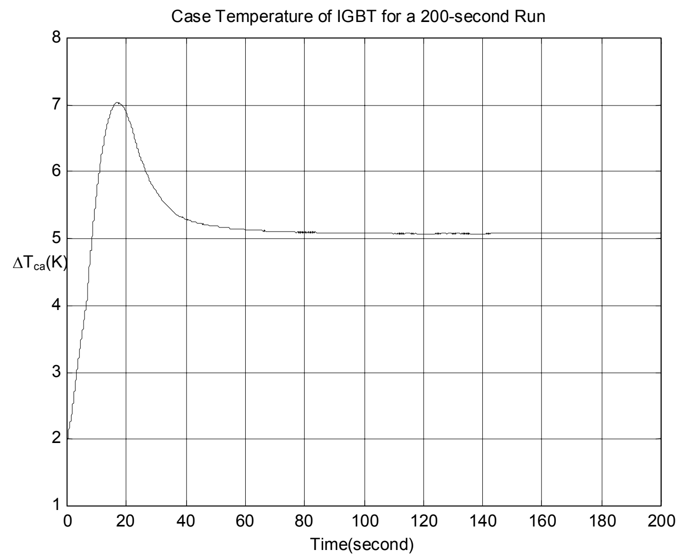

Figure 4.27 Case temperature above the ambient profile of IGBT for a 200-second run.

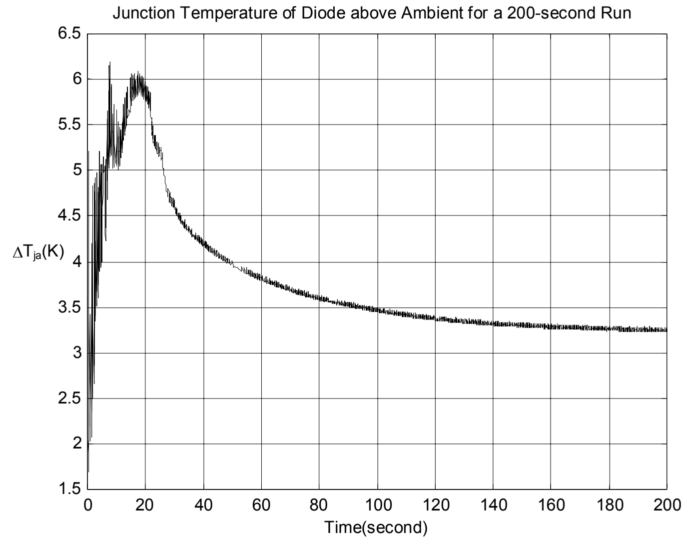

Figure 4.28 Junction temperature above the ambient profile of diode for a 200-second run

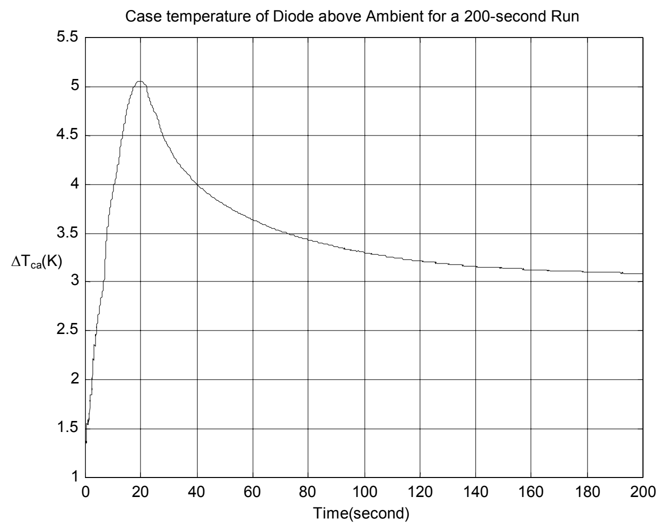

Figure 4.29 Case temperature above the ambient profile of diode for a 200-second run.

4.7 Model Verification By Off-Line Simulation In Matlab

The thermal model built in the real time simulator includes two parts: power losses model and temperature calculation model. The process of testing the whole model thoroughly is shown in Fig. 4.30. We have two ways to test the model: (1) On-line simulation in which the profile information is fed to the real time simulator and the resulting power losses and temperature profile obtained are compared to the experimental data measured in the Power Lab in Fig. 4.31. (2) Off-line simulation in which the power losses profile is input to the thermal model and the temperature from simulation is then compared to the temperature measured on the real train. We will use the second method to verify the thermal RC model. The off-line simulation model is implemented in Simulink.

The motors used in the Power Lab are driven by the three-phase inverter and controlled by the profile information (grade and distance between train stops) to simulate the actual service application. Fig. 4.31 demonstrates the power losses and junction temperature of IGBT modules during the train accelerates, keeping constant speed and decelerates.

The power losses profiles of the IGBT module are recorded during the motor acceleration, while keeping the top speed, and during the deceleration process. The power losses profile of the IGBT and the diode during power acceleration (noted by the interval "A") and deceleration (noted by "D") are shown in Fig. 4.32. The accelerating process lasts 105 seconds and the braking process is accomplished in 25 seconds. Between the acceleration and the braking, the train keeps a constant speed (in the interval noted by "C") about 28 seconds. This last interval is a function of the distance between the stops and the speed of the train. The cycle which includes intervals A, C and D lasts for 158 seconds. In the off-line simulation, the cycle is repeated 15 times which corresponds to the train runs for approximately 40 minutes until the system reach its thermal steady state. The power losses profile from the Power Lab shown in Fig.4.33 is used as the input to the thermal model.

The off-line simulation block in Simulink is shown in Fig. 4.34. The off-line simulation results of junction and case temperature of IGBT and diode are shown in Fig. 4.35 and Fig.4.36 respectively. From Fig.4.35, the case temperature of IGBT module is about 10°C above ambient

(40°C) after the system reaches the thermal steady state. This result is very close to the case temperature 52°C by experimental measurement.

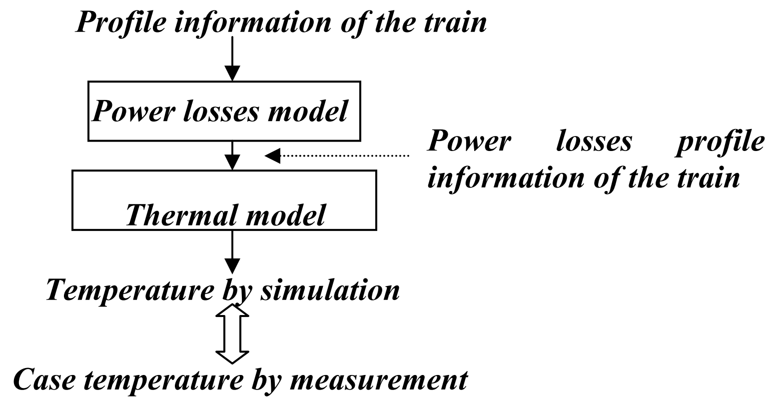

Figure 4.30 Model testing process.

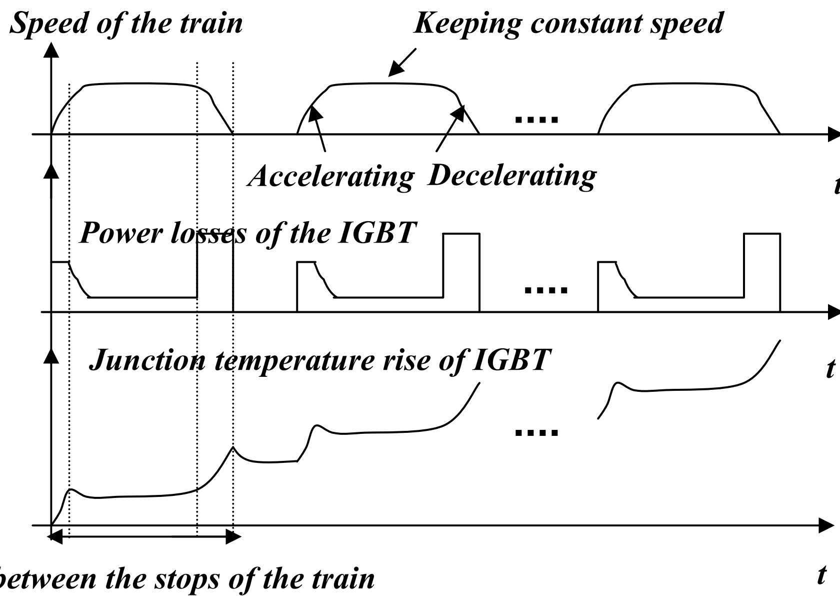

Figure 4.31 Demonstration of power losses and the junction temperature relation during the train accelerates, keeping constant speed and decelerates.

Figure 4.32 Power losses profile of IGBT and diode during train's service period.

(a) IGBT

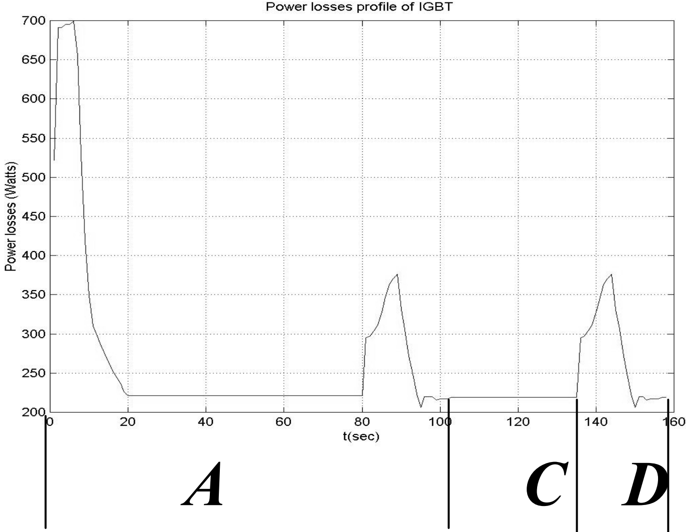

(b) Diode

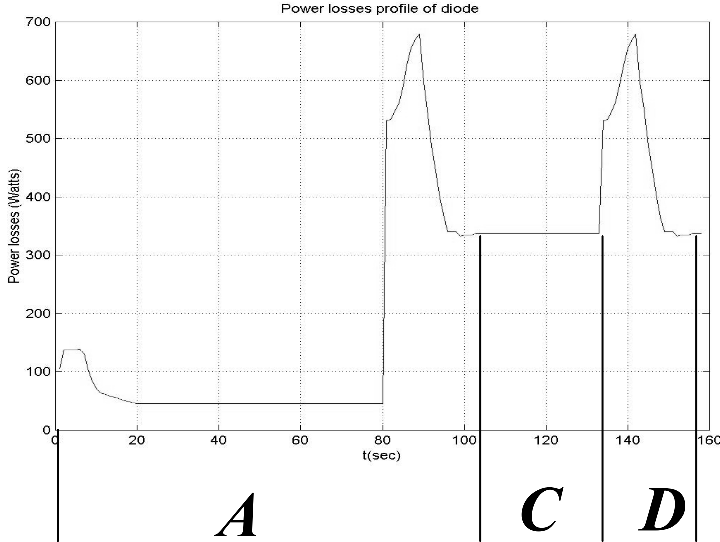

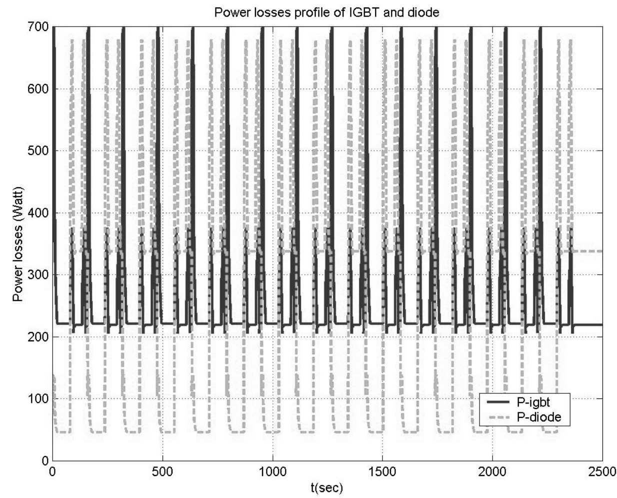

Figure 4.33 Power losses profile of IGBT and diode in the off-line simulation.

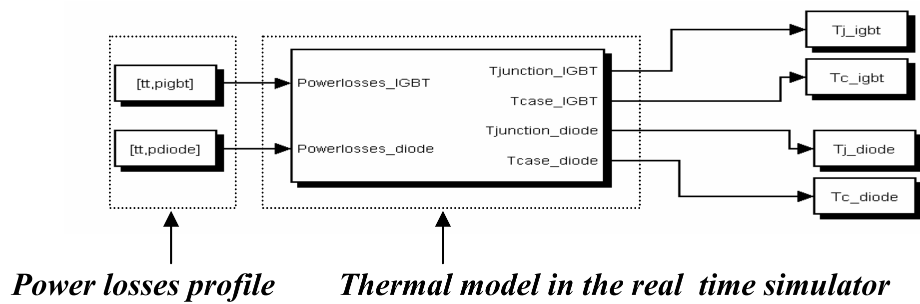

Figure 4.34 Off-line simulation model block in Simulink.

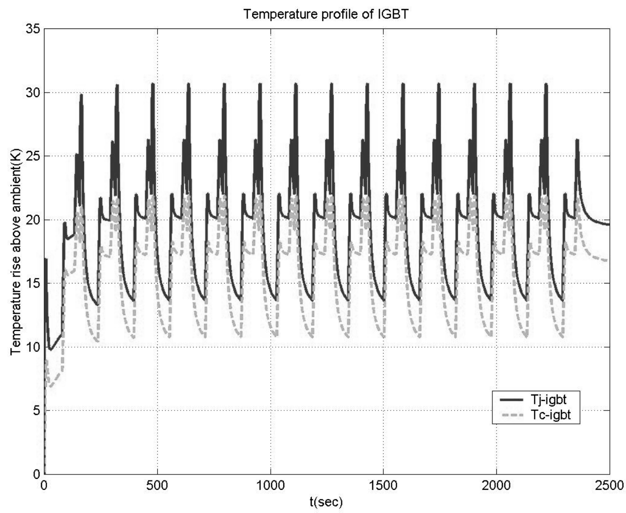

Figure 4.35 Off-line simulation results: temperature profile of IGBT.

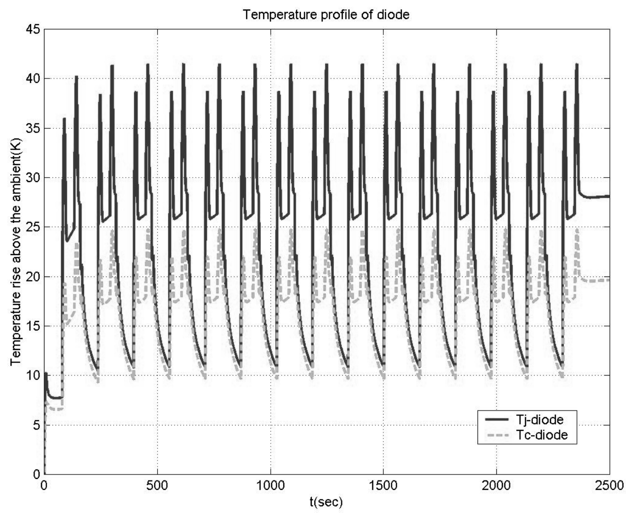

Figure 4.36 Off-line simulation results: temperature profile of diode.

5.0 3-D THERMAL SIMULATION OF IGBT MODULE

5.1 Introduction

In Chapter 3, a thermal RC network is developed for the IGBT module used in the three-phase inverter system. The model requires the availability of the measured transient thermal impedance curve Z_{jc} from the manufacturer and Z_{ca} from user. The RC model is suitable to use in the real time simulator for its implementation simplicity and fast calculation time.

The approach taken in Chapter 3 falls in the category of a behavioral modeling. A model of this type is suitable for a specific situation and depends on the experimental data to extract the model parameters. The model cannot however predict the thermal behavior of the system if the system's physical parameters change unless of course one is provided with a different set of experimental data.

In this Chapter, a physics based model is outlined to perform the thermal analysis. The model is based on the thermal property of the material inside the device, the structure parameter of the device and the characteristics of the cooling technique used in real applications.

The normal methods to solve the heat transfer problems include finite element method (FEM), finite difference method (FDM) and analytical solution. The latter is suitable for simple structures and cannot be easily adapted for the multiple layered structures of the IGBT module and its complicated boundary conditions. FDM and FEM are therefore the most popular numerical methods used in heat transfer analysis.

FDM is conceptually simple and easy to implement. The governing differential equations are solved by approximating differentials by difference expressions. But there is a crucial limitation for the FDM: namely that the domain of interest must be divided into rectilinear cells and for many problems boundaries have to be approximated by a step like pattern. FEM does not suffer from any such limitation. The domain of interest is divided into a number of simple areas or volumes (elements) of variable size. The field variable in the differential equation is assumed

to vary within the element according to a chosen interpolation function. This allows a high degree of flexibility in FEM as accurate results may be obtained by either, using few elements with higher order interpolation, or a larger number of elements with linear interpolation. Because of these advantages, FEM has become the number one choice of the numerical method for the analysis of heat transfer problems with unrivaled accuracy [41].

In this chapter, we will use 3-D FEM software ANSYS [59] to implement the thermal analysis of IGBT module in the three-phase inverter system. The 3-D simulation will result in the transient thermal impedance curve, heat flux distribution through different layers and maximum junction temperature. For the transient thermal impedance curve, the simulation results will be compared with the experimental data. The 3-D simulation provides an alternative way to extract the thermal RC model parameters which can be implemented in the real time simulator.

5.2 Governing Differential Equations Of Heat Transfer

The principle of thermal analysis using FEM consists in solving the governing partial differential equations of heat transfer by breaking the problem into small elements. The details of the mathematical formulation will not be discussed in this thesis as we have selected to use a commercial package. The emphasis will be directed at introducing the governing equations and the associated boundary conditions [41].

Heat can be transferred from one place to another by three methods: conduction, convection and radiation.

Conduction occurs when molecules of hot substance pass on some of their energy to the adjacent molecules. The governing equation for conduction in isotropic material is given by:

$$\nabla \cdot \left(\kappa\left(\nabla T\right)\right) + Q = \rho c \frac{\partial T}{\partial t} \tag{5.1}$$

Here a heat generating term Q is added compared to Equation (4.1). For non-isotropic material, the thermal conductivity κ is direction dependent and tensor notation is needed in the equation.

Heat transfer by convection takes place when groups of molecules move from one place at a certain temperature to another at a different temperature. It is created by fluid flow. The heat flux term (the heat transfers through the unit area in unit time) due to the convection should be added to Equation (5.1) to yield:

$$\nabla \cdot (\kappa(\nabla T)) + Q = \rho c\left(\frac{\partial T}{\partial t} + u\frac{\partial T}{\partial x} + v\frac{\partial T}{\partial y} + w\frac{\partial T}{\partial z}\right) \tag{5.2}$$

where (u,v,w) is the velocity field of the fluid.

In many applications, the convection occurs between the solid and the fluid boundaries. So the convection can be treated as boundary conditions to the solid. And Equation (5.3) is a very useful equation in this case:

$$q = h(T_s - T_f) \tag{5.3}$$

where q is the heat flux, h is heat transfer coefficient between the solid and the fluid, T_s and T_f are the temperature of the solid and fluid respectively.

The heat transfer rate because of radiation between two systems of temperature T_1 and T_2 is:

$$q = F_{12}\varepsilon A\sigma\left(T_1^{\,4} - T_2^{\,4}\right) \tag{5.4}$$

where F_{12} is a geometry dependent view factor between system 1 and 2, ε is the emissivity of the material, and σ is the Stefan-Boltzmann constant. For radiation always happens between two systems, so radiation can be treated as boundary conditions for Equation (5.2).

ANSYS is commercial finite-element analysis software package. In the thermal analysis area, the software can be used to calculate the temperature gradients, heat transfer and thermal flux of an object. The analysis can be performed using conduction, convection and radiation heat transfer modes. It has the ability to perform the steady and transient analysis under steady state

and time-varying loading conditions respectively. The general process of using ANSYS in the thermal analysis consists in the flowing steps: problem specification, geometry building, material definition, meshing, applying loads, solving the problem and reviewing the results.

5.3 Thermal Behavior Of The IGBT Module

5.3.1 Structure Of The IGBT Module

Fig. 5.1 shows the schematic structure of the IGBT module. The silicon layer is the active device part, while the substrate is made of AlN and the package material is AlSiC. In order to increase the current rating of the IGBT module, 16 IGBT chips and 16 FWD diodes are assembled inside the module and they are connected in parallel and soldered to the ceramic substrate. The thick ceramic substrate provides the electrical isolation and thermal contacts. The base plate provides the mechanical support for the whole module. From the thermal requirement, all the material for the high power IGBT module should have high thermal conductivity and matched coefficients of thermal expansion.

5.3.2 3-D Thermal Modeling

5.3.2.1 Procedure. Taking advantage of the system symmetry, only half of the IGBT module is modeled and simulated.

The model uses 8-noded 3-D thermal solid elements (SOLID 70). The finite element mesh is constructed to obtain optimum mesh size. The final structured mesh of the IGBT module is shown in Fig.5.2. Finer mesh is used for the silicon region while the substrate and base plate is meshed coarsely. The final structured mesh has 13844 elements and 4747 nodes. Inside the IGBT module, the dominant heat transfer mechanism is thermal conduction between different layers, convection and radiation of the different materials to ambient is ignored.

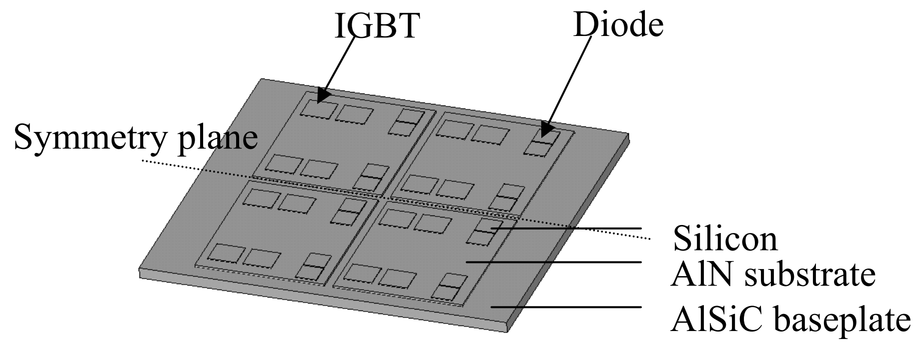

Figure 5.1 Schematics of the IGBT module.

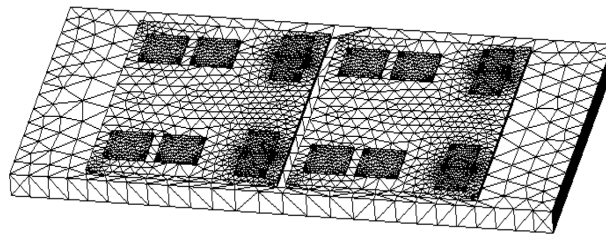

Figure 5.2 Mesh structure for half of the IGBT module.

5.3.2.2 Material Properties. The physical dimensions of each layer within the module and the material properties [60] are listed in Table 5.1. Although the properties of the three materials are temperature-dependent, only the thermal conductivity of silicon varies sufficiently over the temperature range of interest. The silicon layer is thus modeled using isotropic nonlinear thermal properties, while the remaining material use constant linear properties. The temperature dependent thermal conductivity of silicon is listed in Table 5.2[46].

5.3.2.3 Loading And Boundary Condition. Since the device active region results in most of the heat generation, and since the active region is small compared to the device dimension while close to the top surface of the silicon chip, the electrical power losses will be treated as surface load which is applied uniformly on the silicon chip surface.

In order to get the junction to case transient thermal impedance curve for the IGBT, a constant power of1000 watts is applied as surface heat flux load uniformly on the 8 IGBT chips surface, while the temperature of all the nodes at the bottom of the base plate is kept at a constant value T_c. This boundary condition is in conformity with the measurement procedure outlined in Chapter 3. All the other boundaries are assumed adiabatic (thermally insulated).

5.3.2.4 Fem Results And Verification. The heat flux is applied as a sudden load in the transient thermal analysis. After the load is applied for 20 seconds, the temperature distribution of the IGBT module is shown in Fig. 5.3. Pick the hottest spot temperature to correspond to the junction temperature T_j(t). By using Equation (3.5), the transient thermal impedance curve of IGBT from junction to case can be derived. In Fig.5.4, the simulation results are compared with experimental data and are shown to be with good agreement. The error in the thermal resistance from junction to case R_{jc} (the steady state value of the thermal impedance $Z_{jc}(t)$) between the simulation result and experimental data is 0.3%.

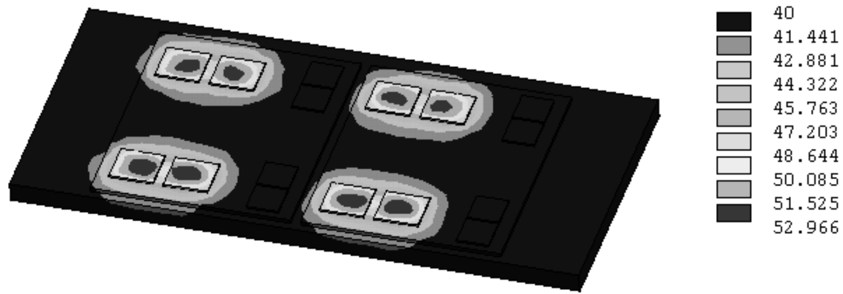

Figure 5.3 Temperature distribution of the module after power applied on IGBT chips.

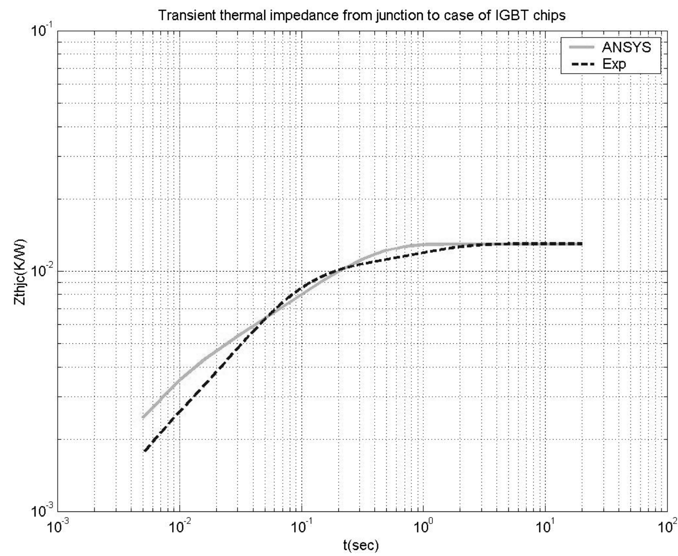

Figure 5.4 Transient thermal impedance from junction to case of IGBT chips. Solid line: simulation results by ANSYS, dash line: experimental data

Table 5.1 Model physical dimensions and material properties used for simulation

Material	*Dimensions(cm)*	*K(W/m-K)*	*c (J/g-K)*	*ρ(g/cm^3)*
Silicon	0.051×1×1.1(IGBT) 0.051×0.8×0.8(Diode)	See Table 5.2	0.712	2.33
AlN	0.1×5.8×5	190	0.74	3.26
AlSiC	0.5×13×14.2	180	0.72	3
Al	See Table 5.3	237	0.91	2.702

Table 5.2 Temperature dependent thermal conductivity of silicon used for simulation

Temperature (℃)	*K(W/m-K)*
25	153
77	119
127	98.9
227	76.2

If we apply the constant heat flux load to the 8 diode chips for 20 seconds and keep the base plate temperature as constant, we obtain the temperature distribution of the module as shown in Fig.5.5. Picking the hottest spot on the surface of the diode to represent T_j and by using Equation (3.5), the junction to case transient thermal impedance of diode is derived as shown in Fig. 5.6. The experimental data from the manufacturer is also shown in the same figure. For the thermal resistance from junction to case of diode R_{jc}, the difference between the simulation result and experimental data is 18.6%.

5.4 Thermal Behavior Of The IGBT Module With Heatsink In The Three-Phase Inverter

5.4.1 System Description

In the three-phase inverter, there are 6 IGBT modules for acceleration and there are 2 extra IGBT modules for the braking process of the motor. All the eight IGBT modules are mounted on the heatsink which is made of aluminum. The heatsink has plate fins on the bottom of the base plate in order to increase the contact area between the heatsink and the cooling air from the fan. So besides the conduction, now the forced convection plays an important role.

5.4.2 3-D Thermal Modeling

5.4.2.1 Procedure. Fig. 5.7 shows the schematic of the whole system. Taking into consideration the limit on the maximum number of nodes of the FEM software and the CPU and storage requirements, we need to simplify the system before building the model. Because of the symmetry of the structure, only half of the system is modeled. Furthermore, although the modules are not located symmetrically on the half plane of the base of the heatsink and while the loading conditions are not the same (one IGBT is for braking while the other three are for acceleration), we will simplify the analysis by assuming that the middle line between the IGBT modules are insulated. So only 1/8 of the system is modeled. The model structure is shown in Fig.5.8.

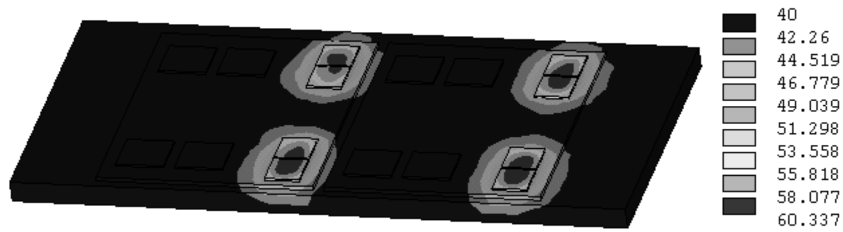

Figure 5.5 Temperature distribution of the module after power applied on diode chips.

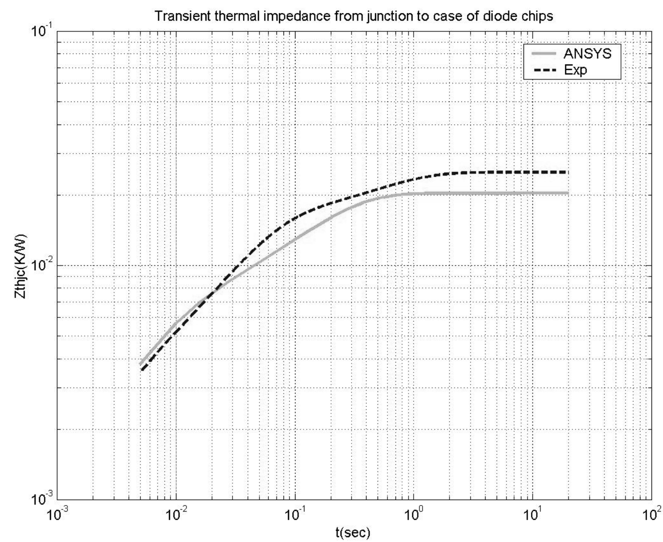

Figure 5.6 Transient thermal impedance from junction to case of diode chips.
Solid line: simulation results by ANSYS, dash line: experimental data

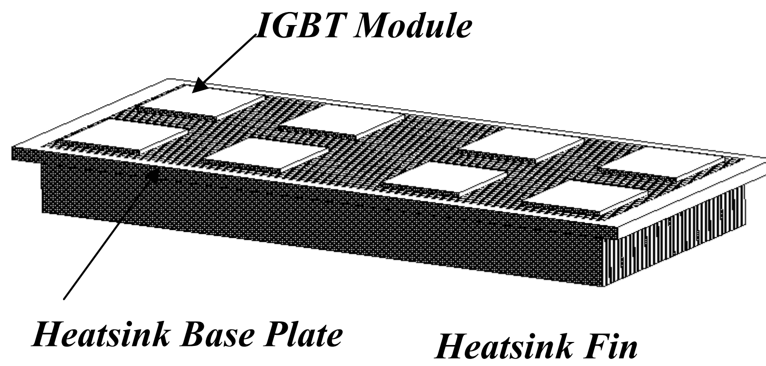

Figure 5.7 Schematic of the whole system.

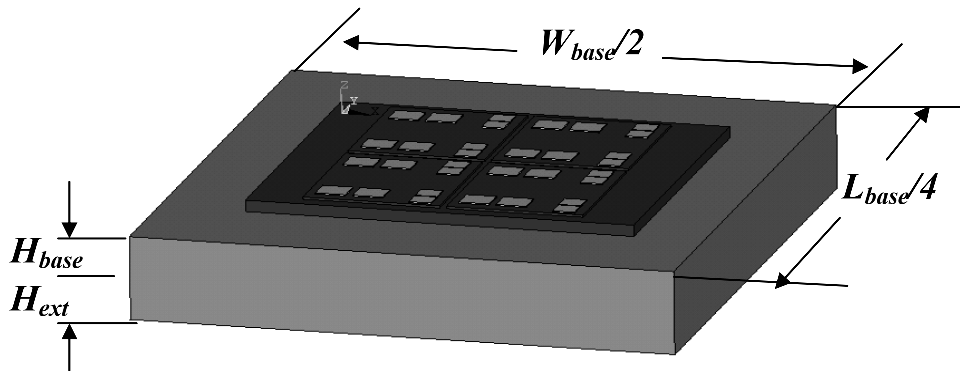

Figure 5.8 Simplified structure of the system.

The simplified model will not include the details of the heatsink fins which act as effective heat transfer coefficients on the base plate of the heatsink. Furthermore, the conduction within the heatsink fins will be equalized as the extension of the base plate of the heatsink. As a result, the heatsink base plate will have the same boundary condition as before with fins [61].

The extension height of the base plate H_{ext} is calculated as the ratio of the volume of the heatsink fins V_{hs} to the area of the base plate of the heatsink A_b:

$$H_{ext} = \frac{V_{hs}}{A_b} = \frac{816 \times 75 \times 3 \times 36}{880 \times 398} = 18.8mm \tag{5.5}$$

5.4.2.2 <u>Calculation Of The Effective Heat Transfer Coefficient H_{eff}</u>. The relation between the effective heat transfer coefficient $\boldsymbol{h_{eff}}$ and the heat transfer coefficient of the heatsink h_{hs} is given by [60]:

$$h_{eff} = \frac{A_{hs}}{A_b} h_{hs} \tag{5.6}$$

where A_{hs} and A_b are the total surface area of the heatsink and the base area, respectively.

The schematic of the finned heatsink is shown in Fig.5.9 (a). The finned heatsink increases the effective surface area for convective heat transfer, and reduces the thermal resistance between the junction to ambient thus lowering the junction temperature of the operating device. The detail of the cross section of the heatsink is shown in Fig.5.9 (b). The serrated fins are used here in order to increase the effective surface area more efficiently.

The heatsink consists of 36 parallel, uniform array of thin, conductive plates of length L, height H and thickness t, mounted on a baseplate of dimensions $L \times W$. Heat is convected from the heatsink by fan through the channels formed between the fins in a direction parallel to the base plate. The heatsink dimensions are listed in Table 5.3.

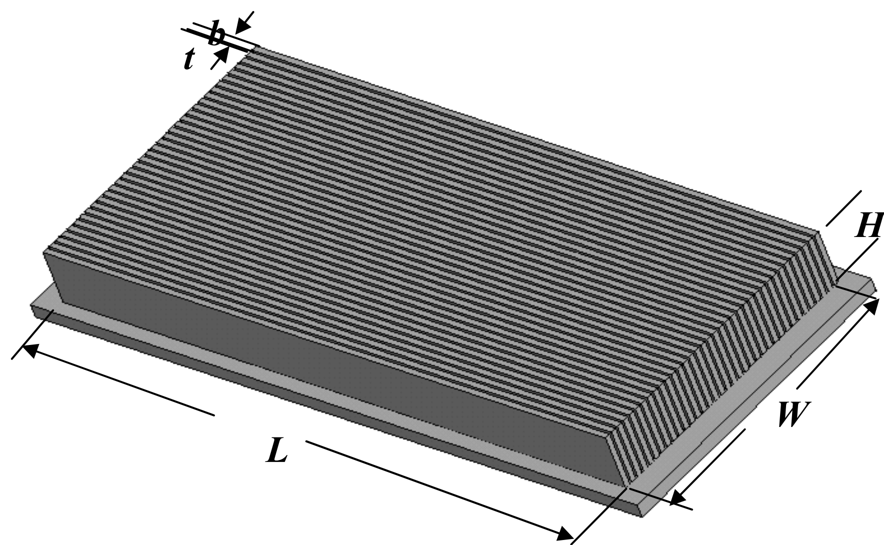

(a)

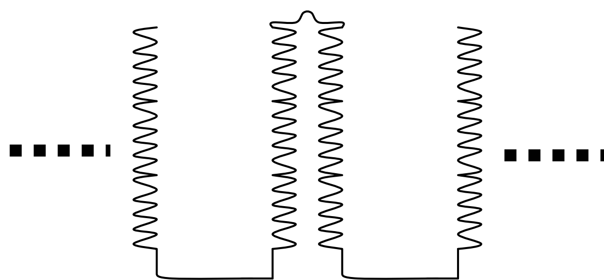

(b)

Figure 5.9 Schematics of the heatsink and the serrated fins.

The average heat transfer coefficient h_{hs} of the heatsink with plane fins is calculated using the equations developed in Reference [62]. The accuracy of these equations was established by comparing predictions with the experimental data and found them in good agreement.

Nusselt number N_u is calculated by using the following relation [62]:

$$N_u = \left[\frac{1}{\left(\frac{\mathrm{Re}_b^{*}\,\mathrm{Pr}}{2} \right)^3} + \frac{1}{\left(0.664\sqrt{\mathrm{Re}_b^{*}}\,\mathrm{Pr}^{1/3}\sqrt{1+\frac{3.65}{\sqrt{\mathrm{Re}_b^{*}}}} \right)^3} \right]^{-1/3} \tag{5.7}$$

where P_r is the Prandtl number and Re_b^* is the channel Reynolds number which can be calculated from Reynolds number Re_b as:

$$\mathrm{Re}_b^{*} = \mathrm{Re}_b \cdot \frac{b}{L} = \frac{Ub}{\nu} \cdot \frac{b}{L} = \frac{Ub^2}{\nu L} \tag{5.8}$$

where ν is the kinematic viscosity of air, b and L are the thickness and length of the plane fins respectively, U is the average air velocity in the channels. The average air velocity can be calculated from the volumetric air flow rate U^* as:

$$U = \frac{U^*}{A - A_f} \tag{5.9}$$

Here A is the cross section area of the wind channel $A=H\times W$, and A_f is the heatsink cross sectional area: $A_f=nHt,$ n is the number of fins.

Table 5.3 Dimensions of finned heatsink

Dimension of finned heatsink	*Values(mm)*
L	816
W	362.4
H	75
B	3
T	7.15
H_{base}	18
H_{ext}	18.8
$W_{base}/2$	199
$L_{base}/4$	220

Table 5.4 Thermochemical properties of air at room temperature used in the calculation

Thermochemical properties	*Values*
Kinematic viscosity ν *(m^2/s)*	1.568×10^{-5}
Thermal conductivity K(W/m-K)	2.62×10^{-2}
Prandtl number P_r	0.708

Combining Equations (5.7) through (5.9) which using the Prandtl number P_r of air as 0.708 [63] and the volumetric air flow rate U^* as 700 cfm(feet^3/minute) as provided by the company allows us to calculate the Nusselt number N_u.

The average heat transfer coefficient h is calculated as [62]:

$$h_{hs} = N_u \cdot \frac{k_f}{b} \tag{5.10}$$

where k_f is the thermal conductivity of the air, and is chosen as 0.000262W/cm·C. The value of h_{hs} calculated using the procedure is 0.00355W/cm^2·C which is within the reasonable range of h for the forced convection [64].

The effective heat transfer coefficient h_{eff} is then estimated from Equation (5.6). The serrated surface area is used in the equation resulting in effective heat transfer coefficient of 0.21W/cm^2·C.

5.4.2.3 Material Properties. The heatsink is made of aluminum, its thermal properties are listed in table 5.1. The thermal properties of the air at room temperature are listed in table 5.4 [64].

5.4.2.4 Loading And Boundary Conditions. A constant power losses of 1000 watts is applied as surface heat flux load uniformly on the 8 IGBT chips surface, while h_{eff} calculated above is added as a convection load on the base of the heatsink. All the other boundaries are assumed adiabatic.

5.4.2.5 Fem Results And Verification. The meshed structure is shown in Fig. 5.10. The model has 3944 nodes and 4410 elements.

5.4.2.5.1 IGBT Powered. In the transient thermal analysis mode, 1000 Watts power is applied as surface load suddenly on the 16 IGBT chips in order to simulate the step response of the system. After 1000 seconds, the temperature distribution of the IGBT modules is shown in Fig. 5.11.

From the simulation data, the junction to ambient thermal impedance curve Z_{ja} of the IGBT can be derived. This curve is shown in Fig.5.12. The Z_{ja} curve predicted from the RC network derived from experimental data is shown on the same figure. The two curves agree with each other and it verifies the accuracy of the RC network derived in Chapter 3 for predicting junction temperature of the IGBT chips. The difference in the thermal resistance between the simulation and the RC model is 6.3%.

Because the transient thermal impedance from case to ambient Z_{ca} is directly derived from the experiment data, so it can be used as criteria to verify the simulation result. The comparison of the simulation result and the experimental data is shown in Fig.5.13. The difference between the simulation and the experimental data for the thermal resistance is 10%.

Because of thermal coupling between the IGBT and diode, so the junction temperature of diode will rise when IGBT chips are powered. This effect is shown in Fig. 5.14. The transient thermal impedance $Z_{IGBT\text{-}diode}$ represents the thermal coupling effect of IGBT on the diode is shown in Fig.5.15. The curve derived from experimental data is shown on the same figure. For the thermal resistance $R_{IGBT\text{-}}diode$, the difference between the result of 3-D simulation and the RC model is 12.5%.

5.4.2.5.2 Diode Powered. Apply 1000 Watts power as surface load on the 16 diode chips for 1000 seconds, the temperature distribution of the system are shown in Fig.5.16.

From the simulation results, we derive the transient thermal impedance of diode from junction to ambient Z_{ja} and it is shown in Fig.5.17. On the same curve, the RC model results are shown for comparison. For the thermal resistance R_{ja}, the difference between the simulation and RC model is 6.8%. This result verifies the RC model for predicting the junction temperature of diode in the IGBT module.

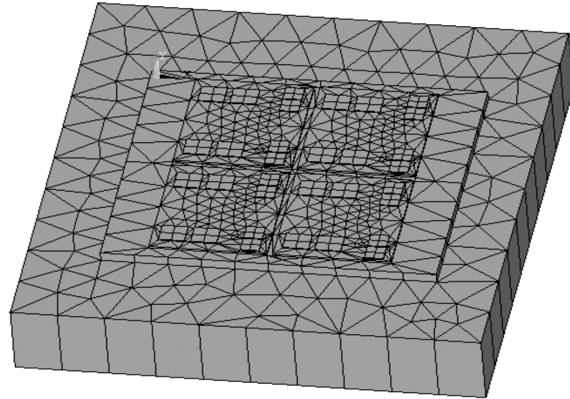

Figure 5.10 Mesh structure of the system.

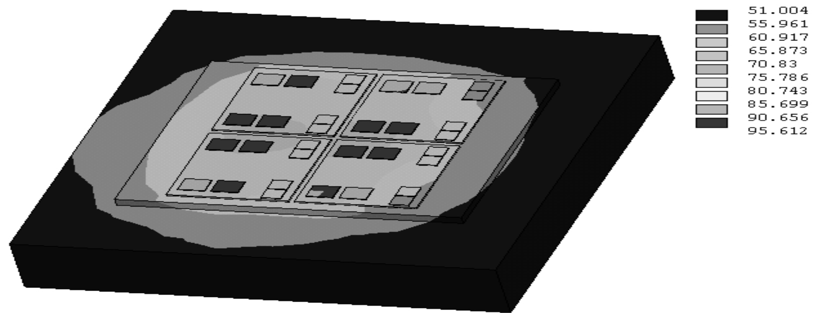

Figure 5.11 Temperature distribution of the system after power applied on IGBT chips.

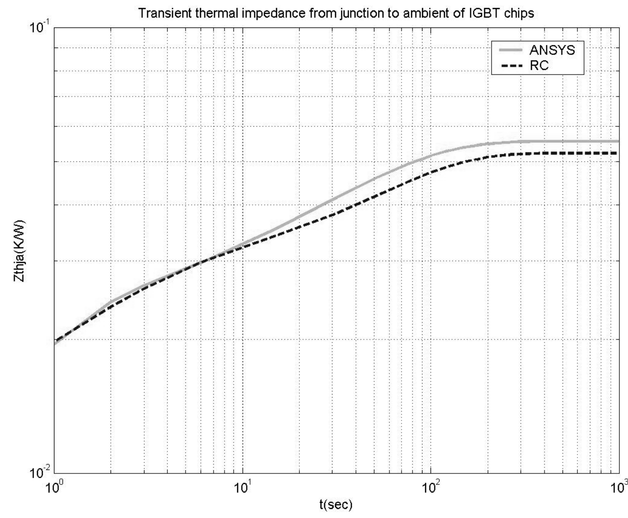

Figure 5.12 Transient thermal impedance from junction to ambient of IGBT chips. Solid line: simulation results by ANSYS, dash line: prediction by RC network

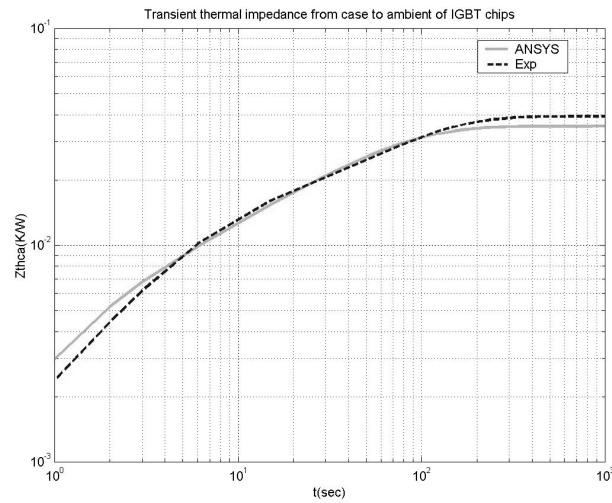

Figure 5.13 Transient thermal impedance from case to ambient of IGBT chips. Solid line: simulation results by ANSYS, dash line: experimental data

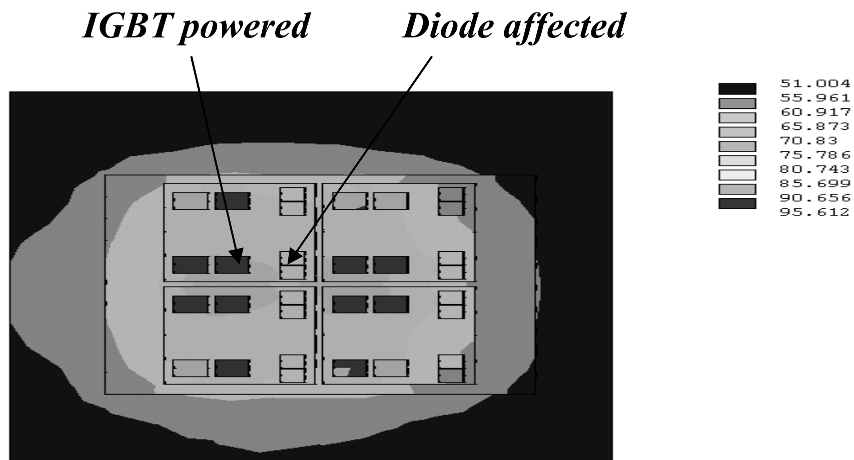

Figure 5.14 Thermal coupling effect of IGBT chips on the diode chips.

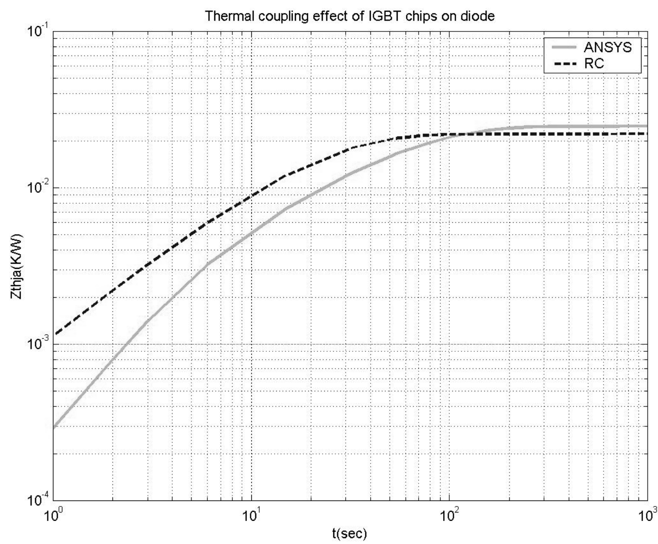

Figure 5.15 Transient thermal impedance representing the thermal coupling effect of IGBT chips on the diode chips. Solid line: simulation results by ANSYS, dash line: prediction by RC network

For the transient thermal impedance from case to ambient of diode, the simulation results and experimental data are shown in Fig.5.18. For the thermal resistance R_{ca}, the difference between the simulation and experimental data is 13.8%.

The thermal coupling effect of diode chips on the IGBT chips are shown in Fig.5.19. The transient thermal impedance $Z_{diode\text{-}IGBT}$ represents the thermal coupling of diode on the IGBT is shown in Fig.5.20. The curve derived from experimental data is shown on the same figure. For the thermal resistance $R_{diode\text{-}IGBT}$, the difference between the simulation and the RC model is 8.7%.

Finally, it is worth mentioning that the thermal conductivity of silicon is a function of temperature, and because the convection is a nonlinear process, the system described is nonlinear. The transient thermal impedance is therefore a function of power. Fig. 5.21 compares the transient thermal impedance $Z_{ja}(t)$ of IGBT at two different power levels. In steady state, the difference between the thermal resistance is within 11%. We can then conclude that the assumption of a system is linear is quite reasonable in the device application condition. This also supports the approach to use RC network to model the thermal behavior of the system.

5.5 Summary

Using 3-D FEM software ANSYS, we have analyzed the thermal behavior of the IGBT module in a three-phase inverter with and without a heatsink. The emphasis of the simulation was to derive the transient thermal impedance curve of the system. The simulation results were compared with the experimental data and found to be in very good agreement. The numerical simulation therefore provides an alternative way to extract thermal RC network parameters which can be implemented in the real time simulator.

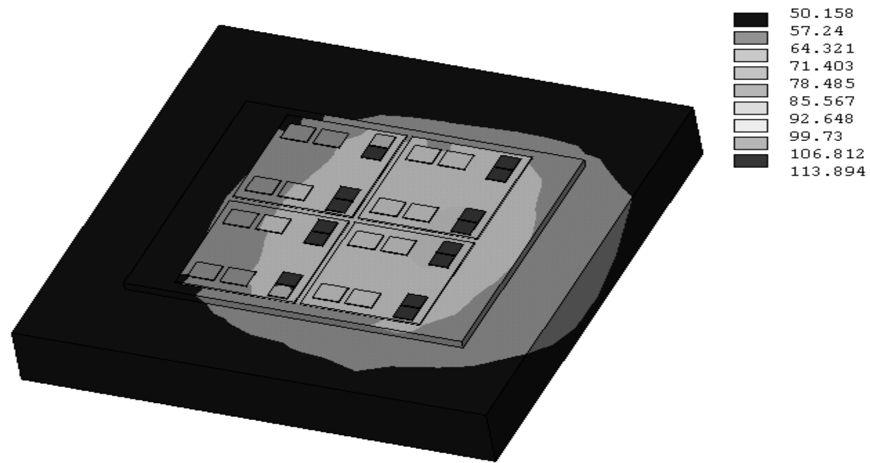

Figure 5.16 Temperature distribution of the system after power applied on diode chips.

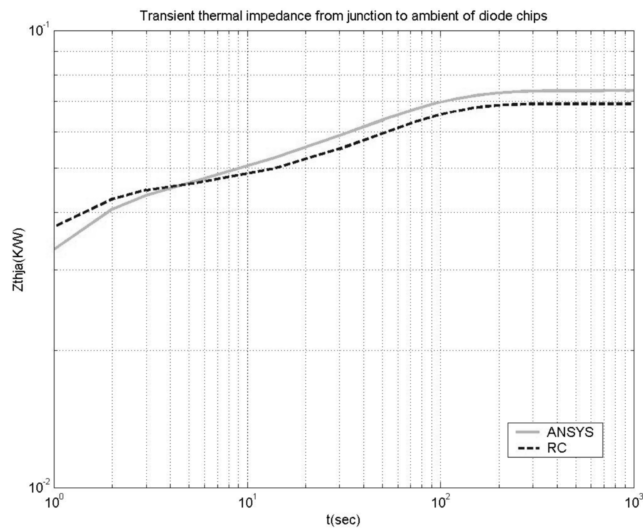

Figure 5.17 Transient thermal impedance from junction to ambient of diode chips. Solid line: simulation results by ANSYS, dash line: prediction by RC network

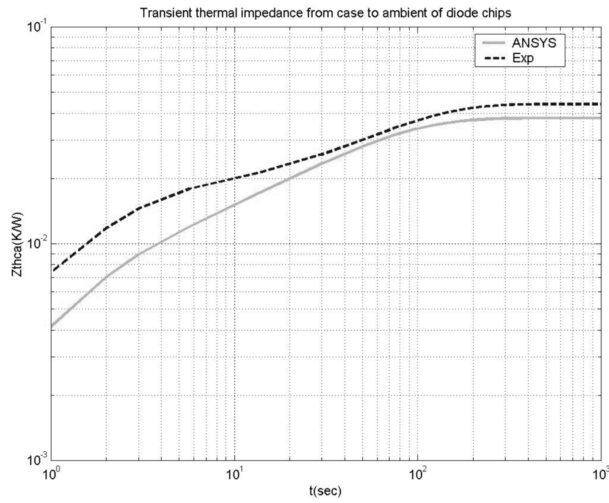

Figure 5.18 Transient thermal impedance from case to ambient of diode chips. Solid line: simulation results by ANSYS, dash line: experimental data

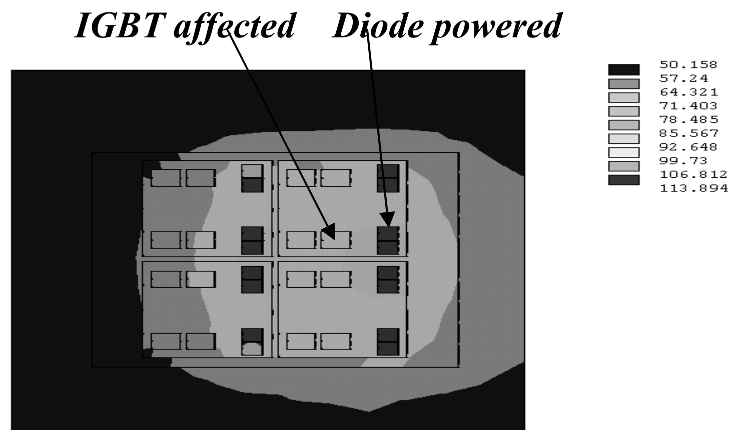

Figure 5.19 Thermal coupling effect of diode chips on the IGBT chips.

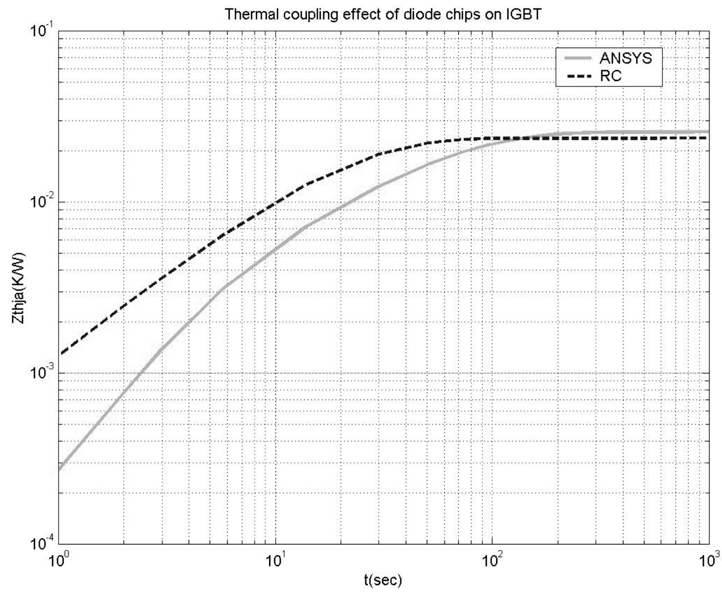

Figure 5.20 Transient thermal impedance representing the thermal coupling effect of diode chips on the IGBT chips. Solid line: simulation results by ANSYS, dash line: prediction by RC network

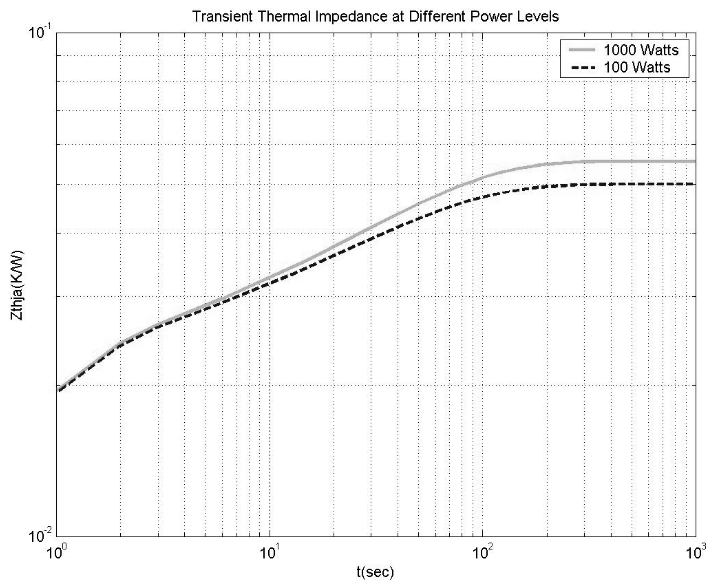

Figure 5.21 Transient thermal impedance Z_{ja} of IGBT at different power levels.

6.0 CONCLUSION

6.1 Summary

A thermal model for the IGBT modules in a three-phase inverter is developed , implemented and tested in the real time simulator.

The model is built in two steps: first the power losses in the IGBT and diode used in a three-phase inverter operating on-line with real time simulator are derived. The power losses in IGBT include the conduction, turn-on and turn-off switching losses. The losses in a diode consists of conduction and recovery losses. The model is based on the curve-fitting results of the power loss data provided by the IGBT module manufacturer. An algorithm is used to catch the switching event in the real time simulator so all switching losses are picked up and accounted for. Besides instantaneous power losses (data sampling time is 50 μs), the model also provides the average power losses for a long average window size such as 1 second. This makes the observation of power losses over a long time run possible.

After the initial step is performed, a thermal RC model of the IGBT module is built. The model is suitable for implementation in a real time simulator. The parameters of the model are derived from two sources: (1) The dynamic thermal impedance from junction-to-case of the IGBT module provided by the IGBT module's manufacturer. (2) The dynamic thermal impedance from case-to-ambient of the IGBT module provided by the user from their experiment on the real application system. The RC thermal circuit is solved in **Simulink** by using "transfer" function. The thermal model includes the thermal coupling between IGBT and the free-wheeling diode. From this model, the instantaneous junction and case temperature of IGBT and diode is calculated on-line in the real time simulator when the three-phase inverter is operating. The transient and steady state junction and case temperature of the IGBT and diode when the train is accelerating and decelerating can be obtained from the real time simulator.

Besides extracting RC thermal model parameters from experimental data, 3-D FEM modeling of the thermal behavior of the IGBT module in the three-phase inverter system is also

performed and the simulation results shows good agreement with the experimental data. From the step response of the system in the 3-D simulation, the transient thermal impedance from junction to case, from case to ambient and the thermal coupling of IGBT and diode chips can be derived. This provides an alternative method to extract thermal RC model parameters which can be implemented in the real time simulator to predict the junction temperature of IGBT module dynamically. The relation between different modeling approach are shown in Fig.6.1.

An off-line simulation is performed to test the thermal model in the real time simulator. Power losses profile corresponding to the process of train's accelerating, keeping constant speed and braking between stops is given as input to the thermal model in the Simulink off-line simulation block, the result of case temperature of the IGBT module when the system reaches thermal steady state agreed well with the experimental data.

In conclusion, the thermal RC model developed for the IGBT module in the three-phase inverter are tested and verified by the experimental data and 3-D numerical simulation results. It will be a useful tool to predict the junction and case temperature of IGBT module dynamically in the real time simulator. The model parameters extracting methods are easy to adapt to other type of IGBT power modules in an industrial application environment.

6.2 Suggestion For Future Work

As mentioned in Chapter 1, the more realistic and accurate model to predict the junction temperature of a device should include the electro-thermal coupling effect. This effect is ignored in our system-level model. If we want to build a device-level thermal model to predict the temperature distribution in the junction region or the junction temperature rise response to very short power losses pulses, electro-thermal coupling effect must be considered. Based-on the electro-thermal model of the IGBT module, an electro-thermal simulation of the device or the system can be further performed [65].

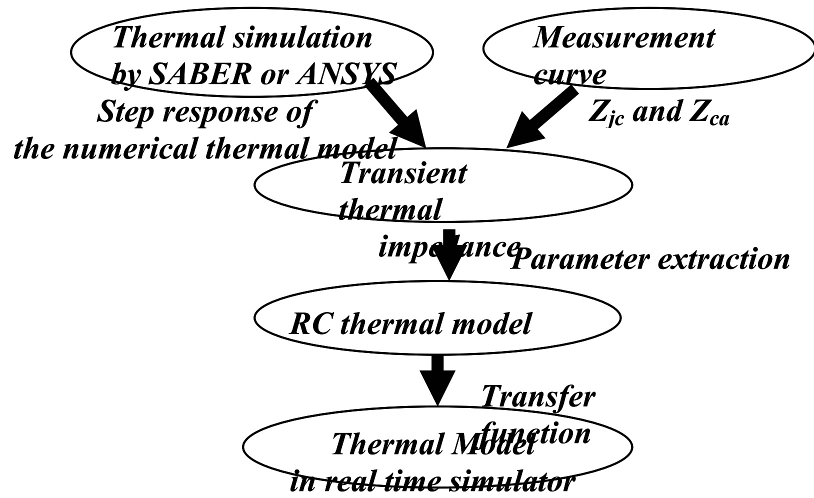

Figure 6. 1 Relation between different approaches of thermal modeling of IGBT module.

APPENDIX

Appendix A

Modeling Approach Including Temperature-Dependency Of Power Losses

A.1 Introduction

Suppose the data shows the relation between the power losses and the device junction temperature T_j is provided by the manufacturer, we can further improve our model to include the temperature dependency on the power losses.

Eupec company does not provide the relation between the switching losses and temperature, so here we use the data sheet of an IGBT device by another company (International Rectifier) as an example to develop the algorithm. The device name is: IRG4BC30KD.

A.2 Curve-Fitting

A.2.1 Switching Losses

The typical switching losses vs. junction temperature is shown here:

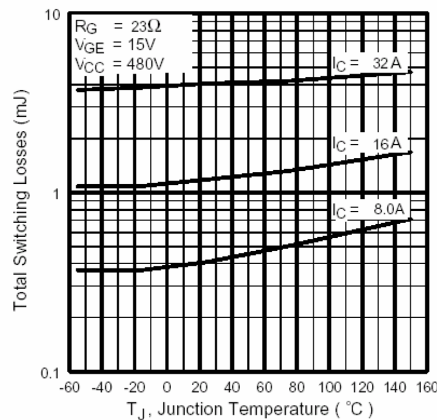

Figure A.1 Typical switching losses vs. junction temperature.

The data points taken from the curve is shown in Table 1.In order to make the current rating matching the Eupec device, we scale up the current and the switching losses both by 31.25 times(=1000/32). The data points after scale-up is shown in Table 2.

Here the switching losses is noted as “Total switching losses”, and we assume the switching-on and switching-off losses are equal, so take half of the value of Table 2 and got Table 3. We will apply curve-fitting method to Table 3.

Table A.1 Data from Fig. A.1

Tj(°C)	-40	0	40	80	120	140
E(mJ)@8A	0.36	0.37	0.43	0.5	0.62	0.68
E(mJ)@16A	1.1	1.2	1.3	1.4	1.5	1.6
E(mJ)@32A	3.8	4	4.1	4.2	4.4	4.6

Table A.2 Scaling–up data on Table A.1

Tj(°C)	-40	0	40	80	120	140
E(mJ)@250A	11.25	11.56	13.44	15.63	19.38	21.25
E(mJ)@500A	34.38	37.5	40.63	43.75	46.88	50
E(mJ)@1000A	118.75	125	128.13	131.25	137.5	143.75

Table A.3 Dividing data on Table A.2 by 2

Tj(°C)	-40	0	40	80	120	140
E(mJ)@250A	5.625	5.78	6.72	7.815	9.69	10.625
E(mJ)@500A	17.19	18.75	20.315	21.875	23.44	25
E(mJ)@1000A	59.375	62.5	64.065	65.625	68.75	71.875

The curve-fitting result for the switching energy losses is:

$$E(Ic,Tj) = m_0 + m_1 \times Tj + m_2 \times Tj^2 + m_3 \times Tj^3$$

where:

$$m_0 = 7.7012 \times Ic + 65.126 \times Ic^2 - 10.266 \times Ic^3$$

$$m_1 = -1.1917 + 72.716 \times Ic + 3.3904 \times Ic^2 - 21.452 \times Ic^3$$

$$m_2 = 2039.2 \times Ic - 6264.8 \times Ic^2 + 3682.8 \times Ic^3 \quad m_3 = -3769.4 \times Ic + 13918 \times Ic^2 - 5509.8 \times Ic^3$$

Here Ic is in Kilo-Ampere, Tj is in Kilo-°C. And E is in Mill-Joules.

A.2.2 Conduction Losses

For the conduction losses calculation, we need to curve fit out-put data curve of Fig. A.2. Figure A.2 was taken from the manufacturer's data sheet. And we also need to scale-up the current rating and after the scale-up, the data points are shown in Table 4. The V_{ce} value is too large for the scaled-up current range and in order not to exaggerate the contribution of the conduction losses, assumption is made that the curve will saturate around 3 Volts and the V_{ce} values are divided by 2. And Table 5 shows the data we took for the curve-fitting of conduction losses calculation.

The curve-fitting result for the out put characteristics is:

$$Vce(Ic,Tj) = m_0 + m_1 \times Ic + m_2 \times Ic^2$$

where:

$$m_0 = 0.63747 - 0.001255 \times Tj$$

$$m_1 = 3.3433 + 0.015519 \times Tj$$

$m_2 = -1.5836 - 0.010252 \times Tj$

Here Ic is in Kilo-Ampere, and Tj is in °C.

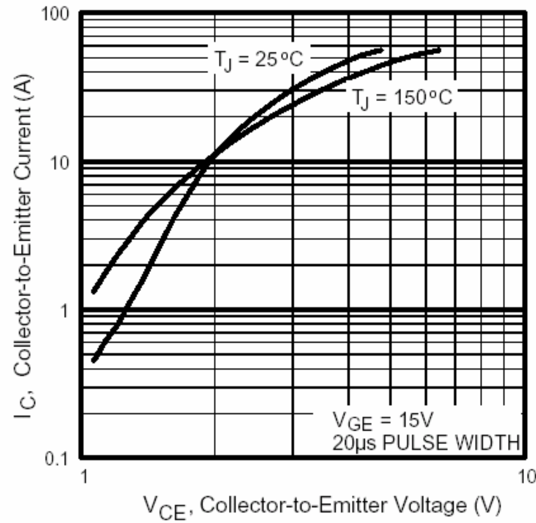

Figure A.2 Typical output characteristics.

Table A.4 Data from Fig.A.2

Ic(A)	20	100	500	1000
Vce(V)@25°C	1.3	2	4	5
Vce(V)@150°C	1.1	2	5	6

Table A.5 Scaling-down the data from Table A.4

Ic(A)	20	100	500	1000
Vce(V)@25°C	0.65	1	2	2.5
Vce(V)@150°C	0.55	1	2.5	3

The model block built in Simulink is shown in the upper part of Fig. A.3. The lower part of Fig. A.3 shows the model which ignore the temperature dependency of the power losses (the

model has no iteration and the power losses is calculated using Tj=125°C). All the inside of the two models are identical.

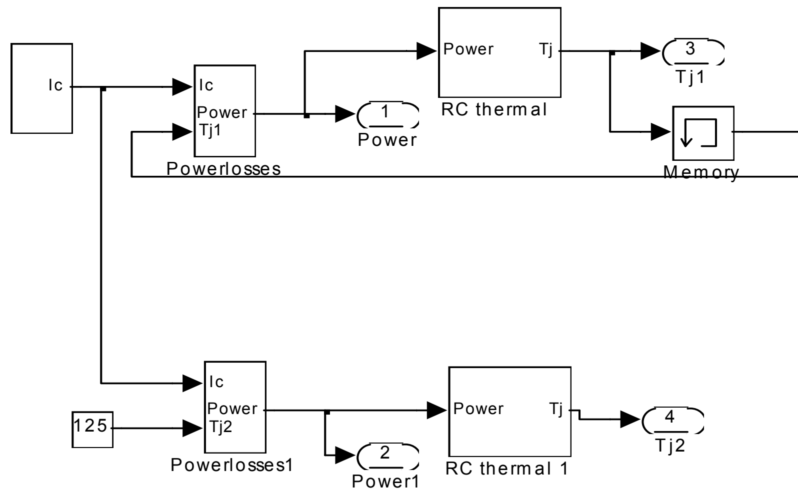

Figure A.3 Simulation models built in Simulink : with and without temperature dependency of power losses.

The RC thermal model is for the Eupec device developed in the thesis. The RC network representing the thermal behavior of the IGBT with heatsink as shown in Fig. 3.10 is repeated here. This model describes the IGBT modules mounted on an air-forced flow heatsink in a three-phase inverter system. And the thermal resistance and capacitance values are listed in Table 3.5.

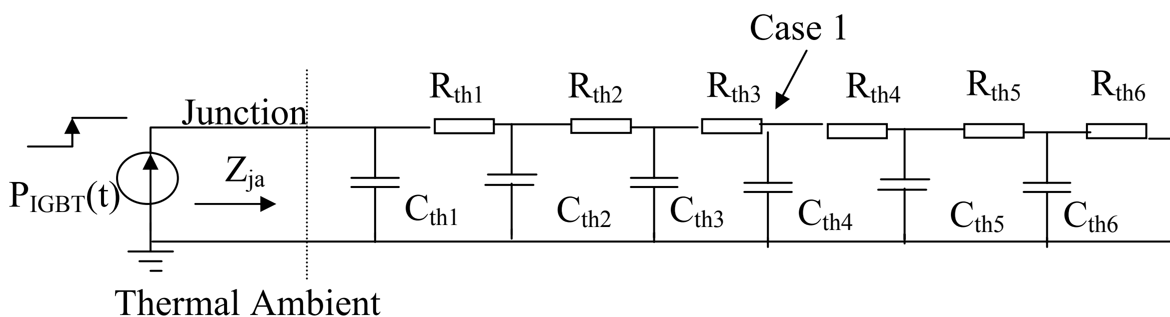

Fig.3.10 RC network representing the thermal behavior of IGBT with heatsink.

Table 3.5 Parameters of the RC network of IGBT from junction to ambient.

i	1	2	3	4	5	6
Thermal R_{thi}(K/Watt)	0.0023	0.0078	0.0019	0.0076	0.0102	0.0225
Thermal C_{thi}(Watt·Sec/K)	1.8	5.5	82.7	123	363.2	2955.5

The process of calculating these values are described in Chapter 3 (behavior modeling approach) and Chapter 5 (physical modeling approach) in parallel. The RC network parameters are extracted from the thermal step response of the device. For Chapter 5 describes the physical modeling approach, all the physics parameters and the device geometry can be found there.

Fig. A.4 shows the input Ic waveform. It is a periodical signal. Fig. A.5 shows the corresponding power losses waveform. Fig. A.6 shows the junction temperature excursions from the temperature-dependency model when ambient temperature is setup as 25°C.

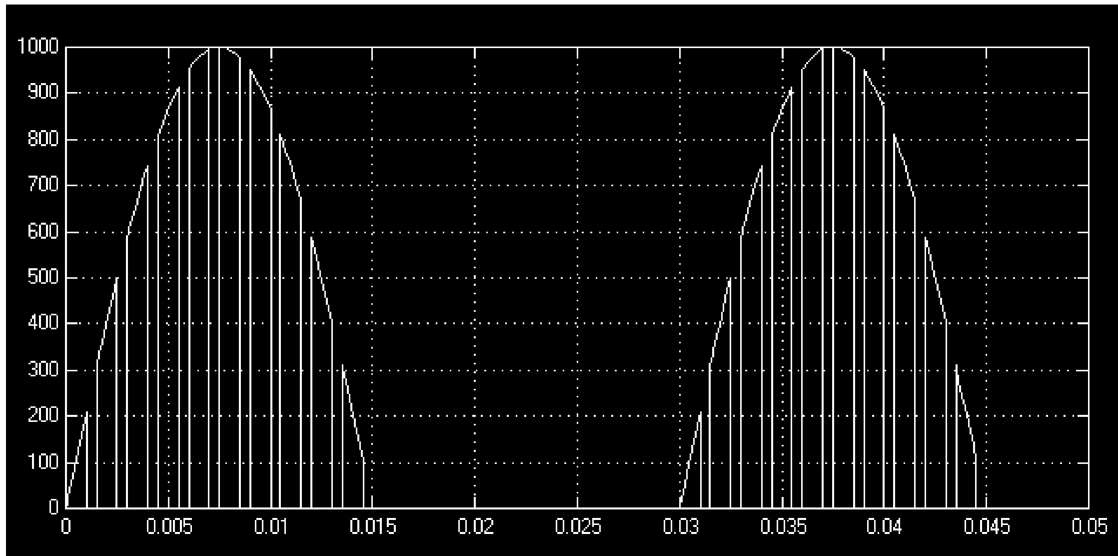

Figure A.4 Input Ic waveform. X-time(second); Y-current(A)

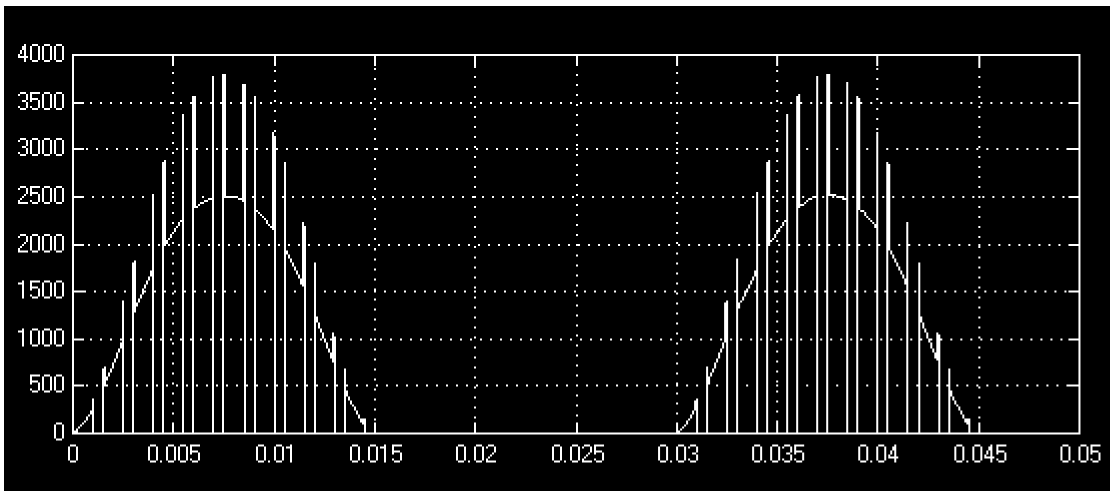

Figure A.5 Power losses waveform. X-time(second); Y-power losses(Watts)

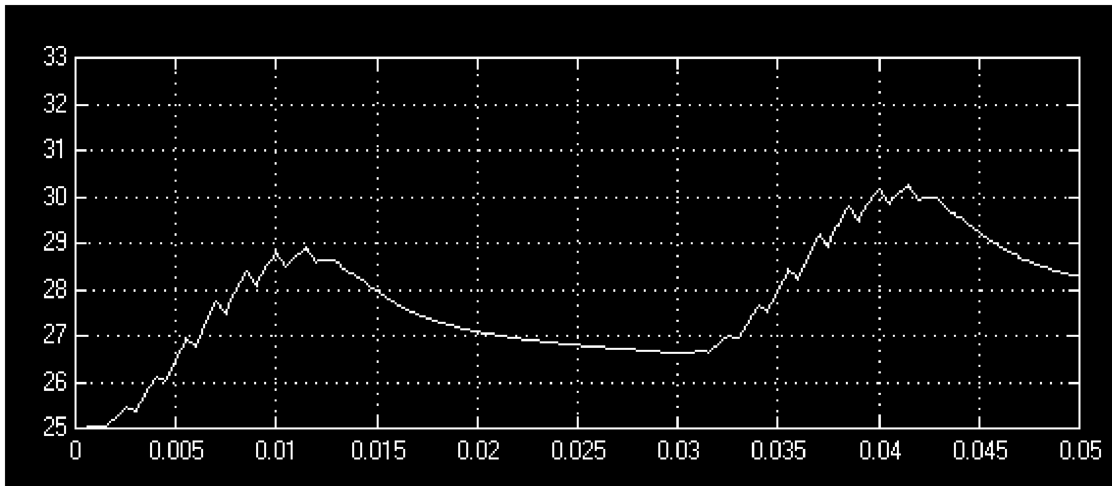

Figure A.6 Junction temperature waveform. X-time(second); Y-temperature(°C)

A.3 Case Study: Simulation Results

A.3.1 The Difference Between The Temperature-Dependency Model And The Non-Temperature-Dependency Model

A.3.1.1 With Assumption Of Ambient Temperature Of 0 °C. Fig. A.7 shows the simulation results of junction temperature of two models. The difference between the two models is about 20%.

A.3.1.2 With Assumption Of Ambient Temperature Of 25 °C. Fig. A.8 shows the simulation results of junction temperature of two models. The difference between the two models is about 5%.

A.3.1.3 With Assumption Of Ambient Temperature Of 40 °C. Fig. A.9 shows the simulation results of junction temperature of two models. The difference between the two models is about 4%.

The difference between the two models will decrease when the working junction temperature increases.

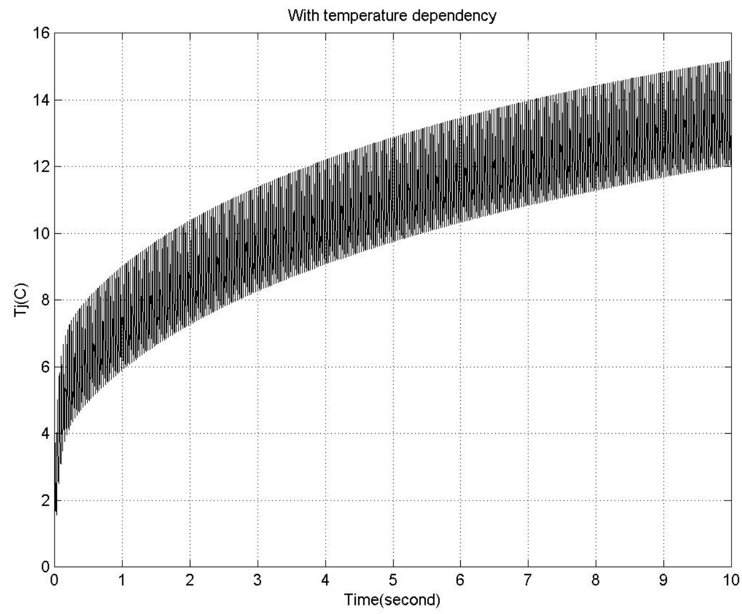

Figure A.7 Junction temperature Tj simulation results by two model when ambient =0°C.

(a) With temperature dependency

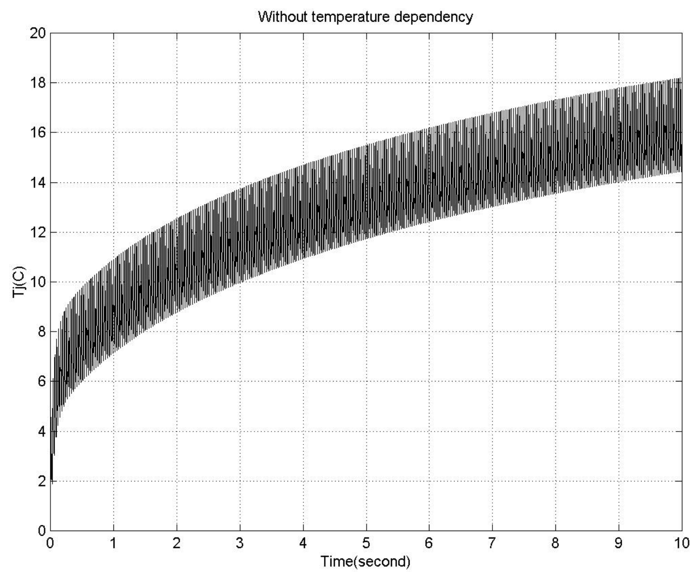

(b) Without temperature dependency

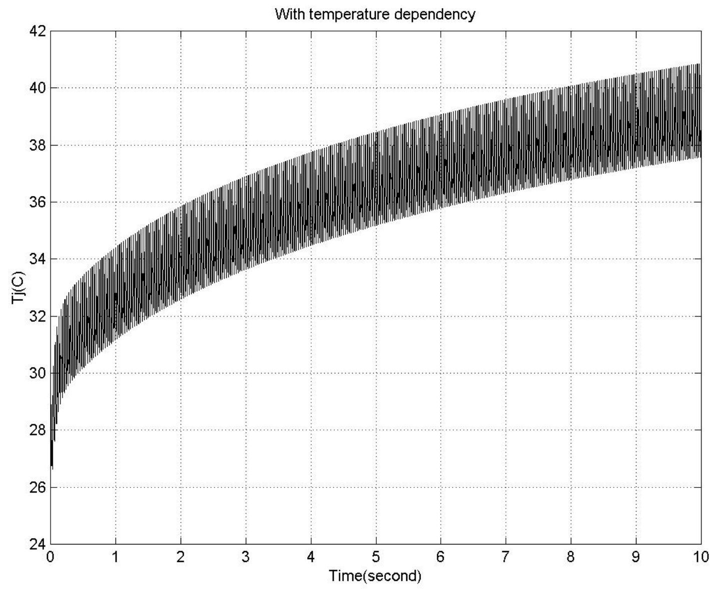

Figure A.8 Junction temperature Tj simulation results by two model when ambient =25°C.

(a) With temperature dependency

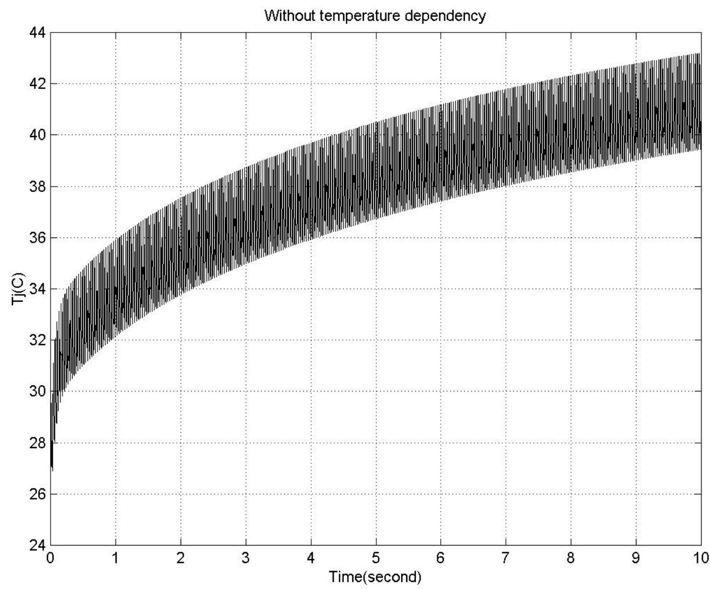

(b) Without temperature dependency

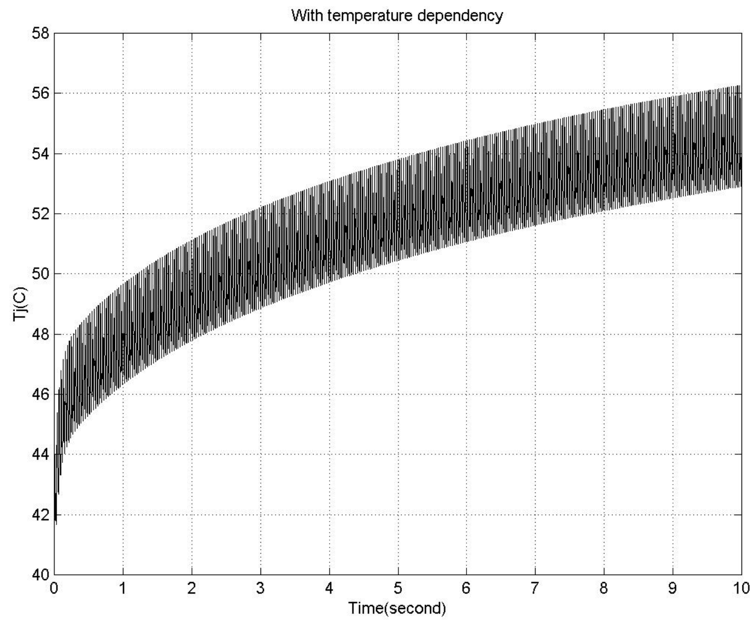

Figure A.9 Junction temperature Tj simulation results by two model when ambient =40°C.
(a) With temperature dependency

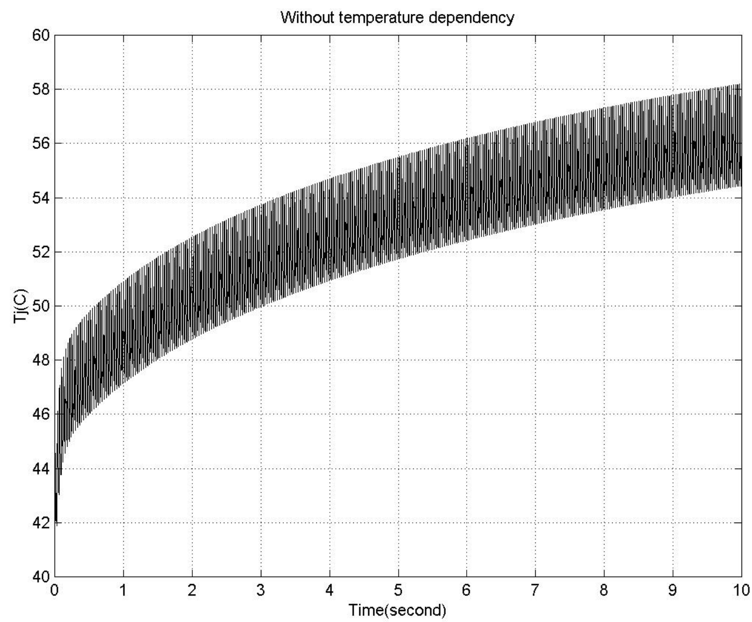

(b) Without temperature dependency

A.3.2 Verification Of The Junction Temperature Excursion Per Pulses In Fig.A.6

There is about 3 °C junction temperature excursion for per 33Hz pulses. In order to show this result is reasonable, we need to verify the result by using the experimental data of the Eupec device.

The available thermal performance data is the transient thermal impedance curve from junction to case of IGBT module as shown in Fig. 3.5. It is repeated here for convenience.

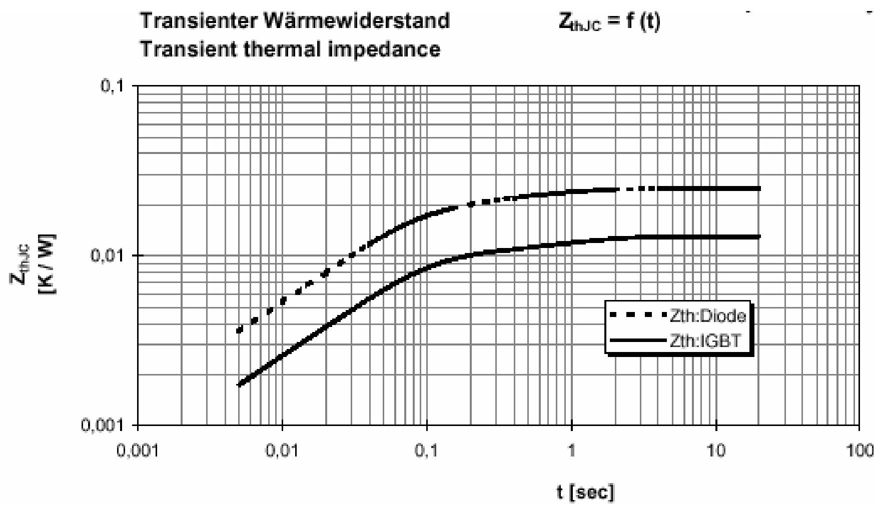

Fig. 3.5 Transient thermal impedance curve of IGBT module including the diode.

The available experimental data on Fig. 3.5 goes down to 0.005 seconds. This means we can tell how much is the junction temperature rise when we apply a power losses step with certain amplitude for a short period 0.005 seconds to the device. We need to mention that although this data is the performance of the IGBT device with idea heatsink attached, for we are down to this small time period, the heat from the IGBT chip have not transmitted to the heatsink yet, so the thermal behavior of the IGBT can not be affected by the heatsink, so we can also use this data for the performance of IGBT with non-ideal heatsink (the real device in application) attached in this short period.

If we average the power losses waveform in Fig.A.5 for every 0.005 seconds, we will have three pulses as shown in Fig. A.10. Here we got the three values: P1=525 Watts, P2=1175 Watts and P3=500 Watts. Please notice the delay comes from the averaging algorithm and will not affect the averaging power losses values here.

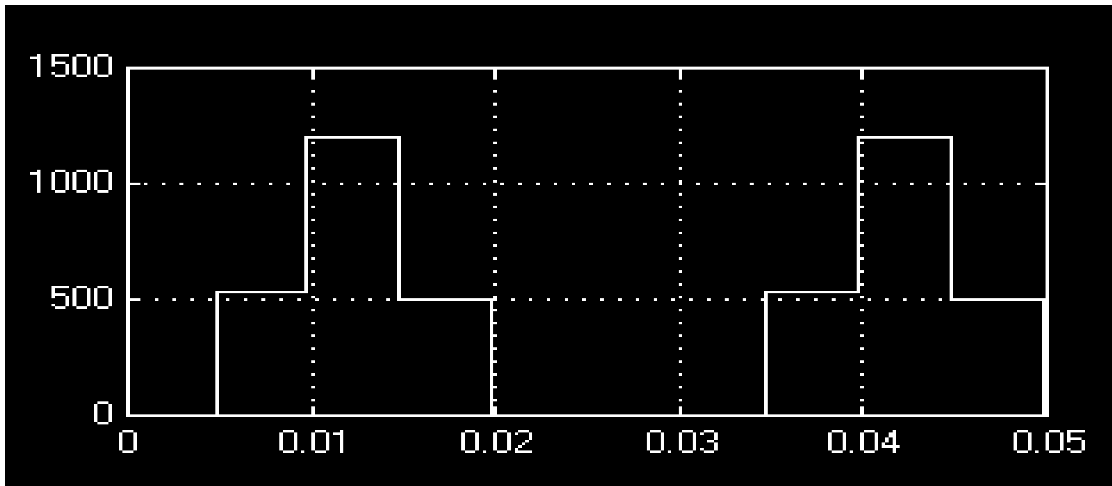

Figure A.10 Averaged power losses waveform. X-time(second); Y-power losses(Watts)

These three power losses pulses shown in Fig.A.11(a) are equaled to combining three power losses steps as shown in Fig.A.11(b) to Fig.A.11(d).

The junction temperature rise at 0.005, 0.01 and 0.015 seconds can be predicted by the supposition of the temperature rise stimulated by each power losses steps. The calculation process is shown below.

From the experimental curve shown in Fig. 3.5, the thermal impedance of IGBT module are:

@ t=0.005 sec, Zth(t)=0.0017 °C/Watt

@ t=0.010 sec, Zth(t)=0.0026 °C/Watt

@ t=0.015 sec, Zth(t)=0.0032 °C/Watt

For P1:

@ t=0.005 sec, $\Delta Tj=P1\times Zth(t)=525\times 0.0017=0.89$°C (For it is the temperature difference, the unit in K or °C is the same).

@ t=0.01 sec, $\Delta Tj=P1\times Zth(t)=525\times 0.0026=1.365$°C

@ t=0.015 sec, $\Delta Tj=P1\times Zth(t)=525\times 0.0032=1.68$°C

For P2-P1:

@ t=0.005sec, $\Delta Tj=0$

@ t=0.01sec, $\Delta Tj=(P2-P1)\times Zth(t)=650\times 0.0017=1.105$°C

@ t=0.015sec, $\Delta Tj=(P2-P1)\times Zth(t)=650\times 0.0026=1.69$°C

For P3-P2-P1:

@ t=0.005sec, $\Delta Tj=0$

@ t=0.01sec, $\Delta Tj=0$

@ t=0.015sec, $\Delta Tj=(P3-P2-P1)\times Zth(t)= -1200\times 0.0017= -2.04$°C

So the excursion of junction temperature is:

@ t=0.005sec, $\Delta Tj=0.89$°C

@ t=0.01sec, $\Delta Tj=1.365+1.105=2.47$°C

@ t=0.015sec, $\Delta Tj=1.68+1.69-2.04=1.33$°C

This result verified the simulation results shown in Fig. A.6.

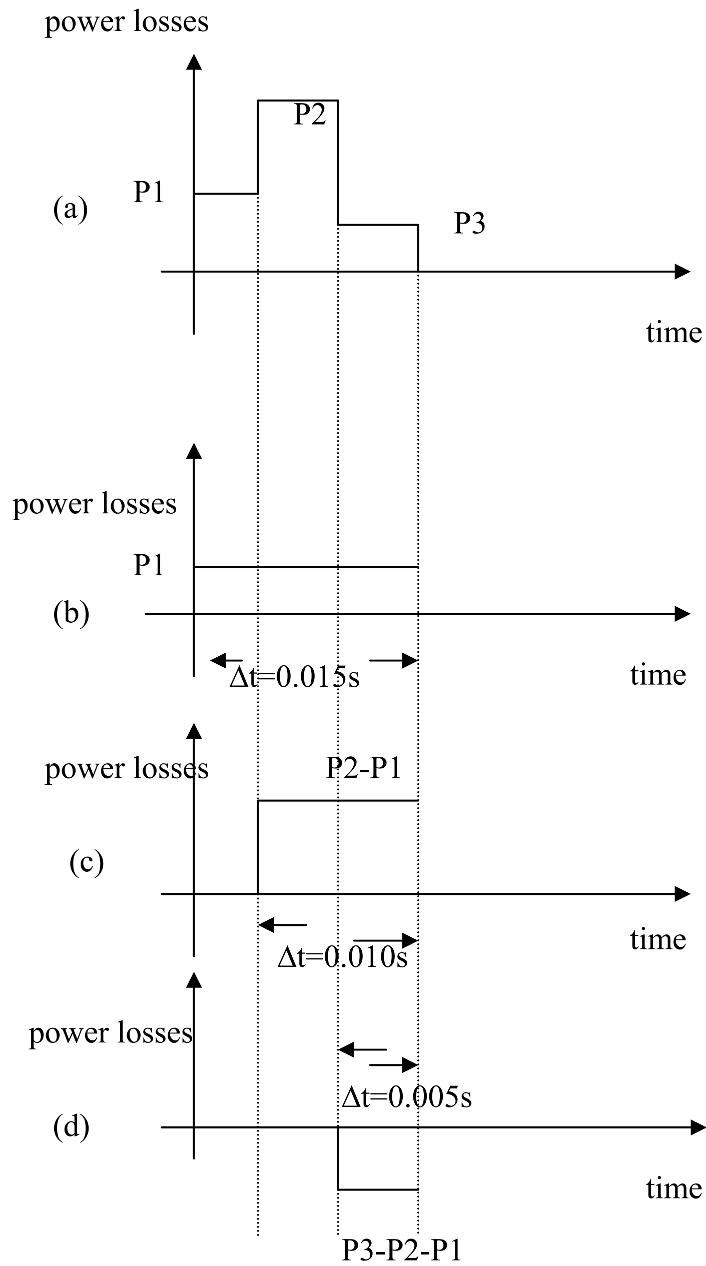

Figure A.11 Pulses vs. step as input function.

BIBLIOGRAPHY

BIBLIOGRAPHY

[1] Bimal K. Bose, "Power electronics and drives-technology advances and trends", Industrial Electronics, ISIE '99. Proceedings of the IEEE International Symposium on, Volume: 1 , 1999. Page(s): TU1 vol.1

[2] B.Jayant Baliga, "Trends in power semiconductor devices", IEEE Trans. on Electron Devices, Vol. 43, No. 10, October 1996.

[3] Steffen Bernet, "Recent developments of high power converters for industry and traction applications", IEEE Trans. on Power Electronics, vol. 15, No 6, November 2000.

[4] IGBT designer's manual, International Rectifier Corp., El Segundo, CA, 1997.

[5] B.J. Baliga, Power Semiconductor Devices. Boston, MA:PWS Publishing, 1995, p.433.

[6] Kuang Shen, Stephen J. Finney, and Barry W. Williams, "Thermal Stability of IGBT High-frequency operation", IEEE Trans. on Industrial Electronics, vol. 47, No 1, February 2000.

[7] Powerex, "IGBTMOD and Intellimod, Application and Technical data book".

[8] Wuchen Wu, Marcel Held, Peter Jacob, Paolo Scacco, and Alessandro, " Thermal stress related packaging failure in power IGBT modules", Proc. of 1995 International Symposim on Power Semiconductor Devices and ICs, Yokohama.

[9] Francesco Profumo, Alberto Tenconi, Simone Facelli, and Bruno Passerini, "Implementation and validation of a new thermal model for analysis, design, and characterization of multichip power electronics devices", IEEE Trans. On Industry Applications, vol. 35, No. 3, May/June 1999.

[10] J.Sigg, P.Turkes, R. Kraus, "Parameter extraction methodology and validation for an electro-thermal physics-based NPT IGBT model", IEEE Industry Applications Society Annul Meeting, New Orleans, Louisiana, October 5-9, 1997.

[11] Anis Ammous, Kaiçar Ammous, Hervé Morel, Bruno Allard, Dominique Bergogne, Fayçal Sellami, and Jean Pierre Chante, "Electrothermal modeling of IGBT's: application to short-circuit conditions", IEEE Trans. On Power Electronics, Vol.,15, No. 4, July 2000.

[12] Eupec, Web site: http://www.eupec.com

[13] Heinz Willi Van Der Broeck, Hans-christoph Skudelny, and Georg Viktor, "Analysis and realization of a pulsewidth modulator based on voltage space vectors", IEEE Trans. On Industry Applications, vol. 24, No. 1, January/February 1988.

[14] Allen R. Hefner, Jr., Daniel M. Diebolt, "An experimentally verified IGBT model Implemented in the SABER circuit simulator", IEEE Power Electronics Specialist Conference, Conf. Rec., pp. 10-19, 1991.

[15] Allen R. Hefner, Jr., and S. Bouché, "Automated parameter extraction software for advanced IGBT modeling", Computers in Power Electronics, 2000. COMPEL 2000. The 7th Workshop on , 2000. Page(s): 10 -18

[16] Chuck Wong, "EMTP modeling of IGBT dynamic performance for power dissipation estimation", IEEE Trans. On Industry Applications, vol. 33, No. 1, January/February 1997.

[17] Allen R.Hefner and David L.Blackburn, "Thermal Component models for electrothermal network simulation", IEEE Trans. On Components, Packaging, and Manufacturing Technology, Part A, vol.17, no. 3, September 1994

[18] Tien-Yu Lee, "Design optimization of an integrated liquid-cooled IGBT power module using CFD technique", IEEE Trans On Components and packaging Technologies, vol. 23, No.1, March 2000.

[19] ANSYS analysis manual; ANSYS is a trade mark of ANSYS Inc., Houston, PA,USA.

[20] Flotherm analysis manual; Flotherm is a trademark of Flometrics Limited, Surrey, England.

[21] Anis Ammous, Sami Ghedira, Bruno Allard, Hervé Morel, and Denise Renault, "Choosing a thermal model for electrothermal simulation of power semiconductor devices", IEEE Trans. On Power Electronics, vol.14, No.2, March 1999.

[22] D.J. Jamieson, A.D. Mansell; Staniforth, J.A. Staniforth, and D.W. Tebb, "Application of finite difference techniques for the thermal modelling of power electronic switching devices", Power Electronics and Variable-Speed Drives, 1994. Fifth International Conference on, 1994. Page(s): 313 -318

[23] Chan-Su Yun, Peter Regli, Jürg Waldmeyer, and Wolfgang Fichtner, "Static and dynamic thermal characteristics of IGBT power modules", Power Semiconductor Devices and ICs, 1999. ISPSD '99. Proceedings.,

[24] Gary l. Skibinski, and William A. Sethares, " Thermal parameter estimation using recursive identification", IEEE Trans., On Power Electronics, Vol., 6, No. 2, April 1991.

[25] Allen R. Hefner, "A dynamic electro-thermal model for the IGBT", IEEE Trans. On Industry Applications, vol.30, No. 2, March/April 1994.

[26] B.Kaku, I. Miyashita, S.Sone, “Switching loss minimized space vector PWM method for IGBT three-level inverter”, IEE Proc-Electr. Power Appl.,Vol.144, No. 3, May 1997.

[27] B.Weis, and M.Bruckmann, “A new gate driver circuit for improved turn-off characteristics of high current IGBT modules”, Industry Applications Conference, 1998. Thirty-Third IAS Annual Meeting. , 1998 .Page(s): 1073 –1077.

[28] B.Jayant Baliga, Power Semiconductor Devices, PWS Publishing Company, 1996.

[29] Robert W.Erickson, Fundamentals of Power Electronics, Kluwer Academic, Publishers, 1997.

[30] H.S.Oh, Ph.D thesis, University of Pittsburgh, July, 2000.

[31] Joseph Vithayathil, Power electronics: principles and applications. McGraw-Hill, Inc., 1995.

[32] J.W.Kolar, H. Ertl, and F.C. Zach, “Influence of the modulation method on the conduction and switching losses of a PWM converter system”, Industry Applications Society Annual Meeting, 1990., Conference Record of the 1990 IEEE, 1990. Page(s): 502 –512.

[33] Casnellas, “Losses in PWM inverters using IGBTs”, IEE Proc.-Electr. Power Appl. 1994, 141, pp.235-239.

[34] Jinrong Qian, Aslam Khan, and Issa Batarseh, “ Turn-off switching loss model and analysis of IGBT under different switching operation modes”, Industrial Electronics, Control, and Instrumentation, 1995, Proceedings of the 1995 IEEE IECON 21st International Conference on, Volume: 1, 1995 .Page(s): 240 -245.

[35] Osama Al-Naseem, Robert W. Erickson and Palmer Carlin, “ Prediction of switching loss variations by averaged switch modeling”, Applied Power Electronics Conference and Exposition, 2000. APEC 2000. Fifteenth Annual IEEE , Volume: 1 , 2000 . Page(s): 242 -248.

[36] Abraham L., and M.Reddig, “ Determination of switching losses in IGBT’s by loss summation-method”. Industry Applications Conference, 1995. Thirtieth IAS Annual Meeting, IAS '95., Conference Record of the 1995 IEEE , Volume: 2 , 1995. Page(s): 1061 –1068.

[37] T.Reimann, R. Krümmer, U.Franke, J.Petzoldt, L.Lorenz, “Real time calculation of the chip temperature of power modules in PWM inverters using a 16bit microcontroller”, Power Semiconductor Devices and ICs, 2000. Proceedings. The 12th International Symposium on , 2000 . Page(s): 127 -130.

[38] S. Azuma, M. Kimata, M. Seto, Xinjian Jiang, Haiwei Lu, Dewei Xu, and Lipei Huang, “Research on the power loss and junction temperature of power semiconductor devices for inverter”, Vehicle Electronics Conference, 1999. (IVEC '99) Proceedings of the IEEE International , 1999 . Page(s): 183 -187 vol.1.

[39] Ronald H. Randall, and Alain Laprade, “Analyze IGBT losses with behavioral models”, PCIM Magazine, March 2001.

[40] Fabio Filicori, Corrado Guarino Lo Bianco, “A simplified thermal analysis approach for power transistor rating in PWM-controlled DC/AC converters”, IEEE Trans. On Circuit and Systems-I, vol.45, No. 5, May 1998.

[41] Hou-cheng Huang and Asif S. Usmani, Finite Element Analysis for Heat Transfer: Theory and Software, springer-verlag, chapter 1.

[42] H.S.Carslaw and J.C.Jaeger, Conduction of Heat in Solids. England: Oxford Science Section 2.9.

[43] Steve Clemente, “Transient thermal response of power semiconductors to short power pulses”, IEEE Trans. On Power Electronics, Vol. 8, No. 4, October 1993.

[44] Y.Jay Min, Arthur L. Palisoc, and Chin C. Lee, “ Transient thermal study of semiconductor devices”, IEEE Trans. On Components, Hybrids, and Manufacturing Technology, Vol. 13, No. 4, December 1990.

[45] Jean-Marie Dorkel, Patrick Tounsi, and Philippe Leturcq, “ Three-dimensional thermal modeling based on the two-port network theory for hybrid or monolithic integrated power circuits”, IEEE Trans. On Components, Hybrids, and Manufacturing Technology, -Part A, Vol. 19, No. 4, December 1996.

[46] N.Y.A. Shammas, M.P.Rodriguez, A.T.Plumpton, and D.Newcombe, “Finite element modeling of thermal fatigue effects in IGBT modules”, IEE Proc. –Circuit Devices Syst.,Vol.148, No. 2, April 2001.

[47] Toshiyuki kikunaga and takesshi Ohi, “ Analysis and simulation technologies for high reliability design of power modules”, R& D Progree Report, Mitsubishi.

[48] Jia Tzer and loc Vu-Quoc, “ A rational formulation of thermal circuit models for electrothermla simulation-Part I: Finite element method”, IEEE Trans. On Circuits and Systems-I: Fundamental and Applications, Vol., 43, No. 9, September 1996.

[49] Torsten Hauck and Tina Bohm, “ Thermal RC-network approach to analyze multichip power packages”, Semiconductor Thermal Measurement and Management Symposium, 2000. Sixteenth Annual IEEE, 2000. Page(s): 227 –234.

[50] Martin März, Paul Nance, Application Note, “Thermal modeling of power electronic systems”, Infineon, Web page: http://www.infineon.com

[51] F.P. Incropera and D.P. Dewitt, Fundamentals of Heat and Mass Transfer, 3 rd ed. New York, NY: Wiley,1990, p.51.

[52] Chan-Su Yun, Paolo Malberti, Mauro Ciappa, and Wolfgang Fichtner, "Thermal component model for electrothermal analysis of IGBT module systems", IEEE Trans. On Advanced Packaging, Vol., 24, No. 3, August 2001.

[53] F. Blaabjerg, J.K. Pedersen, K.D. Madsen, and K.F. Rasmussen, "An advance microprocessor based temperature controlled heatsink", Industrial Electronics, Control, and Instrumentation, 1993. Proceedings of the IECON '93., International Conference on, 1993. Page(s): 785 –789. vol.2.

[54] John W. Sofia, Application note, " Fundamentals of thermal resistance measurement",Analysis Tech, web page: www.analysistech.com.

[55] Peter Terwiesch, Thomas Keller and Erich Scheiben, "Rail vehicle control system integration testing using digital hardware-in-the-loop simulation", IEEE Trans. On Control Systems Technology, vol. 7, no. 3, may 1999.

[56] Ying-Yu Tzou, and Hau-Jean Hsu, "FPGA realization of space-vector PWM control IC for three-phase PWM inverter", IEEE Trans On Power Electronics, Vol. 12, No. 6, November 1997.

[57] Simulink Manual, Mathworks Inc., web page: www.mathworks.com

[58] P.Barnard, "New power system blockset enables you to model electrical power systems", Matlab Newsletter, pp. 10-11, Summer 1998.

[59] ANSYS manual, ANSYS Inc., web page: www.ansys.com

[60] Jerry E.S, and Al Krum, Thermal Management Handbook for Electronic Assemblies, McGRAW-HILL, 1998.

[61] Susheela Narasimhan and Joseph Majdalani, "Characterization of compact heat sink models in natural convection", IEEE Trans. On Components and Packaging Technologies, Vol. 25, No. 1, March 2002.

[62] P. Teertstra, M.M. Yovanovich and J.R. Culham, "Analytical forced convection modeling of plate fin heat sinks", Semiconductor Thermal Measurement and Management Symposium, 1999. Fifteenth Annual IEEE, 1999. Page(s): 34 –41.

[63] Chan-Ki Kim, and Kee-Man Nho, "Heatsink design of high power converter",

[64] Tummala R.R, Eugene J.R, and Alan G.K, Microelectronics Packaging Handbook, Van Nostrand Reinhold, 1989.

[65] H.Alan Mantooth, and Allen R. Hefner, "Electrothermal simulation of an IGBT PWM inverter", IEEE Trans. On Power Electronics, Vol. 12, No. 3 May 1997.